Control of Dynamically Substructured Systems for Testing Generic Vibrating Structures

Thesis submitted in accordance with the requirements of
the University of Liverpool for the degree of
Doctor of Philosophy

by

An Hu

School of Engineering
University of Liverpool
September 2019

Declaration

This work has not been submitted in substance for any other degree or award at this or any other university or place of learning, nor is being submitted concurrently in candidature for any degree or other award. This thesis is being submitted in partial fulfilment of the requirements for the degree of PhD. This thesis is the result of my own independent work/investigation, except where otherwise stated. Other sources are acknowledged by explicit references. The views expressed are my own. I hereby give consent for my thesis, if accepted, to be available for photocopying and for interlibrary loan, and for the title and summary to be made available to outside organisations.

Abstract

Currently, the mainstream structure testing methods include physical tests via experiments and numerical simulations. The advantage of physical tests is obvious: the reality can be fully reflected, which means uncertainties and realistic results can be obtained. However, it can be time consuming for the preparation and post processing, as well as it is expensive. Numerical simulations are economic and have simplified operation procedures compared with physical tests, but it may be time consuming to simulate complex structures and cannot reflect the reality such as uncertainties in all circumstances. Then, considering the challenges and the cost of testing the large and complex structures using the physical test, and in order to avoid such disadvantages, several techniques have been proposed to combine the advantages of physical tests and numerical simulations. Such techniques are categorised as the hybrid testing. The basic idea is to place some parts of structures under test with a numerically simulated system while the rest of structures are physically tested. Dynamically structured systems (DSS) are a typical example of hybrid testing; by combining real-time numerical simulation with physical components, it allows dynamic testing of structures with high accuracy and fidelity, while reducing cost. In this thesis, a comprehensive analysis of DSS approaches for generic lumped parameter vibration problems is conducted to find explicit conditions under which DSS is a feasible approach for dynamic testing. At present, the feasibility analysis of generic vibrating structure is missing. The work presented in

this thesis is a step towards filling this gap. Analytical conditions for structural properties such as causality, observability and controllability are derived for a generalised vibration system represented as a chain of mass-spring-damper systems. The method is based on a novel recursive representation of transfer functions, which eliminates the need for deriving fully explicit symbolic expressions. This in turn, allows performing the causality analysis without the exact knowledge of the structure parameters, meaning that the procedure can be largely simplified. In addition, it enables the verification of structural properties such as controllability and observability with the reduced knowledge of the structure compared to standard approaches. Such generic conditions complement specific examples available in the literature and provide guidelines for DSS implementation in vibration problems. Another issue tackled in this thesis is the hybrid testing of the marginally stable structures. Previous research neglected this kind of structures or designed controllers that are only valid for specific models, which severely limits their application. This thesis highlights a systematic flaw of the traditional displacements error based feedback control, which makes it difficult to achieve synchronisation and prevent drifts of marginally stable structures. In order to overcome such issues, a novel control architecture is proposed based on the error between velocities instead of the displacements. This method can prevent instability and potential drifts during hybrid testing of marginally stable structures. The benefit also includes the expansion of the applications of DSS to other types of structures.

Acknowledgements

I would like to express all my gratitude to my supervisor Dr Paolo Paoletti for his academic supports, kindness, patience and guidance throughout my PhD study. I also would like to express my gratitude to Jack Carter-Hallam, his help kept me on track of my PhD project when unprecedented incidents occurred to me. Special thanks to my family and friends for their love and invaluable encouragement.

Contents

List of Publications

Journal articles:

A. Hu and P. Paoletti, A novel control architecture for marginally stable dynamically substructured systems, *Mechanical Systems and Signal Processing*, vol. 143, p. 106834, 2020.

A. Hu and P. Paoletti, On the feasibility of dynamic substructuring for hybrid testing of vibrating structures, *Journal of Sound and Vibration*. (Under Review)

List of Figures

List of Tables

Notation

$b_{1(j)}$

j-th implicit term of coefficients of Den_{n-i} when analysing controllability and observability

$b_{2(j)}$

j-th implicit term of coefficients of Den_{n-i+1} when analysing controllability and observability

c_i

damping coefficient of i-th damper in the generic vibrating mass chain system

d

disturbance acting on the system

Den_i

denominator of i-th mass in the generic vibrating mass chain system when input is y_{i-1}

Den_{1i}

denominator of i-th mass in the generic vibrating mass chain system when input is F

Den_d

generic denominator in substructure A for type 1 and type 2 decomposition as input is d

Den_{F_p}

generic denominator in substructure A for type 1 decomposition as input is F_p

Den_{2F_p}

generic denominator in substructure B for type 2 decomposition as input is F_p

Den_{y_l}

generic denominator in substructure B for type 1 decomposition as input is y_l

$Den_{y_{l+1}}$

generic denominator in substructure A for type 2 decomposition as input is y_{l+1}

e

error between physical and numerical signals

F

applied force to the generic vibrating mass chain system

F_n

numerical force

F_p

force of DSS actuator (physical force)

k_i

stiffness of i-th spring in the generic vibrating mass chain system

$K_{1(n-j+1)}$

simplified $n-j+1$-th explicit term of coefficients of Den_{n-i} when analysing controllability and observability

$K_{2(n-j+1)}$

simplified $n-j+1$-th explicit term of coefficients of Den_{n-i+1} when analysing controllability and observability

l

location of DSS interface

m_i

i-th mass in the generic vibrating mass chain system

n

number of masses

Num_i^d

i-th generic numerator in substructure A for type 1 and type 2 decomposition as input is d

$Num_i^{F_p}$

i-th generic numerator in substructure A for type 1 decomposition as input is F_p

$Num_j^{F_p}$

j-th generic numerator in substructure B for type 2 decomposition as input is F_p

$Num_j^{y_l}$

j-th generic numerator in substructure B for type 1 decomposition as input is y_l

$Num_i^{y_{l+1}}$

i-th generic numerator in substructure A for type 2 decomposition as input is y_{l+1}

$\angle P(s)$

degree of polynomial $P(s)$

$\lfloor P(s) \rfloor$

maximum degree of polynomial $P(s)$

r_i

implicit term when analysing stability

U

voltage of DSS actuator

w

objective signal in H_∞ control

y_i

displacement of i-th mass in the generic vibrating mass chain system

y_i^n

numerical displacement of i-th mass in decomposed substructures

y_i^p

physical displacement of i-th mass in decomposed substructures

$\dot{y}_i$

velocity of i-th mass in the generic vibrating mass chain system

Chapter 1

Introduction

At present, the most common structure testing methods for vibrating structures include physical tests (experiments) and numerical simulations. Physical tests have obvious advantages, including the reflection of reality, as they are able to capture uncertainties and disturbances, thus providing realistic results. However, they are time consuming for setting up and post processing, and usually expensive as well. Numerical simulations are economic and simpler to run compared with physical tests, but they cannot fully reflect the reality under all circumstances. Moreover, simulating complex structures is still time consuming. In order to avoid these disadvantages and combine advantages of both techniques, hybrid testing is proposed. The basic idea of hybrid testing is to implement some parts of the structure under test via numerical simulations, while the rest of the structure is physically tested. Synchronisation between the two parts is then required to make the hybrid tested structure behave as the original structure. Dynamically substructured systems (DSS) belong to the class of hybrid testing techniques [1]. Extra actuators are used to simulate the response at the interface and the actuator dynamics should be controlled to achieve the required synchronisation. Current challenges include dealing with the actuator delays

that can lead to system instability and with the uncertainty that may affect the accuracy of testing results [2]. Other open challenges include the limited focus of research that on specific structures, as well as no general solution for marginally stable DSS. All of them will be discussed below.

The current research about DSS mainly focuses on specific structures, for which decompositions and control strategies are designed on a case-by-case basis, and generic structures are neglected, which leads to inevitable limitations of DSS applications. This thesis is mainly aimed at filling this gap by developing analyses that are valid for a whole class of vibrating structures. A benchmark structure is selected to show the proposed procedures first, but the results are generic and it will be shown that they hold for more complex structures as well. The main contribution includes establishing generic procedures for feasibility analysis of DSS, which is aimed to show whether a desired physical decompositions can be implemented and what controller design is required, as well as providing a novel control architecture of DSS with marginally stable generic substructures. The feasibility analysis is composed of series of steps, including the analysis of causality, controllability and observability. At present, the feasibility analysis of generic vibrating problems is missing. Most of the available literature has been focused on simple benchmark systems or specific examples, with only limited exceptions such as [3] where the effect of the interface location on DSS performance was studied for generic two degree-of-freedom systems. Li [4] performed causality analysis in DSS, but only limited to specific models as well. As for the controllability and observability of generic vibration problems, general results are missing as well. In this thesis, a frequency domain approach is proposed based on a novel recursive form of the transfer functions involved in DSS design, which avoids obtaining the fully explicit symbolic expression of such transfer functions, as numerators and denominators of the transfer functions are not described by detailed polynomials, the recursive form of numerators and

denominators is used instead. This formulation allows to assess if DSS controllers can be designed for a *generic* lumped parameter vibration system without the exact knowledge of the structure parameters, which is aimed to describe systems by obtaining their generic properties, thus significantly simplifying the whole procedure. In addition, knowledge of a reduced set of system parameters is only required for the verification of system controllability and observability. Conditions of controllability and observability satisfaction are analytic and explicit, at odd with the most commonly used purely numeric matrix rank calculation. In addition, a novel control architecture is proposed to solve the issue of DSS with marginally stable substructures. In fact, previous research only focused on specific models and structures, which severely limits wider applications of DSS to other classes of structures, and control algorithms were based on the minimisation of displacement error. However, as highlighted in this thesis, displacement error control has an intrinsic issue that makes it difficult to achieve synchronisation and to prevent drifts when the external excitation is applied. This, in turn, requires the accurate tuning of the controller to achieve the synchronisation. A novel control architecture is proposed to provide a comprehensive solution to DSS testing of structures with marginally stable substructures, successfully avoiding issues of synchronisation and drifts by using the error between velocities and adding an extra controller. This is a breakthrough for this type of problems, as the current literature only focuses on specific models and no general solutions are provided. This architecture is also suitable for all DSS testing with marginally stable structures, including mass split decompositions. Therefore, it largely broadens the application of DSS without the limitations of previous approaches.

1.1 Aim and Objectives

The main aim of this thesis is to provide generic procedures for feasibility analysis for generic vibrating structures, which is missing in the current literature. Another goal is the solution of synchronisation issue when DSS or hybrid testing includes marginally stable substructures. In order to fulfil such goals, the following objectives are met:

- Propose a novel recursive form of the transfer functions that can avoid obtaining fully explicit expressions to describe the system dynamics in the frequency domain.
- Analyse causality, controllability and observability of DSS decomposition strategies to provide generic procedures of feasibility of hybrid testing of generic vibrating structures.
- Propose a novel control architecture to solve the synchronisation issue when DSS or hybrid testing includes marginally stable substructures.

1.2 Contributions and Novelty

The main contributions of this thesis include:

- The novel recursive form of the transfer functions is used to describe the dynamics of structures tested via DSS. The recursion can be used to avoid the calculation of the detailed transfer functions, which significantly reduces the calculation difficulty, especially for the complex structures. This form is suitable for different types of structures, therefore it is helpful to obtain the transfer functions of similar structures with different degrees of freedom, thus overcoming the drawback of traditional approaches by avoiding using the detailed system parameters and the degrees of freedom.

- The conditions of the controllability and observability are made analytically explicit by using the novel recursive form of the transfer functions, compared with the most commonly used matrix based approaches. In addition, the causality analysis can avoid using system parameters, which significantly simplifies the procedure, as the analysis can be used for the controller design after the decomposition.

- The novel control architecture for the marginally stable DSS is proposed, which solves a challenging problem by significantly reducing the difficulty of synchronisation between the numerical substructure and the physical substructure. The available literature either uses accurate tuning to achieve the synchronisation via complex algorithms, or modifications to the original structure to avoid making one substructure marginally stable after the decomposition.

- More potential scenarios of applications can be achieved with the help of the proposed novel control architecture when the marginally stable substructure is included. One direction of applications is to reduce the degrees of freedom in the physical substructure, which can simplify the experimental apparatus while the numerical substructure is marginally stable. This aspect is scarcely considered in the literature and in Chapter 6 a concept is proposed to show a potential application with strong novelty.

1.3 Thesis Structure

This thesis is organised as follows

- Chapter 2 reviews the current literature, with the aim of introducing DSS and other types of real time hybrid simulation(RTHS), as well as of introducing background knowledge which will be used for the following analyses.

- Chapter 3 describes the original benchmark lumped structure which will be used for decomposition. Structrual properties of the original structure such as causality, controllability, observability and stability are analysed as well. Such properties will also be used for the generic feasibility analysis of DSS.

- Chapter 4 carries out a comprehensive analysis of DSS decompositions, aimed at providing generic procedures for feasibility analysis for generic vibration problems.

- Chapter 5 introduces a novel control architecture for the mass split decomposition, which is suitable for all of DSS with marginally stable substructures.

- Chapter 6 proposes the concept of a beam split structure, which is aimed to prove that the novel architecture proposed in Chapter 5 is helpful to broaden the application of DSS to a larger class of structures.

- Chapter 7 contains some conclusions and suggestions for future work.

Chapter 2

Literature Review

This chapter reviews the current literature to provide a brief introduction to hybrid testing and dynamically substructured systems, as well as their applications. In addition, the background knowledge about control concepts used in the rest of this thesis is introduced. In the last section of this chapter, the gaps in the current research are summarised in order to motivate the research direction of this thesis.

2.1 Hybrid Testing and Relative Applications

Challenges and costs of testing large complex structures by experiments are not negligible at present. To alleviate this problem, several techniques have been proposed in the literature to replace part of the structure by a numerical simulator and then designing a control system so that the combination of numerical and physical subsystems behaves in the same way of the original structure. These techniques are known as hybrid testing. Most of them are classified as real time hybrid simulation (RTHS) or real time hybrid testing (RTHT). Generally speaking, the principle is that some parts of structures will be tested numerically while the rest will be physically tested with the help of extra hardwares such as actuators

and computers. Silva provided comprehensive guidance for the applications of RTHS [5]. Currently the potential defects of such techniques include the delay of the actuator and the system robustness [6, 7]. The actuator delay and the system robustness can lead to the instability of whole system. A number of researches have focused on these issues. Some approaches use robust control technique to compensate the actuator delay and to ensure the whole system is robust [8, 9]. Other methods include the adaptive control technique [10, 11], which is aimed to reduce the modelling difficulty and to adapt to different input in a certain range. Saturation control technique [12, 13] is also used to avoid the potential occurrence of system instability, when the maximum power input of the actuator is considered. In addition, control techniques based on structural dynamics [14, 15] are also proposed to better reflect the dynamics of structure. Furthermore, the inverse compensation is applied as the basic principle to measure the delay in an experiment and then control laws are implemented for its compensation in single degree of freedom [16, 17] and multiple degree of freedom (MDOF) systems [18]. Predictive methods have been proposed to avoid the instability caused by delay [19], as the delay is compensated by predicting the future motion. The Model based control strategy for RTHS provided comprehensive guidance for the applications of RTHS [20], where the models are expressed in the framework of structural dynamics. One of the most commonly used applications for these techniques are related to the verification of the design of large-scale structures, which is helpful to reduce the costs, as well as the time required in the design stage. For example, Christenson [21] used RTHS to verify the semi-active control effect of Magneto-rheological (MR) damper in the building, and the physical structure does not include any components of the original frames. Zhang [22] optimised control effect of MR damper using real time optimisation framework and Shan [23] applied an adaptive algorithm to control MR damper. Moreover, Asai [24] designed a smart base-isolated building, with the help of RTHS. Shaking tables

and actuators were used in order to better simulate large structures as well [25, 26]. In addition, the research also expanded into the identification of system parameters, where the response signals estimate the parameters with the help of RTHS, see for example [27]. Furthermore, Ou [28] explored the possibility of using online updating of the numerical model parameters, so that this technique can be applied to make RTHS more flexible. Another important application is to reduce the damage of earthquake with the help of RTHS. The control strategy is proposed for the semi-active control using MR damper in order to expand the application of semi-active control to RTHS [29]. Kim [30] combined RTHS and the semi active control of MR damper to reduce the damage of earthquake. Mahmoud [31] discovered the damage of the structure with the semirigid partial-strength steel frames during the earthquake with the help of RTHS, as the investigation has been applied to the damage of structures with MR damper subjected to seismic loading [32, 33]. Another important application includes the prediction of hydraulics capacity when drilling [34]. Bonnet [35] and Botelho [36] implemented the multiple decomposition for the test structure, meaning only some substructures need to be physically tested. When assessing performance, the mainstream performance index is the standard deviation of relative error [37, 38]. The comprehensive development overview of RTHS can be seen in [39].

2.2 Introduction to Dynamically Substructured Systems

Dynamically Substructured Systems (DSS) are part of the family of hybrid testing techniques. Hakuno [40] applied DSS to test a cantilever beam with the help of an analog computer, which was a typical example of DSS applications at the early stage. Other contributions at the early stage include the simplified control algorithm proposed by Leung [41], Hale [42] applying DSS to complex structures and Nakashima [43] developing DSS including the introduction of digital servo-mechanism in the hardware and the introduction

of direct force measurement. In the DSS framework, the original structure is decomposed into two main substructures, the physical substructure and the numerical substructure, as shown in figure 2.1. The numerical substructure simulates a subsystem of the original structure. On the other hand, the physical substructure consists of a physical structure and of an actuator which is used to simulate the presence of the subsystem that has been replaced by the numerical substructure. The challenge is then to control the actuator so that the overall DSS behaves as the original structure [44, 45].

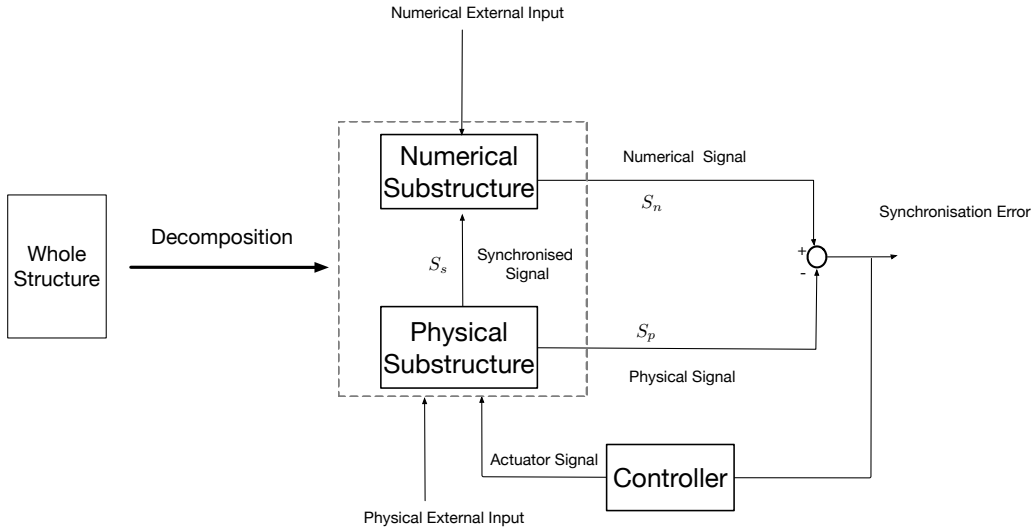

Figure 2.1: Typical dynamic substructuring layout in the time domain

DSS is a method to achieve the physical test and the numerical test at the same time by replacing part of a structure with a numerical simulation. Therefore, the cost of testing can be significantly reduced. The difference between the dynamical behaviour of the original and the substructured structures should be minimised. At present there are two main approaches to solve such challenge: force control and displacement control. The force control is aimed at minimising the error between the physical force and the numerical force, while the displacement control minimises the error between the physical displacement and

the numerical displacement. In the force control setting, the displacement of the physical substructure at the interface is measured and transmitted as an input to the numerical substructure (indicated by *synchronised signal* S_s in figure 2.1). The simulator used in the numerical substructure then calculates the force at the interface (*numerical signal* S_n) which is compared with the force generated by the actuator situated at the corresponding interface in the physical substructure (*physical signal* S_p). A feedback controller is then designed to minimise the *synchronisation error* e between the simulated force and the actuator force, so that the interface becomes transparent and the DSS behaves as the original system. In the displacement control setting, the role of force and displacement is swapped, except for the mass split decomposition that will be shown in Chapter 5. The presence of delays, disturbances and model uncertainties prevents exact cancellation of the error between numerical and physical signals, therefore feedback control is needed to control the actuator in order to minimise the synchronisation error. Model-in-the-loop (MIL) and hardware-in-the-loop (HIL) have some similarities to DSS, such as the actual hardwares in the testing loop [46, 47]. However, MIL and HIL are mainly used for verifying the subsystems for various types of systems ranging from mechanical systems and electronic systems [48, 49], rather than achieving the synchronisation between the numerical substructure and the physical substructure as in DSS.

2.3 Applications of DSS

Various control techniques have been successfully used to test dynamical systems in different domains. For example, in the railway industry Stoten and colleagues have tested a pantograph using a DSS approach where only the pantograph is physical, whereas the electric cable is simulated [50, 51]. The benefit is that it can largely simplify the mechanism simulating the movement of electric cable when the cable touches the pantograph.

Similarly, models of motorcycles have been tested using DSS techniques, see for example [52] and [44]. In addition, Wallace [53], Neild [54], Bursi [55], Tu [56] and Terkovics [3] discussed the effect of decomposition on marginally stable structures, as the key is to find the stable region and then different algorithms are used to accurately tune the actuators for the purpose of eliminating the error between the displacements in the marginally stable substructure and the stable substructure. The focus was on the actuator compensation delay which can lead to system instability, and the controller was designed to eliminate the error and compensate the delay. However, the main limitation of such methods that they require much information about the structure and a detailed analysis to ensure the effectiveness of DSS substructuring. In addition, accurate tuning is required to achieve the best performance of controller, otherwise the effect can be really limited, which lead to significant limitations in real applications. In order to avoid such issue in the analysis, some researchers changed the original test structure to ensure stability after decomposition. For example, an extra spring and damper in the original system were added in [7] to let all substructures be stable after the decomposition. In addition, the similar substructuring techniques have also been recently proposed to understand vibration and uncertainty propagation in complex structures in presence of limited knowledge about the structures themselves [57]. Other applications include the use of sliding mode control in DSS [58], the use of neural network control in DSS [59], the application to rotational structures in order to simulate the helicopter rotor blade [60] and DSS application to analyse the soil-structure interaction [61]. Nonlinear structures have also been analysed using the integration method [62], as a similar research being carried out to design protective devices for bridge structures [63] and flexible frames [64]. Applications also include the mechanics analyses of artificial disc in the biomechanics of the implanted and adjacent spinal segments [65] and the modelling of flexible structures [66]. Control of multiple actuators was also implemented using

polynomial fitting [67]. Like in RTHS, the effect of actuator delay has also been researched quite extensively [68, 69], as well as in the nonlinear system [70]. The performance assessment of the most representative underdamped system was also carried out in [71]. In the automotive industry, DSS is also helpful to measure the performance at the development stage [72], as well as for the development of rail vehicles [73, 74]. In addition, the application includes the identification of parametric variation in vibrating structures [75] and the test of complex structures using shaking tables.

Another application of dynamic substructuring is on the evaluation of frequency response, instead of the time domain response. A comprehensive review of dynamic substructuring techniques can be found in [45]. In this case the aim is to find out the characteristics of frequency response function (FRF) on substructures and components. Hong used dynamic substructuring to analyse the characterisation of rail track in order to avoid serious accidents [76]. The rail track can be tested from different layers and with the help of dynamic substructuring the analysis of frequency response of coupled track structures can be performed more clearly, which is helpful to avoid the difficulty of finding out the cause of cracks and defects. Allen used dynamic substructuring to aid the design of NASA rocket launcher [77]. The whole structure consisted of the rocket and its launcher. The interface was the touch plane between rocket and launcher and it is fixed, compared with the flexible interface in reality. The purpose was to measure the mode shapes of the whole structures. With the help of numerical simulation combined with actual measurement of natural frequencies the mode shapes were close to the results obtained by finite element method (FEM), but the analysis was more effective and efficient. Mayes developed the applications of dynamic substructuring to find out the frequency response of the transmission structures, instead of using FEM. This approach is helpful for experiments on rotational structures such as wind turbines [78, 79]. Model reduction is also used for complex struc-

tures in order to simplify the testing procedure [80], as well as for reducing the calculation cost for the continuous structure [81]. Random uncertainties in dynamic substructuring were modelled with the nonparametric approach in [82]. Inverse dynamic substructuring is also used when the substructure is difficult to be tested, as the method is based on the hybrid assembly in the frequency domain [83, 84], and has been used to predict the dynamics of mobile machine tool [85]. The effect of damping of the interface was also considered in [86]. In addition, DSS can be applied to vehicle development, see for example [87] where the authors proposed a DSS framework for a variety of experiments on vehicle structures. This series of analyses and experiments include noise measurement, frequency response of decoupled structures etc. It was shown that DSS helps to improve the level of noise, vibration and harshness (NVH), as well as the structure design. A comprehensive analysis on the gear noise propagation in the automotive was carried out in [88] and the crankshaft was also optimised to improve the ride comfort in [89]. In addition, uncertainty propagation has also been considered in FRF analysis [90, 91, 92].

2.4 Structural Properties of Dynamical Systems

This section is the brief introduction of the background knowledge about structural properties of dynamical syatems, which will be used in the following chapters to perform the relevant analyses.

2.4.1 Causality

A dynamical system called causal when the system outputs only depend on the current and previous value of inputs and not on the future inputs [93]. From a physical prospective, a causal system means that the system is implementable.

Mathematically, a transfer function of the impulse response of a causal system has a region

of convergence (ROC) lying on the right hand side (RHS) of the complex plane. Here, ROC is defined as the range of variation of σ such that

$$\int_0^\infty |h(t)|e^{-\sigma t}dt \leq \infty \tag{2.1}$$

where $h(t)$ is the impulse response of the system under study.

The Laplace transform of $h(t)$ is defined as

$$H(s) = \int_0^\infty h(t)e^{-st}dt \tag{2.2}$$

and $H(s)$ can be rearranged as

$$H(s) = \frac{a_n s^n + a_{n-1}s^{n-1} + \cdots + a_0}{b_m s^m + b_{n-1}s^{m-1} + \cdots + b_0} = \frac{(s+z_n)\ldots(s+z_i)\ldots(s+z_0)}{(s+p_m)\ldots(s+p_i)\ldots(s+p_0)} \tag{2.3}$$

where $-z_i$ are zeros and $-p_i$ are poles.

Let us then assume that $-p_j$ is the rightmost pole. Then ROC can be represented by

$$\sigma = Re[s] > Re[-p_j] \tag{2.4}$$

Most of the transfer functions describing mechanical systems are rational except infinite dimensional systems [94] and systems with time delay [95], and for a rational transfer function of mechanical system ROC is on the real part of the rightmost poles. The degree of numerator and denominator of the rational transfer function should be also checked to assess causality. If the degree of the numerator is less than the degree of the denominator the system is strictly proper, or the degree of numerator is equal to the degree of denominator the system is bi-proper [96]. Bi-proper systems are causal and proper systems are strictly

causal (outputs only depend on past inputs). Therefore, causality verification of DSS can be converted to the testing of relative degrees of the relevant transfer functions. This is the approach used in the rest of the thesis to assess if a given strategy is feasible.

If any of the signal used a DSS decomposition is non causal with respect to some of the inputs, then such decomposition can not be physically implemented and should be discarded. However, an alternative decomposition of the same original structure may involve only causal signals. Therefore, the first step of the approach proposed in this thesis is aimed at obtaining conditions for which a given DSS decomposition involves only causal signals and can be physically implemented. An example of such analysis has been performed by Li [4] and Gawthrop [97], but only for a specific dynamical system.

2.4.2 Controllability and Observability

Once all the signals required for DSS decomposition have been proven to be causal, the next step is to check if the dynamical system under control has the structural properties of *controllability* and *observability*. A system is called *controllable* if an external input can move the internal states of the system from any initial state to any other final state in a finite time interval. Similarly, a system is *observable* if its initial state can be determined based on the sequence of inputs and output signals [98]. Such structural properties are sufficient conditions to ensure that a stabilising controller can be designed. Note that observability and controllability are not necessary conditions. In fact, a stabilising controller can still be designed in presence of unobservable/uncontrollable states as long as these latter are stable. However, such weaker conditions can only be studied on a case by case basis, therefore they are not useful to develop the generic framework considered in this thesis.

A traditional result of control theory states that a linear dynamical system is controllable and observable if there are no pole-zero cancellations between the numerator and the

denominator of the transfer function describing the system behaviour [99]. Such analytical test will then be applied in Chapter 4 to obtain conditions under which a given DSS decomposition is feasible and can be implemented.

2.4.3 System Stability

The system stability is the important part for the control design. Consider a linear time invariant (LTI) system with natural response $x(t)$. If

$$\lim_{t\to\infty} x(t) = 0 \tag{2.5}$$

then the system is stable, if

$$\lim_{t\to\infty} x(t) = x(\infty) \neq 0 \tag{2.6}$$

the system is marginally stable, and if

$$\lim_{t\to\infty} |x(t)| = \infty \tag{2.7}$$

the system is unstable.

Stability can be studied in the frequency domain by looking at the position of poles in transfer functions. If any of $-p_i$ in Equation (2.3) are located on the right half of complex plane, the system is unstable. If all of $-p_i$ are located on the left half of complex plane, the system is stable. If any of $-p_i$ are located in the imaginary axis and the rest of $-p_i$ are not located on the right hand side then the system is marginally stable [100]. In this thesis systems with repeated poles at the origin are defined as marginally stable system. Therefore, stability analysis of DSS decomposition strategies will be performed by analysing the location of the poles of the transfer functions involved in such decomposition.

2.5 Control Techniques and DSS Control Design

2.5.1 General Framework of Combined Feedforward-Feedback Control Techniques

After the verification of the structural properties of a given decomposition, control techniques will be used to eliminate the error between the numerical and physical substructure. Stoten, Hyde [101] and Tu [44] analysed DSS based on some existing models such as the half model of motorcycle and its full model, and then the physical substructure and the numerical substructure were selected after the decomposition. Klerk [45] analysed the conditions for decomposition of a broad range of dynamical substructing and Stoten applied it to DSS. Therefore, the general framework shown in Figure 2.2 was proposed in order to achieve the applications of control techniques to DSS.

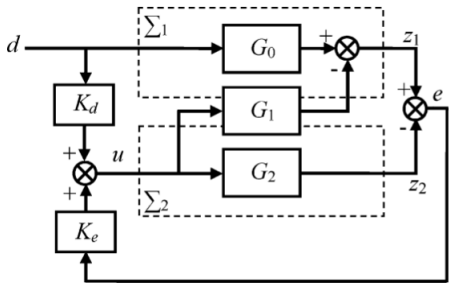

Figure 2.2: General framework of DSS, taken from [101]

This general framework is based on the single input and single output (SISO) system and can be applied to multiple input and multiple output (MIMO) system by adding additional control gains. System $\sum_1$ and system $\sum_2$ are included after the decomposition. System $\sum_1$ and system $\sum_2$ can either be the physical system or the numerical system. In the physical substructure, the physical signal is entirely or partly excited by the actuator.

In this framework, $\boldsymbol{d}$ is a disturbance applied to the system and z_1, z_2 can either be the numerical or the physical signals, meaning the error between them should be minimised. Input u is signal of the actuator, which typically is the voltage or the current of an electric actuator. The response of the system shown in Figure 2.2 can be described in the frequency domain as

- System $\sum_1$:

$$z_1(s) = \boldsymbol{G}_0(s)\boldsymbol{d}(s) - \boldsymbol{G}_1(s)u(s) \tag{2.8}$$

- System $\sum_2$:

$$z_2(s) = \boldsymbol{G}_2(s)u(s) \tag{2.9}$$

- Error:

$$e = z_1 - z_2 = \boldsymbol{G}_0(s)\boldsymbol{d}(s) - [\boldsymbol{G}_1(s) + \boldsymbol{G}_2(s)]u(s) \tag{2.10}$$

  where G_0, G_1 G_2 are the transfer functions for two systems, $\boldsymbol{K}_d$ is the feedforward control gain relating to the disturbance d and $\boldsymbol{K}_e$ is the feedback control gain relating to the error e.

Typical linear hybrid controller (feedforward plus feedback) design techniques used for eliminating the synchronisation error in DSS applications include linear substructing control (LSC) and minimal control with error feedback (MCEF)[102]. In this thesis LSC will be described in the next subsection.

Linear Substructuring Controller (LSC)

Typically, the control technique used for driving the actuator is based on the linear feedforward plus feedback system. Linear Substructuring Controller (LSC) was developed by

Stoten in [101]. Nonlinear substructructuring controller (NLSC) was also developed from LSC [103]. LSC is based on the general framework introduced above and the controller has the form

$$u(s) = \boldsymbol{K}_d(s)\boldsymbol{d}(s) + \boldsymbol{K}_e(s)e(s) \tag{2.11}$$

By plugging (2.11) into (2.10), one obtains

$$\begin{aligned} e(s) &= \boldsymbol{G}_0(s)d(s) - [\boldsymbol{G}_1(s) + \boldsymbol{G}_2(s)]u(s) \\ &= \boldsymbol{G}_d(s)d(s) - \boldsymbol{G}_u(s)u(s) \\ &= [\boldsymbol{I} + \boldsymbol{G}_u(s)\boldsymbol{K}_e(s)]^{-1}[\boldsymbol{G}_d(s) - \boldsymbol{G}_u(s)\boldsymbol{K}_d(s)]d(s) \end{aligned} \tag{2.12}$$

Given that the control goal is ensuring $e \to 0$, the control gain $\boldsymbol{K}_d$ is set to

$$\boldsymbol{K}_d(s) = \frac{\boldsymbol{G}_d(s)}{\boldsymbol{G}_u(s)} \tag{2.13}$$

if $\boldsymbol{G}_u$ is a non-minimum phase and non-singular. Which means, parameter variations in $\sum_1$ may be unstable due to the inverted dynamics, as seen from the open-loop solution of Equation (2.13). Therefore, closed-loop stability and robustness must be guaranteed via appropriate synthesis of $\boldsymbol{K}_e$ to obtain desirable roots of the multiple inputs multiple outputs (MIMO) closed-loop characteristic equation

$$\boldsymbol{I} + \boldsymbol{G}_u(s)\boldsymbol{K}_e(s) = 0 \tag{2.14}$$

There are many methods to solve $\boldsymbol{K}_e$ in the above equation. For the simplicity, root locus based synthesis is commonly used in LSC design, and will be the main approach used for the examples in Chapter 5.

Minimal Control with Error Feedback (MCEF)

Minimal Control with Error Feedback (MCEF) is an adaptive controller proposed in [102]. The mathematical description of the controller is listed as follows

$$u(t) = \boldsymbol{K}_d d(t) + \boldsymbol{K}_e e(t) \tag{2.15}$$

where

$$\boldsymbol{K}_d = \alpha \int_0^t y_e(t) d(t) dt + \beta y_e(t) d(t) \tag{2.16}$$

$$\boldsymbol{K}_e = \alpha \int_0^t y_e(t) e(t) dt + \beta y_e(t) e(t) \tag{2.17}$$

$\boldsymbol{K}_d$ and $\boldsymbol{K}_e$ are adaptive gains, with α and β being adaptive weights and $y_e(t)$ being proportional to the error $e(t)$. Adaptive control it will not be used in this thesis as the focus is on the feasibility of control design, rather than optimisation of performance.

2.5.2 H_2 and H_∞ Controller

Feedback controllers are commonly used and can also be used to synchronise numerical and physical signals in the DSS framework. A typical feedback control block diagram for DSS is shown in Figure 2.3, where $P(s)$ is the control plant and $K(s)$ is the feedback controller that is used to drive the actuator in the physical substructure of DSS. In order to compensate for unknown disturbances, H_2 control has been used in [104] and H_∞ control has been used in [105].

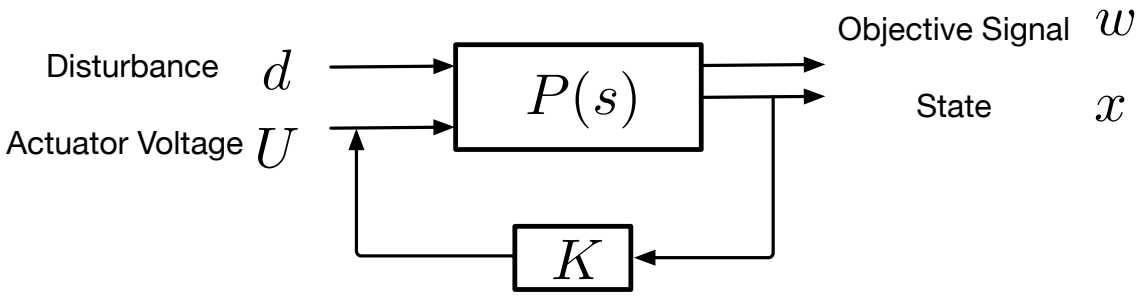

Figure 2.3: General feedback control block diagram

Briefly, the H_∞ controller design process can be summarised as follows. Let us consider the state space form of control plant $\boldsymbol{P}(s)$

$$\begin{cases} \dot{x} = Ax + B_{11}\boldsymbol{d} + B_{12}\boldsymbol{U} \\ w = C_1 x + D_{11}\boldsymbol{d} + D_{12}\boldsymbol{U} \end{cases} \tag{2.18}$$

where $\boldsymbol{d}$ is the disturbance and w is the objective signal that should be minimised in DSS, for example, the synchronisation error $e(t)$. $\boldsymbol{U}$ is the voltage of actuator and w represents the measurable output states.

Then the state feedback of controller $\boldsymbol{K}$ can be written as

$$\boldsymbol{U} = \boldsymbol{K}x \tag{2.19}$$

Therefore, the state space form of the closed loop $\boldsymbol{G}(s)$ can be summarised as

$$\begin{cases} \dot{x}_{cl} = A_{cl}x_{cl} + B_{cl}\boldsymbol{d} \\ w = C_{cl}x_{cl} + D_{cl}\boldsymbol{d} \end{cases} \tag{2.20}$$

where

$$\begin{cases} x_{cl} = x \\ A_{cl} = A + B_{12}\boldsymbol{K} \\ B_{cl} = B_{11} \\ C_{cl} = C_1 + D_{12}\boldsymbol{K} \\ D_{cl} = D_{11} \end{cases} \tag{2.21}$$

The goal of a H_2 controller is to minimise the gain between the H_2 norm of $\boldsymbol{d}$ and the H_2 norm of w, i.e.

$$\|G\|_2 = \frac{\|w\|_2}{\|\boldsymbol{d}\|_2} < \gamma \tag{2.22}$$

where γ is the target performance index which is set in order to reduce the effect of the disturbance $\boldsymbol{d}$ on the output w. In Equation (2.22) the H_2 norm is defined as

$$\|w\|_2 = \left(\int_0^\infty \|w\|^2 dt \right)^{1/2} \tag{2.23}$$

Then the controller $\boldsymbol{K}$ and performance index γ can be obtained by using the linear matrix inequalities (LMI) or Riccati equations [106]. The details of LMI based procedure is described below, as this is the approach used for the mechanical examples in Chapter 4. For the case with state feedback controller, Equation (2.24) can be solved by following the procedure below.

Let us assume that there exist three matrices $\boldsymbol{Z}$, $\boldsymbol{R}$ and $\boldsymbol{X}$ such that

$$\operatorname{tr} \boldsymbol{Z} < \gamma^2$$

$$\begin{bmatrix} \boldsymbol{Z} & \boldsymbol{C}_1\boldsymbol{X} + \boldsymbol{D}_{12}\boldsymbol{R} \\ (\boldsymbol{C}_1\boldsymbol{X} + \boldsymbol{D}_{12}\boldsymbol{R})^T & \boldsymbol{X} \end{bmatrix} > 0 \tag{2.24}$$

$$\boldsymbol{A}\boldsymbol{X} + \boldsymbol{X}\boldsymbol{A}^T + \boldsymbol{B}_{12}\boldsymbol{R} + (\boldsymbol{B}_{12}\boldsymbol{R})^T + \boldsymbol{B}_{11}\boldsymbol{B}_{11}^T < 0$$

Such LMI can be solved for any value of γ in MATLAB by using the relative toolbox, for example, by using the function $h2syns$.
The H_2 controller gain $\boldsymbol{K}$ can then be obtained as

$$\boldsymbol{K} = \boldsymbol{R}\boldsymbol{X}^{-1} \tag{2.25}$$

The goal of a H_∞ controller is to minimise the gain between the ℓ_2 norm of $\boldsymbol{d}$ and the ℓ_2 norm of w.

$$\|G\|_\infty = \sup |G(s)| = \sup \left\{ \frac{\|w\|_2}{\|\boldsymbol{d}\|_2} \right\} < \gamma \tag{2.26}$$

where γ is the performance index which is set in order to reduce the effect of disturbance on the output w.

Then the controller $\boldsymbol{K}$ and performance index γ can be obtained by using the linear matrix inequalities(LMI) or Riccati equations [107]. The details of LMI based procedure are briefly described below
H_∞ control synthesis can be converted to the LMI optimisation problem

$$\boldsymbol{min}(\gamma)$$

$$\begin{bmatrix} \boldsymbol{A}_{cl}\boldsymbol{X}_{cl} + (\boldsymbol{A}_{cl}\boldsymbol{X}_{cl})^T & \boldsymbol{B}_{cl} & (\boldsymbol{C}_{cl}\boldsymbol{X}_{cl})^T \\ \boldsymbol{B}_{cl}^T & -\boldsymbol{I} & \boldsymbol{D}_{cl}^T \\ \boldsymbol{C}_{cl}\boldsymbol{X}_{cl} & \boldsymbol{D}_{cl} & -\gamma^2\boldsymbol{I} \end{bmatrix} < 0 \tag{2.27}$$

$$\boldsymbol{X}_{cl} > 0$$

where $\boldsymbol{X}_{cl}$ is the unknown variable.

For the system with state feedback controller, Equation (2.27) can be solved by calculating the following inequality

$$\begin{bmatrix} \boldsymbol{A}\boldsymbol{X}^* + \boldsymbol{B}_{12}\boldsymbol{U}_1 + (\boldsymbol{A}\boldsymbol{X}^* + \boldsymbol{B}_{12}\boldsymbol{U}_1)^T & \boldsymbol{B}_{11} & (\boldsymbol{C}_1\boldsymbol{X}^* + \boldsymbol{D}_{12}\boldsymbol{U}_1)^T \\ \boldsymbol{B}_{11}^T & -\boldsymbol{I} & \boldsymbol{D}_{11}^T \\ \boldsymbol{C}_1\boldsymbol{X}^* + \boldsymbol{D}_{12}\boldsymbol{U}_1 & \boldsymbol{D}_{11} & -\gamma^2\boldsymbol{I} \end{bmatrix} < 0 \tag{2.28}$$

$$\boldsymbol{X} > 0$$

with $\boldsymbol{U}_1$ and $\boldsymbol{X}$ as unknowns. Such LMI can be solved in MATLAB by using the relative toolbox. The state feedback control gain can then be calculated as

$$\boldsymbol{K} = \boldsymbol{U}_1\boldsymbol{X}^{*-1} \tag{2.29}$$

2.6 Research Gaps

Currently most of the literature on DSS mainly focused on specific models, and a rigorous framework to study the feasibility of such hybrid testing approach for generic vibration problems is missing, as the analysis does not depend on the certain system parameters and degrees of freedom, which is beneficial for a range of structures, especially for those

with different degrees of freedom. In addition, delay is also a common issue in DSS and hybrid testing applications, however, there is no generic analytical approach to deal with it. Given the research direction of this thesis, which is aimed at establishing the generic procedures of DSS, no discussion of delay is included in this thesis. One main objective of this thesis is to fill this gap by using a novel recursive expression for transfer functions. The generic feasibility analysis of DSS will be established in Chapter 4, including the analysis of causality, controllability and observability. Such an analysis will make the conditions of generic feasibility explicit and there is no need to focus on specific models anymore, in contrast to current approaches.

Another gap in the current literature is related to robust techniques for DSS or RTHS with marginally stable substructures, with limited exceptions that only focused on specific models. In order to solve this problem, a novel control architecture will be proposed in Chapter 5 to provide a comprehensive solution of generic DSS with marginally stable substructures, with the help of novel recursive transfer functions. This solution significantly broadens the scope of structures that can be hybrid tested using DSS by allowing testing of marginally stable structures. In addition, unlike other approaches that require accurate tuning to achieve the synchronisation, this proposed solution will provide complete freedom to design the needed controllers to achieve synchronisation and no accurate tuning will be required as well.

Chapter 3

Benchmark Structure and its Structural Properties

This chapter is to introduce the generic benchmark structure and its structural properties including causality, controllability, observability and stability. Such knowledge is the preparation of the following analyses that will be used to analyse the feasibility of the decomposed structures (Chapter 4) and to reveal the difficulty of achieving the synchronisation of DSS with marginally stable substructures (Chapter 5). Such content will be in the following chapters.

3.1 Original Structure

The generic lumped parameter vibration model considered in this thesis can schematically be represented as chain of n spring-damper-mass systems as shown in Figure 3.1. This model is selected for the comprehensive guidance of generalised DSS. It is worth noting that, despite its simplicity, such representation can describe a wide range of vibration problems [3, 44, 52]. Therefore, it is still a very useful benchmark structure, as its mathematical

model will still be helpful to explore other types of structures, considering the mathematical similarities among discretely distributed structures. Results obtained for this benchmark system are easily generalisable to other complex structures, as will be shown in Chapter 4. Previously, analyses mainly focused on specific models, meaning conclusions are only suitable for particular models and no conclusions can be drawn about other structures. In order to overcome this shortfall, a generic procedure is introduced in this chapter. All of analyses are generic in the sense of not requiring detailed knowledge about the system, and the same procedures can be applied to different types of structures. Therefore it is suitable to derive general conclusions about DSS design for generic vibrating structures. Here, the disturbance $d(t)$ is applied as displacement of the support at one end of the structure, whereas an external force $F(t)$ is applied to the other end. Such force will represent, for example, the action of the actuator used in substructures. A semi-implicit form for the generalised transfer function and the degree of relative coefficients will be obtained in this chapter to analyse the aspects of feasibility such as causality, controllability and observability with minimal knowledge of system parameters, which significantly simplifies such analysis.

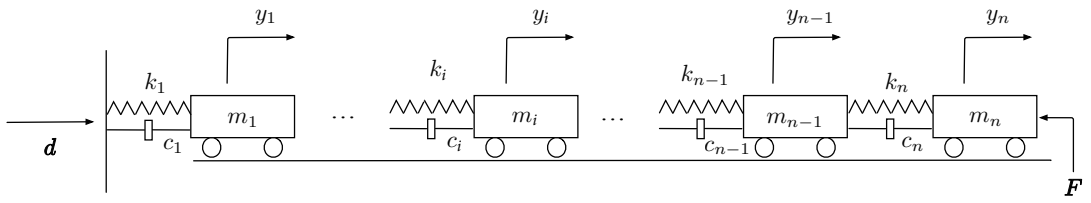

Figure 3.1: Schematics for a generic lumped parameter vibration problem.

3.2 Mathematical Description

The equations of motion describing the behaviour of the system shown in Figure 3.1 (sometimes referred to as *emulated system* in the DSS literature [44]) can be obtained by imposing force balance at each mass

$$\begin{cases} m_n\ddot{y}_n = -k_n(y_n - y_{n-1}) - c_n(\dot{y}_n - \dot{y}_{n-1}) - F \\ m_{n-1}\ddot{y}_{n-1} = -k_{n-1}(y_{n-1} - y_{n-2}) - c_{n-1}(\dot{y}_{n-1} - \dot{y}_{n-2}) + k_n(y_n - y_{n-1}) + c_n(\dot{y}_n - \dot{y}_{n-1}) \\ \qquad\qquad\qquad\qquad\qquad\qquad\qquad\qquad\qquad\qquad\qquad\qquad\qquad\qquad\qquad\qquad i = n-1 \\ \qquad\qquad\vdots \\ m_i\ddot{y}_i = -k_i(y_i - y_{i-1}) - c_i(\dot{y}_i - \dot{y}_{i-1}) + k_{i+1}(y_{i+1} - y_i) + c_{i+1}(\dot{y}_{i+1} - \dot{y}_i) \\ \qquad\qquad\qquad\qquad\qquad\qquad\qquad\qquad\qquad\qquad\qquad\qquad\qquad\qquad\qquad\qquad 2 \leq i \leq n-1 \\ m_1\ddot{y}_1 = -k_1(y_1 - d) - c_1(\dot{y}_1 - \dot{d}) + k_2(y_2 - y_1) + c_2(\dot{y}_2 - \dot{y}_1) \end{cases} \tag{3.1}$$

where m_i is the i-th mass, c_i the i-th damping coefficient, k_i is the i-th spring stiffness, y_i the displacement of the i-th mass and the dot indicates time derivative. The displacement of the support is indicated as $y_0 = d$ and is considered unknown. An equivalent expression in the frequency domain can then be written as

$$y_i(s) = \frac{Num_i(s)}{Den_i(s)} y_{i-1}(s) - \frac{Num1_i(s)}{Den1_i(s)} F(s) \tag{3.2}$$

where $Num_i(s)$ and $Den_i(s)$ represent, respectively, the numerator and the denominator of the transfer function between the position of the i-th and $(i-1)$-th masses. Similarly $Num1_i(s)$ and $Den1_i(s)$ refer to the transfer function between the position of the i-th mass and the applied force F. All of numerators and denominators will use the recursive form in order to reduce the complexity of calculations in the following.

The linearity of the system dynamics (3.1) allows studying the influence of the disturbance d and the force F independently, thanks to the superposition principle. For example, the transfer function between i-th mass displacement y_i and the disturbance d can be written as

$$\frac{y_i}{d} = \frac{y_1}{d}\frac{y_2}{y_1}\cdots\frac{y_i}{y_{i-1}} = \frac{Num_i^d}{Den_1} = \begin{cases} \dfrac{Den_{i+1}\prod_1^i (c_i s + k_i)}{Den_1} & i \leq n-1 \\ \dfrac{\prod_1^i (c_i s + k_i)}{Den_1} & i = n \end{cases} \tag{3.3}$$

where

$$Den_i = \begin{cases} m_n s^2 + c_n s + k_n & i = n \\ (m_n s^2 + c_n s + k_n)[m_{n-1} s^2 + (c_{n-1} + c_n)s + k_{n-1} + k_n]... & \\ \quad -(c_n s + k_n)^2 & i = n-1 \\ [m_i s^2 + (c_i + c_{i+1})s + k_i + k_{i+1}]Den_{i+1} - (c_i s + k_i)^2 Den_{i+2} & i \leq n-2 \end{cases} \tag{3.4}$$

A similar procedure can also be applied to derive the transfer functions between the i-th displacements y_i and the external force F, which read

$$\frac{y_i}{F} = \frac{y_n}{F}\frac{y_{n-1}}{y_n}\cdots\frac{y_i}{y_{i+1}} = -\frac{Num_i^F}{Den1_n} = \begin{cases} -\dfrac{\prod_{i=2}^n (c_i s + k_i)}{Den1_n} & i = 1 \\ -\dfrac{Den1_{i-1}\prod_{i+1}^n (c_{i+1} s + k_{i+1})}{Den1_n} & 1 < i \leq n \end{cases} \tag{3.5}$$

where

$$Den1_i = \begin{cases} m_1 s^2 + (c_1 + c_2)s + k_1 + k_2 & i = 1 \\ [m_1 s^2 + (c_1 + c_2)s + k_1 + k_2][m_2 s^2 + (c_2 + c_3)s + k_2 + k_3] & \\ \quad - (c_2 s + k_2)^2 & i = 2 \\ [m_i s^2 + (c_i + c_{i+1})s + k_i + k_{i+1}]Den1_{i-1} - (c_i s + k_i)^2 Den1_{i-2} & 2 < i \leq n-1 \\ (m_n s^2 + c_n s + k_n)Den1_{n-1} - (c_n s + k_n)^2 Den1_{n-2} & i = n \end{cases} \tag{3.6}$$

and $Den1_n$ is equal to Den_1. The degree of the numerators and the denominators is summarised in Table 3.1 for reference, based on the assumption that there are no poles and zeros cancellations. Note that observability and controllability are not necessary conditions. Such structural properties are sufficient conditions to ensure that a stabilising controller can be designed. In fact, a stabilising controller can still be designed in presence of unobservable/uncontrollable states as long as these latter are stable. However, such weaker conditions can only be studied on a case by case basis, therefore they are not useful to develop the generic framework considered in this thesis.

Table 3.1: Degrees of numerators and denominators for the transfer functions between input displacements and force.

Index i	$\angle Num_i$	$\angle Den_i$	$\angle Num1_i$	$\angle Den1_i$
n	n	2	$2n-2$	$2n$
$n-1$	$n+1$	4	$2n-3$	$2n-2$
$n-2$	$n+2$	6	$2n-4$	$2n-4$
$\vdots$	$\vdots$	$\vdots$	$\vdots$	$\vdots$
i	$2n-i$	$2n-2i+2$	$n+i-2$	$2i$
$\vdots$	$\vdots$	$\vdots$	$\vdots$	$\vdots$
1	$2n-1$	$2n$	$n-1$	2

3.3 Causality

For DSS, the first property that needs to be checked before designing any controller is *causality*. Based on the knowledge introduced in Chapter 2, if any of the signal used a DSS decomposition is non causal with respect to some of the inputs, then such decomposition can not be physically implemented and should be discarded. However, an alternative decomposition of the same original structure may involve only causal signals. Therefore, the first step of the approach proposed in this thesis is aimed at obtaining conditions for which a given DSS decomposition involves only causal signals and can be physically implemented. From Table 3.1 it can be seen that the original structure is causal, because the degree of numerators is less than the degree of denominators when the system inputs are d and F.

3.4 Controllability and Observability

A traditional result of control theory states that a linear dynamical system is controllable and observable if there are no pole-zero cancellations between the numerator and the denominator of the transfer function describing the system behaviour [99]. The proof of controllability and observability for the original structure is reported in this section, as it will form the basis for DSS analysis. Let us assume that the following conditions hold

$$\begin{cases} (c_n s + k_n) \perp m_n s^2 + c_n s + k_n & \\ (c_i s + k_i) \perp m_i s^2 + (c_i + c_{i+1}) s + k_i + k_{i+1} & i \leq n-1 \\ (c_{i+1} s + k_{i+1}) \perp m_i s^2 + (c_i + c_{i+1}) s + k_i + k_{i+1} & \\ (c_j s + k_j) \perp Den_i & j = 1, \ldots, n-i+1;\ i \leq n \end{cases} \tag{3.7}$$

where $A(s) \perp B(s)$ indicates that the polynomials $A(s)$ and $B(s)$ do not share any common root.

From a physical point of view, most of the conditions listed in Equation (3.7) are satisfied if none of the mass, spring or damping coefficients are zero in the original structure. Moreover, if the system is underdamped all conditions are automatically satisfied.

An induction procedure can then be performed to show that under such hypotheses there are no common roots between any denominator and numerator of the transfer functions considered in DSS design. In fact, the constraints listed in Equation (3.7) imply that the first two denominators Den_n and Den_{n-1} in Equation (3.4) do not have any common root. Let us then assume that two adjacent denominators Den_{n-i+1} and Den_{n-i} do not share any common root. Equation (3.4) implies that for any index j between $i+1$ and n, the following relations hold

$$Den_{n-i-1} = K_{1(n-i-1)} Den_{n-i} - K_{2(n-i-1)} Den_{n-i+1} \tag{3.8}$$

$$Den_{n-i-2} = K_{1(n-i-2)} Den_{n-i-1} - K_{2(n-i-2)} Den_{n-i} \tag{3.9}$$

$$\vdots$$

$$\begin{aligned} Den_{n-j+1} &= K_{1(n-j+1)} Den_{n-j+2} - K_{2(n-j+1)} Den_{n-j+3} \\ &= \left(\prod_{q=i+2}^{j} K_{1(n-q+1)} - b_{1(j)} \right) Den_{n-i} \\ &\quad - \left(K_{2(n-i-1)} \prod_{q=i+3}^{j} K_{1(n-q+1)} - b_{2(j)} \right) Den_{n-i+1} \qquad i+3 \leq j \leq n \end{aligned} \tag{3.10}$$

where

$$K_{1(n-j+1)} = m_{n-j+1}s^2 + (c_{n-j+1} + c_{n-j+2})s + k_{n-j+1} + k_{n-j+2} \tag{3.11}$$

$$K_{2(n-j+1)} = (c_{n-j+2}s + k_{n-j+2})^2 \tag{3.12}$$

$$b_{1(i+2)} = 0 \tag{3.13}$$

$$b_{1(i+3)} = K_{2(n-i-2)} \tag{3.14}$$

$$b_{1(j)} = K_{1(n-j+1)}b_{1(j-1)} + K_{2(n-j+1)} \prod_{q=i+2}^{j-2} K_{1(n-q+1)} - K_{2(n-j+1)}b_{1(j-2)} \qquad i+4 \leq j \leq n \tag{3.15}$$

$$b_{2(i+2)} = b_{2(i+3)} = 0 \tag{3.16}$$

$$b_{2(i+4)} = K_{2(n-i-1)}K_{2(n-i-3)} \tag{3.17}$$

$$b_{2(j)} = K_{1(n-j+1)}b_{2(j-1)} + K_{2(n-j+1)}K_{2(n-i-1)} \prod_{q=i+3}^{j-2} K_{1(n-q+1)} - K_{2(n-j+1)}b_{2(j-2)} \qquad i+5 \leq j \leq n \tag{3.18}$$

The degrees of the polynomials b_1 and b_2 are reported in Table 3.2 for reference.

Let us then proceed with a proof by contradiction. To this end, note that if Den_{n-j+1} and Den_{n-i-1} have common roots, then Equation (3.10) can be rearranged as

$$Den_{n-j+1} = A \cdot Den_{n-i-1} \tag{3.19}$$

When A is a constant or a polynomial, all roots of Den_{n-i-1} are included in the roots of Den_{n-j+1}. On the other hand, if A is a ratio of polynomials and its denominator share some roots with Den_{n-i-1}, then some roots of Den_{n-i-1} are not included in the roots of

Table 3.2: Degrees of polynomials $b_{1(j)}$ and $b_{2(j)}$.

Index j	$\angle b_{1(j)}$	$\angle b_{2(j)}$
i+2	0	0
i+3	2	0
i+4	4	4
i+5	6	6
$\vdots$	$\vdots$	$\vdots$
j	2j-2i-4 ($j \geq i+2$)	2j-2i-4 ($j \geq i+4$)
$\vdots$	$\vdots$	$\vdots$
n	2n-2i-4	2n-2i-4

Den_{n-j+1}. Note that Equation (3.10) can be rewritten as

$$\begin{aligned} Den_{n-j+1} = K_{1(n-i-1)} \left(\prod_{q=i+3}^{j} K_{1(n-q+1)} - \frac{b_{1(j)}}{K_{1(n-i-1)}} \right) Den_{n-i} \\ - K_{2(n-i-1)} \left(\prod_{q=i+3}^{j} K_{1(n-q+1)} - \frac{b_{2(j)}}{K_{2(n-i-1)}} \right) Den_{n-i+1} \end{aligned} \tag{3.20}$$

which, once combined with Equation (3.8) and Equation (3.19), implies

$$A = \prod_{q=i+3}^{j} K_{1(n-q+1)} - \frac{b_{1(j)}}{K_{1(n-i-1)}} = \prod_{q=i+3}^{j} K_{1(n-q+1)} - \frac{b_{2(j)}}{K_{2(n-i-1)}} \tag{3.21}$$

which, in turn, implies

$$\frac{b_{1(j)}}{K_{1(n-i-1)}} = \frac{b_{2(j)}}{K_{2(n-i-1)}} \tag{3.22}$$

It is obvious that Equation (3.22) is trivially not satified for $j = i+3$ due to (3.15)-(3.18), hence the following proof will focus on Equation (3.22) for $j > i+3$. To this end,

note that given generic non-zero polynomials X, Y, a_1, a_2, T the relation

$$\frac{X}{Y} = \frac{TX + a_1}{TY + a_2} \tag{3.23}$$

holds if and only if

$$\frac{a_1}{a_2} = \frac{X}{Y} \tag{3.24}$$

Let us then rewrite Equation (3.22) as

$$\frac{b_{1(j)}}{b_{2(j)}} = \frac{K_{1(n-i-1)}}{K_{2(n-i-1)}} \tag{3.25}$$

and use Equations (3.15) and (3.18) to express $b_{1(j)}$ and $b_{2(j)}$ as

$$b_{1(j)} = TX + a_1, \qquad b_{2(j)} = TY + a_2 \tag{3.26}$$

where

$$T = K_{2(n-j+1)} \prod_{q=i+3}^{j-2} K_{1(n-k+1)} \tag{3.27}$$

$$X = K_{1(n-i-1)} \tag{3.28}$$

$$Y = K_{2(n-i-1)} \tag{3.29}$$

$$a_1 = K_{1(n-j+1)} b_{1(j-1)} - K_{2(n-j+1)} b_{1(j-2)} \tag{3.30}$$

$$a_2 = K_{1(n-j+1)} b_{2(j-1)} - K_{2(n-j+1)} b_{2(j-2)} \tag{3.31}$$

Therefore, (3.25) holds if and only if

$$\frac{K_{1(n-j+1)}b_{1(j-1)} - K_{2(n-j+1)}b_{1(j-2)}}{K_{1(n-j+1)}b_{2(j-1)} - K_{2(n-j+1)}b_{2(j-2)}} = \frac{K_{1(n-i-1)}}{K_{2(n-i-1)}} \tag{3.32}$$

or, by rearranging the terms in a more convenient form, if

$$\frac{K_{1(n-j+1)}}{K_{2(n-j+1)}} = \frac{K_{2(n-i-1)}b_{1(j-1)} - K_{1(n-i-1)}b_{2(j-1)}}{K_{2(n-i-1)}b_{1(j-2)} - K_{1(n-i-1)}b_{2(j-2)}} \tag{3.33}$$

However, according to Equation (3.11)-(3.12) and Table 3.2, the left hand side is a ratio of second order polynomials, whereas the right hand side is a ratio of polynomials of different degrees. Therefore Equation (3.33) can not hold and the proof is concluded. This means that an underdamped original system is automatically controllable and observable. For other types of systems, controllability and observability can be analysed by verifying Equation (3.7). In addition, this method avoids obtaining the analytical solution of Den_{n-i+1} where the total number of coefficients in $b_{1(j)}$ and $b_{2(j)}$ are the Fibonacci numbers.

Such analytical test will then be applied to obtain conditions under which a given DSS decomposition is feasible and can be implemented.

3.5 Stability

The original structure is a typical mass spring and damper system, which is asymptotically stable due to the presence of non-zero damping. However, it is useful to conduct the formal stability analysis, as it will form the basis for the stability analysis of decomposed structures in the following chapters. Indeed, for the decomposed structures, stability can not be assumed a priori, due to the presence of an active element at the interface and the possible structural difference from the original system. In this section a formal stability

analysis of the original structure will be carried out anyway.

In order to prepare for the following stability analysis of the decomposed structures, the denominator in Equation (3.3) can be rearranged as

$$Den_i = \prod_{q=i}^{n}(m_q s^2 + c_q s + k_q) + r_i \quad i \leq n-1 \tag{3.34}$$

where r_i is the implicit form of the rest of the coefficients in Den_i and it contains the common factor s^2. To prove this, let us start from Den_{n-1}. Equation (3.4) implies

$$\begin{aligned} Den_{n-1} &= (m_{n-1}s^2 + c_{n-1}s + k_{n-1})(m_n s^2 + c_n s + k_n) + (c_n s + k_n)m_n s^2 \\ &= \prod_{q=n-1}^{n}(m_q s^2 + c_q s + k_q) + r_{n-1} \end{aligned} \tag{3.35}$$

Therefore, Equation (3.34) is satisfied when $i = n-1$ and then it can also be satisfied when $i = n-2$.

Then let us now assume that Equation (3.34) is satisfied when $i = j+1$ and $i = j$, i.e.

$$Den_{j+1} = \prod_{q=j+1}^{n}(m_q s^2 + c_q s + k_q) + r_{j+1} \tag{3.36}$$

$$Den_j = \prod_{q=j}^{n}(m_q s^2 + c_q s + k_q) + r_j \tag{3.37}$$

where both r_{j+1} and r_j include the common factor s^2. Then Equation (3.4) implies

$$\begin{aligned}
Den_{j-1} &= [m_{j-1}s^2 + (c_{j-1}+c_j)s + k_{j-1}+k_j]Den_j - (c_js+k_j)^2 Den_{j+1} \\
&= (m_{j-1}s^2 + c_{j-1}s + k_{j-1})Den_j + (c_js+k_j)Den_j - (c_js+k_j)^2 Den_{j+1} \\
&= (m_{j-1}s^2 + c_{j-1}s + k_{j-1})Den_j \\
&+ (c_js+k_j)(m_js^2 + c_js + k_j)\prod_{q=j+1}^{n}(m_qs^2+c_qs+k_q) + (c_js+k_j)r_j \\
&- (c_js+k_j)^2[\prod_{q=j+1}^{n}(m_qs^2+c_qs+k_q) + r_{j+1}] \\
&= (m_{j-1}s^2 + c_{j-1}s + k_{j-1})Den_j \\
&+ (c_js+k_j)m_js^2\prod_{q=j+1}^{n}(m_qs^2+c_qs+k_q) + (c_js+k_j)[r_j - (c_js+k_j)r_{j+1}] \\
&= \prod_{q=j-1}^{n}(m_qs^2+c_qs+k_q) + (m_{j-1}s^2 + c_{j-1}s + k_{j-1})r_j \\
&+ (c_js+k_j)m_js^2\prod_{q=j+1}^{n}(m_qs^2+c_qs+k_q) + (c_js+k_j)[r_j - (c_js+k_j)r_{j+1}] \\
&= \prod_{q=j-1}^{n}(m_qs^2+c_qs+k_q) + r_{j-1}
\end{aligned} \tag{3.38}$$

where

$$\begin{aligned}
r_{j-1} = (m_{j-1}s^2 + c_{j-1}s + k_{j-1})r_j + (c_js+k_j)m_js^2\prod_{q=j+1}^{n}(m_qs^2+c_qs+k_q) + \\
+ (c_js+k_j)[r_j - (c_js+k_j)r_{j+1}]
\end{aligned} \tag{3.39}$$

Therefore, r_{j-1} also has the common factor s^2, meaning the proof is complete and Equation (3.34) is satisfied. The proof provided in Appendix A shows that a polynomial with a even maximum degree and all unconditionally positive coefficients can only have

negative real roots, purely imaginary roots or conjugated complex roots with negative real parts. Therefore, it is necessary to prove that all coefficients in $(c_j s+k_j)[r_j-(c_j s+k_j)r_{j+1}]$ are unconditionally positive. Note that this condition is already satisfied for r_{n-2} and r_{n-3}. To use induction, let us then assume that r_{j-1} are unconditionally positive. Then r_{j-2} can be expressed as

$$\begin{aligned}
r_{j-2} &= (m_{j-2}s^2 + c_{j-2}s + k_{j-2})r_{j-1} + (c_{j-1}s + k_{j-1})m_{j-1}s^2 \prod_{q=j}^{n}(m_q s^2 + c_q s + k_q) \\
&\quad + (c_{j-1}s + k_{j-1})[r_{j-1} - (c_{j-1}s + k_{j-1})r_j] \\
&= (m_{j-2}s^2 + c_{j-2}s + k_{j-2})r_{j-1} + (c_{j-1}s + k_{j-1})m_{j-1}s^2 \prod_{q=j}^{n}(m_q s^2 + c_q s + k_q) \\
&\quad + (c_{j-1}s + k_{j-1})\{(m_{j-1}s^2 + c_{j-1}s + k_{j-1})r_j + (c_j s + k_j)m_j s^2 \prod_{q=j+1}^{n}(m_q s^2 + c_q s + k_q) \\
&\quad + (c_j s + k_j)[r_j - (c_j s + k_j)r_{j+1}] - (c_{j-1}s + k_{j-1})r_j\} \\
&= (m_{j-2}s^2 + c_{j-2}s + k_{j-2})r_{j-1} + (c_{j-1}s + k_{j-1})m_{j-1}s^2 \prod_{q=j}^{n}(m_q s^2 + c_q s + k_q) \\
&\quad + (c_{j-1}s + k_{j-1})\{m_{j-1}s^2 r_j + (c_j s + k_j)m_j s^2 \prod_{q=j+1}^{n}(m_q s^2 + c_q s + k_q) \\
&\quad + (c_j s + k_j)[r_j - (c_j s + k_j)r_{j+1}]\}
\end{aligned} \tag{3.40}$$

where

$$\begin{aligned}
&(c_{j-1}s + k_{j-1})[r_{j-1} - (c_{j-1}s + k_{j-1})r_j] = \\
&(c_{j-1}s + k_{j-1})\{m_{j-1}s^2 r_j + (c_j s + k_j)m_j s^2 \prod_{q=j+1}^{n}(m_q s^2 + c_q s + k_q) \\
&+ (c_j s + k_j)[r_j - (c_j s + k_j)r_{j+1}]\}
\end{aligned} \tag{3.41}$$

Therefore, all the coefficients of $(c_{j-1}s + k_{j-1})[r_{j-1} - (c_{j-1}s + k_{j-1})r_j]$ are unconditionally positive, and this implies that the coefficients of r_{j-2} are unconditionally positive as well. Therefore, by induction, all coefficients in r_j are unconditionally positive for each index j, as well as all coefficients in each Den_j. It can also be observed that the maximum degree for Den_j is $2j$, while the maximum degree for r_j is $2j-1$. Moreover, in Den_j the coefficients of odd degree terms are functions of the damping coefficients c_i only. Therefore, the proof provided in Appendix A can be exploited to show that Den_j can only admit negative real roots, complex roots with negative real parts and purely imaginary roots. However, for Den_j to admit purely imaginary roots, at least some of the odd degree terms should be zero, but this would imply that some of the damping coefficients c_i are equal to zero, which is in conflict with the condition that all system parameters are strictly positive. Therefore, Den_j can only have negative real roots or conjugated complex roots with negative real parts, indicating that the original system is asymptotically stable. Equation (3.38) will play a key role in Chapter 4 to analyse the stability for different substructures, as well as to understand the challenges associated to DSS testing of structures in Chapter 5, where the substructuring interface is placed across a mass.

Chapter 4

Control Design Feasibility for Structural Decompositions without Mass Split

In this chapter an analysis of the structural properties of decomposition strategies without the mass split will be carried out. Here "mass split" indicates a decomposition where the DSS interface is placed across a mass. The purpose is to derive analytical conditions for application of DSS to generic vibration problems. The benchmark structure shown in Figure 3.1 is selected, as results for such structure are easily generalised to more complex structures (see examples in section 4.5.2). The analysis is based on properties such as causality, controllability and observability. Therefore, proposed approach is generic and other generalised structures can use these procedures as the reference, and the procedure proposed in this chapter can be applied to other types of structures to obtain similar results.

4.1 Types of DSS Decomposition

In a DSS framework the original system shown in Figure 3.1 is split into two substructures, a physical substructure implemented in hardware and a numerical substructure which is numerically simulated. However, different choices can be made on what substructure should be simulated, where the interface between the two substructures should be placed and whether force or position control should be used. Different choices give raise to different feasibility conditions, which are discussed in the rest of the chapter.

For the sake of reference, in this chapter the decomposition shown in Figure 4.1a will be called *Type 1 decomposition*, whereas the scheme shown in Figure 4.1b will be referred to as *Type 2 decomposition*. The difference between these two options lies in the location of the interface between numerical and physical substructures; in the first type the interface is placed right after the l-th mass, whereas in the second type the interface is placed after the spring-damper connected to the l-th mass.

Once the location of the interface has been finalised, each substructure can be tested either numerically or physically, and force or position control can be used to synchronise the two substructures. Therefore in total eight potential DSS decomposition approaches will be analysed in this chapter.

4.2 Stability Analysis

Obviously, for Type 1 decomposition both substructures are similar to the original structure, which means both substructures are asymptotically stable. However, for Type 2 decomposition substructure B is different from the original structure because the leftmost mass is not linked to a support via a spring and damper on its left side. Therefore, its stability should be carried out separately. In all cases S_1 and S_2 are inputs for substructure

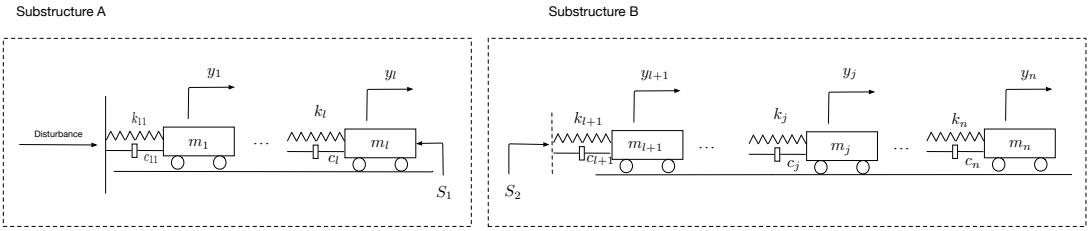

(a) Type 1 decomposition

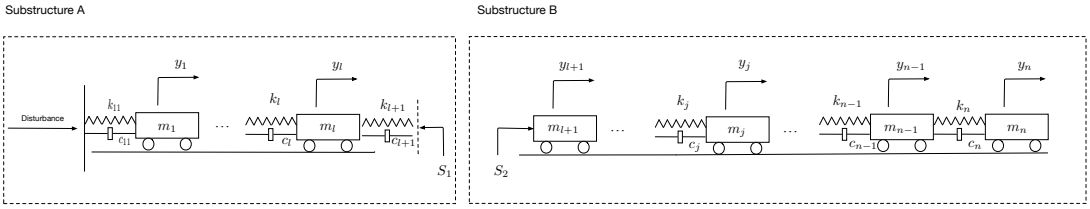

(b) Type 2 decomposition

Figure 4.1: Potential choices of location of substructuring interface: a) Type 1 decomposition where the interface is right after mass l and b) Type 2 decomposition where the interface is located after the spring-mass damper system connected to mass l.

A and substructure B respectively. Then let us assume that S_2 is a force input, hence the generalised equation of motion for substructure B can be written as

$$\frac{y_i}{F} = \frac{y_{l+1}}{F}\frac{y_{l+2}}{y_{l+1}}\cdots\frac{y_i}{y_{i-1}} =$$

$$\frac{Num_i^F}{Den'_{l+1}} = \begin{cases} \dfrac{Den'_{i+1}}{Den'_{l+1}} & i = l+1 \\ \dfrac{Den'_{i+1}\prod_{l+2}^{i}(c_i s + k_i)}{Den'_{l+1}} & l+1 < i \leq n-1 \\ \dfrac{\prod_{l+2}^{i}(c_i s + k_i)}{Den'_{l+1}} & i = n \end{cases} \tag{4.1}$$

where

$$Den'_i = \begin{cases} m_n s^2 + c_n s + k_n & i = n \\ [m_{n-1}s^2 + (c_{n-1} + c_n)s + k_{n-1} + k_n](m_n s^2 + c_n s + k_n) & \\ \quad - (c_n s + k_n)^2 & i = n-1 \\ \vdots & \\ [m_i s^2 + (c_i + c_{i+1})s + k_i + k_{i+1}]Den'_{i+1} & \\ \quad - (c_{i+1}s + k_{i+1})^2 Den'_{i+2} & l+2 \le i \le n-2 \\ (m_{l+1}s^2 + c_{l+2}s + k_{l+2})Den'_{l+2} - (c_{l+2}s + k_{l+2})^2 Den'_{l+3} & i = l+1 \end{cases} \tag{4.2}$$

Note that Equation (4.2), apart from the last denominator, is identical to Equation (3.4). Following the same procedure leading to Equation (3.34), Equation (4.2) can be rearranged as

$$Den'_{l+1} = m_{l+1}s^2 \prod_{q=l+2}^{n} (m_q s^2 + c_q s + k_q) + r'_{l+1} \tag{4.3}$$

where r'_{l+1} also includes the common factor s^2.

Therefore, all coefficients in Den'_l include the common factor s^2, indicating that substructure B is marginally stable, according to the proposed stability analysis shown in Chapter 3. In the following causality analysis Den_2 is used to describe the characteristic equation of substructure B in Type 2 decomposition, in view of its marginal stability.

An example of marginally stable response is shown in Figure 4.2 where four-mass-system with parameters as in Table 4.1 is tested with a sinusoidal external physical force $F_p(t) = 0.003sin(6\pi t)$ which is used to excite the bottom of $4th$ mass. Note that marginal stability may induce a drift in the response.

Table 4.1: Numerical values of parameters used for example of substructure B response

Index	Mass m_i	Stiffness k_i	Damping c_i
1	$380kg$	N/A	N/A
2	$350kg$	$700N/m$	$250Ns/m$
3	$320kg$	$600N/m$	$240Ns/m$
4	$290kg$	$500N/m$	$230Ns/m$

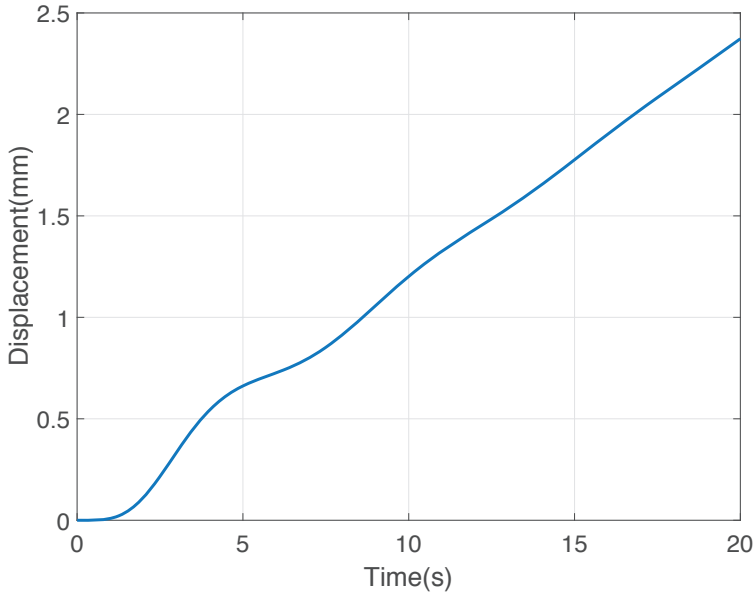

Figure 4.2: Displacement of fourth mass with Type 2 decomposition

4.3 DSS Decomposition: Causality Analysis

In this section, a causality analysis for the eight cases considered in this chapter is performed. Each case is discussed in a separate subsection to improve clarity.

4.3.1 Force Control, Physical substructure A, Type 1 Decomposition

The general scheme for Type 1 decomposition is shown in Figure 4.1a and the control diagram is same as in Figure 2.1. In this section we consider the case

$$S_1 = S_p = F_p, \quad S_2 = S_s = y_l, \quad S_n = F_n \tag{4.4}$$

i.e. the substructure A is a physical substructure and the physical displacement of the interface is passed to the numerical substructure as an input. The goal of the DSS control is therefore to minimise the error between the numerical force F_n at the interface and the physical force F_p that the actuator exerts on the physical substructure.

The equation of motion describing mass displacements in the physical substructure can be written as

$$y_i = \frac{Num_i^d}{Den_d} d - \frac{Num_i^{F_p}}{Den_{F_p}} F_p \qquad 1 \leq i \leq l \tag{4.5}$$

Note that Equations (3.3)-(3.5) and Table 3.1 imply

$$\lfloor y_i \rfloor = \frac{\lfloor 2l - i \rfloor}{\lfloor 2l \rfloor} d - \frac{\lfloor l + i - 2 \rfloor}{\lfloor 2l \rfloor} F_p \tag{4.6}$$

$$\lfloor y_l \rfloor = \frac{\lfloor l \rfloor}{\lfloor 2l \rfloor} d - \frac{\lfloor 2l - 2 \rfloor}{\lfloor 2l \rfloor} F_p \tag{4.7}$$

where $\lfloor y_i \rfloor$ means its maximum degree by obtaining the maximum degree of the relative

transfer functions.

Therefore, all the transfer functions related to quantities to be measured at the interface are causal. Note that for simplicity, all the degrees considered in this analysis are the maximum degrees and no pole-zero cancellations are taken into account. However, the same result holds even in presence of pole-zero cancellations, as the relative degree of the transfer functions is preserved also in such cases.

Similarly, the equations of motion for the numerical substructure read

$$y_j = \frac{Num_j^{y_l}}{Den_{y_l}} y_l = \frac{Num_j^{y_l}}{Den_{y_l}} \left(\frac{Num_l^d}{Den_d} d - \frac{Num_l^{F_p}}{Den_{F_p}} \right) \qquad l+1 \leq j \leq n \tag{4.8}$$

Thanks to Table 3.1, the degree of numerators and denominators of such transfer functions can then be written as

$$\lfloor y_j \rfloor = \frac{\lfloor 2n-j-l \rfloor}{\lfloor 2(n-l) \rfloor} y_l \tag{4.9}$$

$$= \frac{\lfloor 2n-j-l \rfloor}{\lfloor 2(n-l) \rfloor} \left(\frac{\lfloor l \rfloor}{\lfloor 2l \rfloor} d - \frac{\lfloor 2l-2 \rfloor}{\lfloor 2l \rfloor} F_p \right) = \frac{\lfloor 2n-j \rfloor}{\lfloor 2n \rfloor} d - \frac{\lfloor 2n-j+l-2 \rfloor}{\lfloor 2n \rfloor} F_p \tag{4.10}$$

and therefore all the transfer functions involved in calculating mass displacements in the numerical substructure are causal if either the interface displacement y_l is passed as an input (Equation (4.9)) or the combination of physical force F_p and disturbance d are passed as inputs (Equation (4.10)).

On the other hand, the numerical force F_n at the interface also needs to be simulated to compute the synchronisation error which will be fed to the DSS controller. Such numerical

force can be calculated as

$$F_n = (c_{l+1}s + k_{l+1})(y_l - y_{l+1}) = (c_{l+1}s + k_{l+1}) \left(1 - \frac{Num_{l+1}^{y_l}}{Den_{y_l}}\right) y_l \tag{4.11}$$

$$= (c_{l+1}s + k_{l+1}) \left(1 - \frac{Num_{l+1}^{y_l}}{Den_{y_l}}\right) \left(\frac{Num_l^d}{Den_d} d - \frac{Num_l^{F_p}}{Den_{F_p}} F_p\right) \tag{4.12}$$

Once again, Table 3.1 implies that the relative degrees of such transfer functions are

$$\lfloor F_n \rfloor = \frac{\lfloor 2n - 2l + 1 \rfloor}{\lfloor 2(n-l) \rfloor} y_l \tag{4.13}$$

$$= \frac{\lfloor 2n - l + 1 \rfloor}{\lfloor 2n \rfloor} d - \frac{\lfloor 2n - 1 \rfloor}{\lfloor 2n \rfloor} F_p \tag{4.14}$$

Equation (4.13) implies that the numerical force F_n can not be estimated in a causal way if information on y_l only is passed to the numerical substructure. On the other hand, F_n can be obtained in a causal way if information about F_p and d is provided, as indicated by Equation (4.14).

4.3.2 Force Control, Numerical substructure A, Type 1 Decomposition

Let us now consider the case where the role of physical and numerical substructure is swapped compared to the section 4.3.1, i.e.

$$S_1 = S_s = y_l, \quad S_2 = S_p = F_p, \quad S_n = F_n \tag{4.15}$$

In this case, the lack of the spring-damper at the numerical interface prevents the possibility of simulating F_n in a causal way and therefore force control within such decomposition strategy can not be physically implemented.

4.3.3 Position control, Physical Substructure A, Type 1 Decomposition

In this section the case where

$$S_1 = S_p = y_l^p, \quad S_2 = S_s = F_p, \quad S_n = y_l^n \tag{4.16}$$

is considered. This situation is similar to the one considered in section 4.3.1 but with the role of force and position at the interface swapped. In this case, the position actuator used in position control can not independently set the position of the mass m_l in a causal way, therefore this approach is deemed infeasible.

4.3.4 Position Control, Numerical Substructure A, Type 1 Decomposition

The case analysed in this subsection refers to the same schematics of section 4.3.2, but again with the role of force and position at the interface swapped, i.e.

$$S_1 = S_s = F_p, \quad S_2 = S_p = y_l^p, \quad S_n = y_l^n \tag{4.17}$$

The equations of motion for the physical substructure can be written as

$$y_j = \frac{Num_j^{y_l}}{Den_{y_l}} y_l^p \qquad\qquad i+1 \leq j \leq n \tag{4.18}$$

where y_l^p is the physical displacement of the l-th mass, $Num_j^{y_l}$ and Den_{y_l} represent the numerator and the denominator of the transfer function relating to input y_l^p and output y_j respectively According to Table 3.1, the following relation holds

$$\lfloor y_j \rfloor = \frac{\lfloor 2n - j - l \rfloor}{\lfloor 2(n-l) \rfloor} y_l^p \tag{4.19}$$

On the other hand, the equation of motion for the numerical substructure reads

$$y_i^n = \frac{Num_i^d}{Den_d} d - \frac{Num_i^{F_p}}{Den_{F_p}} F_p \qquad 1 \leq i \leq l \tag{4.20}$$

and therefore

$$\lfloor y_i^n \rfloor = \frac{\lfloor 2l - i \rfloor}{\lfloor 2l \rfloor} d - \frac{\lfloor l + i - 2 \rfloor}{\lfloor 2l \rfloor} F_p = \frac{\lfloor 2l - i \rfloor}{\lfloor 2l \rfloor} d - \frac{\lfloor 2n - l + i - 1 \rfloor}{\lfloor 2n \rfloor} y_l^p \tag{4.21}$$

$$\lfloor y_l^n \rfloor = \frac{\lfloor l \rfloor}{\lfloor 2l \rfloor} d - \frac{\lfloor 2n - 1 \rfloor}{\lfloor 2n \rfloor} y_l^p \tag{4.22}$$

where y_i^n is the numerical displacement of i-th mass in the bottom part. Hence, all the transfer functions involved in the substructuring procedures are causal in this scenario.

It is worth noting that the decomposition described in this section is feasible only if the physical force F_p is directly measured. In fact, if one tries to estimate it from measurements of displacements at the interface, namely

$$F_p = (c_{l+1}s + k_{l+1})(y_l^p - y_{l+1}) = (c_{l+1}s + k_{l+1}) \left(1 - \frac{Num_l^{y_l}}{Den_{y_l}}\right) y_l^p \tag{4.23}$$

then such estimation is not causal.

4.3.5 Force Control, Physical Substructure A, Type 2 Decomposition

For Type 2 decomposition, the schematics of Figure 4.1b and Figure 2.1b are used. The case considered in this section corresponds to

$$S_1 = S_p = F_p, \quad S_2 = S_s = y_l, \quad S_n = F_n \tag{4.24}$$

Similar to the case discussed in subsection 4.3.2 above, the numerical force at the interface can not be estimated in a causal manner, making this decomposition strategy not implementable.

4.3.6 Force Control, Numerical Substructure A, Type 2 Decomposition

In this scenario, the original structure is decomposed as shown in Figure 4.1b with

$$S_1 = S_s = y_{l+1}, \quad S_2 = S_p = F_p, \quad S_n = F_n \tag{4.25}$$

The equation of motion for the physical substructure can then be written as

$$y_j = \frac{Num_j^{F_p}}{Den_{2F_p}} F_p \qquad\qquad l+1 \leq j \leq n \tag{4.26}$$

and therefore

$$\lfloor y_j \rfloor = \frac{\lfloor 2n-j-l-1 \rfloor}{\lfloor 2(n-l) \rfloor} F_p \tag{4.27}$$

and the physical substructure is causal, as expected.

Similarly, the displacements of the masses in the numerical substructure can be described as

$$y_i = \frac{Num_i^d}{Den_d} d - \frac{Num_i^{y_{l+1}}}{Den_{y_{l+1}}} y_{l+1} \qquad\qquad 1 \leq i \leq l \tag{4.28}$$

which implies

$$\lfloor y_i \rfloor = \frac{\lfloor 2l-i \rfloor}{\lfloor 2l \rfloor} d - \frac{\lfloor l+i-1 \rfloor}{\lfloor 2l \rfloor} y_{l+1} \tag{4.29}$$

and therefore all the displacements in the numerical substructure can be simulated using causal transfer functions.

On the other hand, the numerical force F_n can be expressed as

$$F_n = (c_{l+1}s + k_{l+1})(y_l - y_{l+1}) = (c_{l+1}s + k_{l+1}) \left[\frac{Num_l^d}{Den_d} d - \left(\frac{Num_l^{y_{l+1}}}{Den_{y_{l+1}}} + 1 \right) y_{l+1} \right] \quad (4.30)$$

which implies

$$\lfloor F_n \rfloor = \frac{\lfloor l+1 \rfloor}{\lfloor 2l \rfloor} d - \frac{\lfloor 2l+1 \rfloor}{\lfloor 2l \rfloor} y_{l+1} = \frac{\lfloor l+1 \rfloor}{\lfloor 2l \rfloor} d - \frac{\lfloor 2n-1 \rfloor}{\lfloor 2n \rfloor} F_p \quad (4.31)$$

Therefore, the numerical force F_n can not be estimated based on the physical displacement y_{l+1} and the disturbance d. However, this causality issue can be avoided if direct measurements of the physical force F_p is available, as suggested by Equation (4.31).

It is worth noting that in the scenario considered here, substructure B may drift as shown in Figure 4.2.

4.3.7 Position Control, Physical Substructure A, Type 2 Decomposition

The setup is similar to the one considered in section 4.3.5, but with the role of force and displacement swapped, i.e.

$$S_1 = S_p = y_{l+1}^p, \quad S_2 = S_s = F_p, \quad S_n = y_{l+1}^n \quad (4.32)$$

In this case, the equation of motion for the physical substructure reads

$$y_i = \frac{Num_i^d}{Den_d} d - \frac{Num_i^{y_{l+1}}}{Den_{y_{l+1}}} y_{l+1} \qquad 1 \le i \le l \quad (4.33)$$

which implies

$$\lfloor y_i \rfloor = \frac{\lfloor 2l - i \rfloor}{\lfloor 2l \rfloor} d - \frac{\lfloor l + i - 1 \rfloor}{\lfloor 2l \rfloor} y_{l+1} \tag{4.34}$$

and therefore all the transfer functions related to displacements are causal. On the other hand, the physical force can be expressed as

$$F_p = (c_{l+1}s + k_{l+1})(y_l - y_{l+1}) = (c_{l+1}s + k_{l+1}) \left[\frac{Num_l^d}{Den_d} d - \left(\frac{Num_l^{y_{l+1}}}{Den_{y_{l+1}}} + 1 \right) y_{l+1} \right] \tag{4.35}$$

with

$$\lfloor F_p \rfloor = \frac{\lfloor l + 1 \rfloor}{\lfloor 2l \rfloor} d - \frac{\lfloor 2l + 1 \rfloor}{\lfloor 2l \rfloor} y_{l+1} \tag{4.36}$$

Therefore, the physical force can not be estimated in a causal way from d and y_{i+1} and needs to be measured directly. Similarly, the equations of motion describing the numerical substructure read

$$y_j = \frac{Num_j^{F_p}}{Den_{2F_p}} F_p \qquad\qquad i + 1 \leq j \leq n \tag{4.37}$$

which implies that no causality problems arise, in fact

$$\lfloor y_j \rfloor = \frac{\lfloor 2n - j - l - 1 \rfloor}{\lfloor 2(n - l) \rfloor} F_p = \frac{\lfloor 2n - j \rfloor}{\lfloor 2n \rfloor} d - \frac{\lfloor 2n - j + l \rfloor}{\lfloor 2n \rfloor} y_{l+1} \tag{4.38}$$

4.3.8 Position Control, Numerical Substructure A, Type 2 Decomposition

The decomposition considered in this section is similar to the one discussed in section 4.3.6, but with the role of force and displacement at the interface swapped, i.e.

$$S_1 = S_s = F_p, \quad S_2 = S_p = y^p_{l+1}, \quad S_n = y^n_{l+1} \tag{4.39}$$

However, similar to section 4.3.5, it is not possible to write down a causal expression for the force at the interface, therefore this decomposition is deemed infeasible as well.

4.3.9 Summary of Causality Analysis

The summary of the results obtained in this section is reported in Table 4.2, showing that only three out of eight decomposition strategies admit a strictly causal implementation with no potential (physical) drifts. Note that in Type 1 decomposition, F_p can either be measured or estimated for the force control while it can only be measured for the position control. In Type 2 decomposition, F_n can only be estimated through F_p for the force control, although substructure B is marginally stable, and it should avoid being physically tested for the safety reason. In addition, F_p can only be measured for the position control in Type 2 decomposition.

Table 4.2: Summary of causality analysis

DSS type	Force Control (A physical)	Force Control (A numerical)	Position Control (A physical)	Position Control (A numerical)
Type 1	✓	×	×	✓
Type 2	×	✓ (Drift)	✓	×

4.4 DSS Decomposition: Structural Properties

In this section the structural properties of controllability and observability of the various DSS decomposition strategies discussed in section 4.1 will be derived to show which strategy is controllable and observable. As mentioned in section 3.1 and 3.3, a frequency domain approach will be taken. Therefore, the analysis of structural properties reduces to obtaining conditions under which no pole-zero cancellations occur in the transfer functions used for control purposes.

Only strategies deemed feasible according to the analysis of section 4.3 are considered here. The main focus in this section is ensuring that all the signals used by the DSS controller, and in particular the synchronisation error $e(t)$, are observable and controllable, so that the controller can effectively synchronise the two substructures.

Let us then start with the case of force control with physical substructure A in Type 1 decomposition (section 4.3.1). In the numerical substructure B, y_l plays the role of the disturbance d in the original system, therefore

$$y_{l+1} = \frac{Num_{l+1}^{y_l}}{Den_{y_l}} y_l \tag{4.40}$$

$$F_n = (c_{l+1}s + k_{l+1})(y_l - y_{l+1}) = (c_{l+1}s + k_{l+1}) \left(1 - \frac{Num_{l+1}^{y_l}}{Den_{y_l}}\right) y_l \tag{4.41}$$

and the synchronisation error can be expressed as

$$e = F_p - F_n = G_u(s)u - (c_{l+1}s + k_{l+1}) \left(1 - \frac{Num_{l+1}^{y_l}}{Den_{y_l}}\right) y_l \tag{4.42}$$

where $G_u(s)$ is the transfer function of the actuator (usually assumed to be a first order system). Note that all the transfer functions considered here are a subset of the transfer functions considered in Chapter 3, therefore no pole-zero cancellation occur and the system

is completely observable and controllable.

Similarly, for the case of position control with numerical substructure A in Type 1 decomposition (section 4.3.4), the equations relative to controller signals can be written as

$$y_l^n = \frac{Num_l^d}{Den_d} d - \frac{Num_l^{F_p}}{Den_{F_p}} F_p \tag{4.43}$$

$$e = y_l^p - y_l^n = G_u(s)u - \frac{Num_l^d}{Den_d} d + \frac{Num_l^{F_p}}{Den_{F_p}} F_p \tag{4.44}$$

The same methods discussed in Chapter 3 can then be applied, yielding that the system is fully controllable and observable if

$$\begin{cases} (c_l s + k_l) \perp m_l s^2 + c_l s + k_l \\ (c_j s + k_j) \perp Den_d \qquad\qquad j = 1, \ldots, l; \end{cases} \tag{4.45}$$

are satisfied in addition to (3.7). These additional constraints are introduced because the denominator Den_d in (4.43)-(4.44) considers only the masses up to l, therefore conditions analogous to the first and the last expressions in (3.7) are needed.

Finally, for the case of position control with physical substructure A in Type 2 decomposition (section 4.3.7) the relevant equations read

$$y_{l+1}^n = \frac{Num_{l+1}^{F_p}}{Den_{2F_p}} F_p \tag{4.46}$$

$$e = y_{l+1}^p - y_{l+1}^n = G_u(s)u - \frac{Num_{l+1}^{F_p}}{Den_{2F_p}} F_p \tag{4.47}$$

Once again, such equations are a subset of the ones considered in section 3.2, therefore also this decomposition strategy is fully controllable and observable. In summary, all the causal DSS decompositions identified in section 4.3 are fully controllable and observable.

4.5 Numerical Examples

For the sake of completeness, in this section three different models are simulated to show the performance that can be obtained when using the DSS decompositions deemed feasible according to the analysis described above.

4.5.1 Benchmark System

For this purpose a system composed of four masses is considered, at first, before progressing to a more complex example in section 4.5.2 the corresponding DSS decomposition is obtained by assigning two masses to the physical system and two masses to the numerical system. The numerical parameters used for simulation are reported in Table 5.1. The natural frequencies are $0.0882Hz$, $0.2382Hz$, $0.3629Hz$ and $0.4455Hz$, respectively. The

Table 4.3: Numerical values of parameters used for simulation examples

Index	Mass m_i	Stiffness k_i	Damping c_i
1	$500kg$	$1200N/m$	$300Ns/m$
2	$470kg$	$1100N/m$	$290Ns/m$
3	$440kg$	$1000N/m$	$280Ns/m$
4	$410kg$	$900N/m$	$270Ns/m$

disturbance $d(t)$ is a chirp signal, in which its amplitude is $1mm$, the frequency increases from $0Hz$ to $0.5Hz$ over $45s$ and then is maintained constant for further $15s$, which is shown in Figure 4.3. For each case, the synchronisation controller in charge of minimising the error $e(t)$ is designed according to the H_2 control design strategy, with $e(t)$ being also the feedback input. The detailed procedure and calculations used to design such controller follow the step which is discussed in section 2.5.

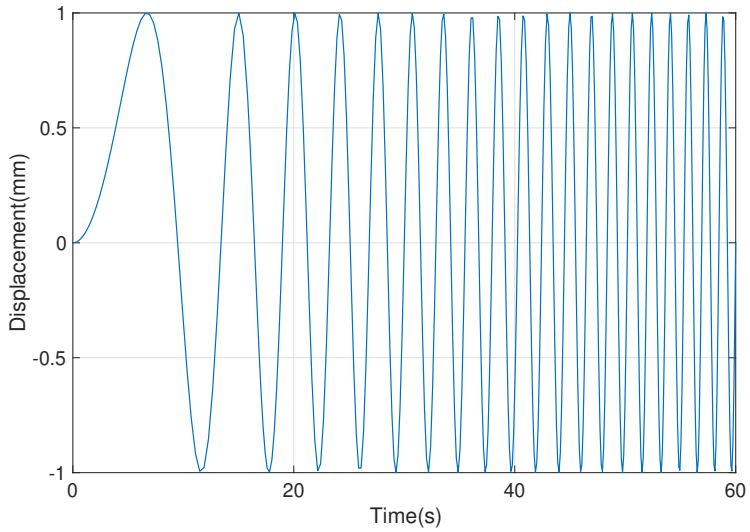

Figure 4.3: Disturbance d in the benchmark system.

In Type 1 decomposition the physical substructure sits in substructure B and the procedure sketched in Section 2.5.2 can be used to obtain the following controller

$$\begin{aligned} K(s) = & \frac{9.2934 \times 10^8 (s+4599)(s+10)(s+3.793)(s+3.571)}{(s+1.009 \times 10^6)(s^2+0.07173s+0.3054)} \\ \times & \frac{(s+0.0001047)(s-0.000104)(s^2+1.272s+4.241)}{(s^2+0.619s+2.255)(s^2+1.447s+5.227)(s^2+2.147s+7.773)} \end{aligned} \tag{4.48}$$

As reported in Figure 4.4. In this case, perfect synchronisation is achieved between the numerical force F_n and the physical force F_p.

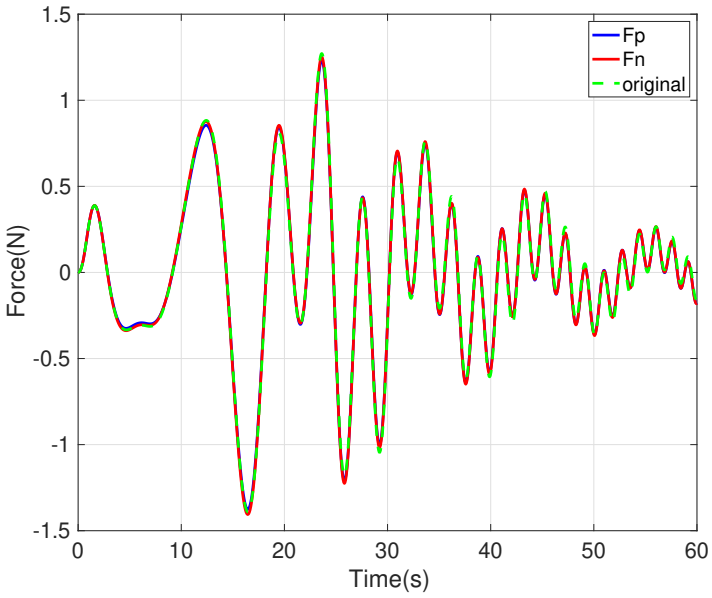

Figure 4.4: Results obtained for DSS with force control in the Type 1 decomposition with physical substructure A.

Similarly, the position control in Type 1 decomposition, where the physical substructure now sits in substructure A. The controller is listed as follows

$$K(s) = \frac{1.0709 \times 10^{11}(s+10)(s+3.793)}{(s+10^9)(s^2+0.08107s+0.3072)(s^2+0.6203s+2.241)} \times \frac{(s^2+0.2534s+0.8867)(s^2+1.655s+5.626)(s^2+533.4s+1.425\times10^5)}{(s^2+1.447s+5.21)(s^2+2.153s+7.813)} \tag{4.49}$$

In this case, almost perfect synchronisation is achieved, with a negligible error between physical displacement y_p and numerical displacement y_n, as the results are reported in Figure 4.5.

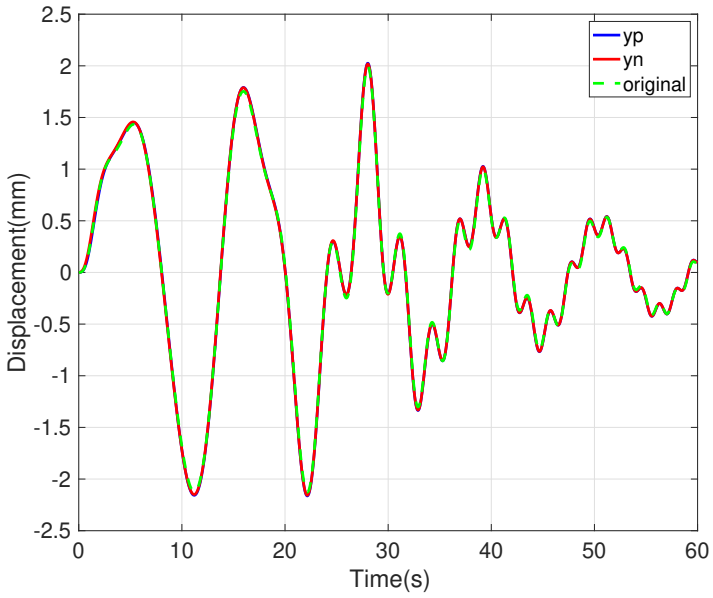

Figure 4.5: Results obtained for DSS with position control in the Type 1 decomposition with physical substructure A.

Finally, results for position control in Type 2 decomposition with numerical substructure A are reported in Figure 4.6, as the controller is provided below

$$K(s) = \frac{9.7305 \times 10^{12}(s+0.8566)(s+10)}{(s+9.902\times 10^{7})(s+9.829\times 10^{5})(s+2.814)} \times \frac{(s^2+0.651s+2.194)(s^2+3.312s+5.248)(s^2+1.369s+12.96)}{(s^2+0.4609s+1.395)(s^2+0.6768s+2.115)(s^2+1.612s+6.121)} \tag{4.50}$$

In this case, some error at the turning points of displacement is present. This is due to limited actuation power and, potentially, a non optimal choice of poles for the closed loop system. This is in accordance with the analysis of section 4.3 where Type 2 decomposition was shown to be harder to control due to the potential drifts in the numerical substructure, as substructure B is marginally stable and the solution to such problem will be introduced in Chapter 5.

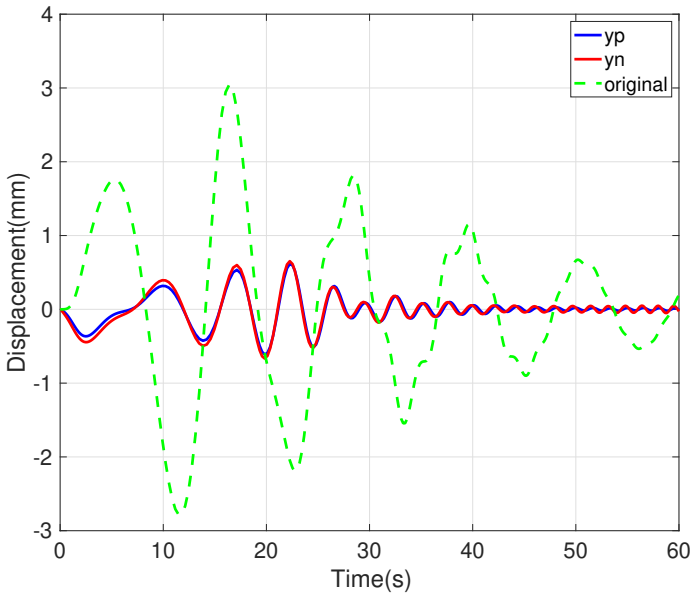

Figure 4.6: Results obtained for DSS with position control in the Type 2 decomposition with numerical substructure A.

4.5.2 Complex Structure

In order to show that the outcomes of the analysis presented in this chapter are suitable for complex structures, a structure with the stronger coupling between DoF is selected and shown in Figure 4.7. The top structure is the conversion to the chain structure while the bottom structure is the actual structure that can represent the building frames in reality.

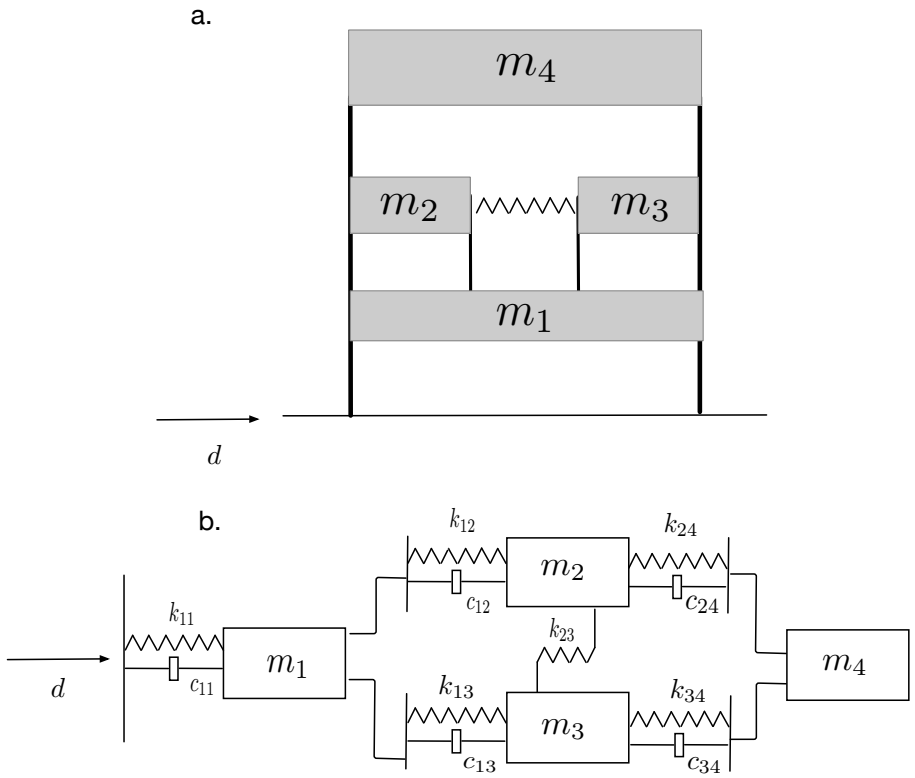

Figure 4.7: Complex benchmark structure: a) sketch of the structure; b) Equivalent Mathematical Model

The equations of motion can be obtained by force balance and read

$$\begin{cases} m_4\ddot{y}_4 = -k_{34}(y_4 - y_3) - c_{34}(\dot{y}_4 - \dot{y}_3) - k_{24}(y_4 - y_2) - c_{24}(\dot{y}_4 - \dot{y}_2) \\ m_3\ddot{y}_3 = k_{34}(y_4 - y_3) + c_{34}(\dot{y}_4 - \dot{y}_3) - k_{23}(y_3 - y_2) - k_{13}(y_3 - y_1) - c_{13}(\dot{y}_3 - \dot{y}_1) \\ m_2\ddot{y}_2 = k_{24}(y_4 - y_2) + c_{24}(\dot{y}_4 - \dot{y}_2) + k_{23}(y_3 - y_2) - k_{12}(y_2 - y_1) - c_{12}(\dot{y}_2 - \dot{y}_1) \\ m_1\ddot{y}_1 = k_{13}(y_3 - y_1) + c_{13}(\dot{y}_3 - \dot{y}_1) + k_{12}(y_2 - y_1) + c_{12}(\dot{y}_2 - \dot{y}_1) \\ \quad - k_{11}(y_1 - d) - c_{11}(\dot{y}_1 - \dot{d}) \end{cases} \tag{4.51}$$

Parameters are same as in the previous example, with k_{34}, k_{13}, k_{12} and k_{11} being respectively, set equal to k_4, k_3, k_2 and k_1. The damping coefficients have been matched as well. In addition, $k_{24} = 800N/m$, $k_{23} = 500N/m$ and $c_{24} = 260Ns/m$. The disturbance $d(t)$ is a chirp signal in which the frequency increases from $0Hz$ to $0.7Hz$ over $50s$ and then is maintained constant for further $30s$, which is shown in Figure 4.8. Note that the natural frequencies of the system are $0.1102Hz, 0.3595Hz, 0.4036Hz$ and $0.4852Hz$. Therefore, the selected chirp signal excites all the resonant modes of the structure. Type 1 decomposition

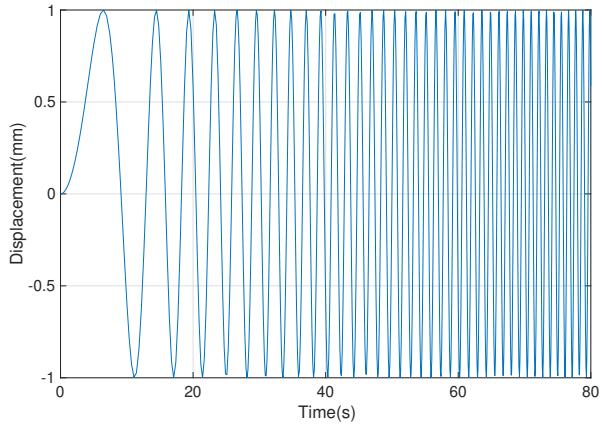

Figure 4.8: Disturbnce d in the complex structure

is implemented by placing the interface at the top of m_1, therefore force and position con-

trol will be included. H_2 controller are then designed to eliminate the error between forces or displacements. The result of force control is shown in Figure 4.9, with the controller as listed below

$$K(s) = \frac{1.4101 \times 10^6 (s + 3.684)(s^2 + 0.002657s + 1.534 \times 10^{-5})}{(s^2 + 0.1155s + 0.4773)(s^2 + 1.517s + 5.154)} \times \frac{(s^2 + 1.856s + 6.01)(s^2 + 1.231s + 6.374)}{(s^2 + 1.224s + 6.405)(s^2 + 2.593s + 9.28)} \tag{4.52}$$

and the result of position control is shown in Figure 4.10, as the controller is listed as follows

$$K(s) = \frac{2.2243 \times 10^{12} (s + 1.112 \times 10^4)(s + 20)(s^2 + 0.3835s + 1.377)}{(s + 2 \times 10^9)(s^2 + 0.1242s + 0.4791)(s^2 + 1.516s + 5.15)} \times \frac{(s^2 + 2.112s + 6.961)(s^2 + 1.218s + 6.357)}{(s^2 + 1.224s + 6.405)(s^2 + 2.589s + 9.246)} \tag{4.53}$$

From both figures it can be clearly observed that signals are well synchronised and the responses are close to those in the original structure, in accordance with the results of section 4.5.

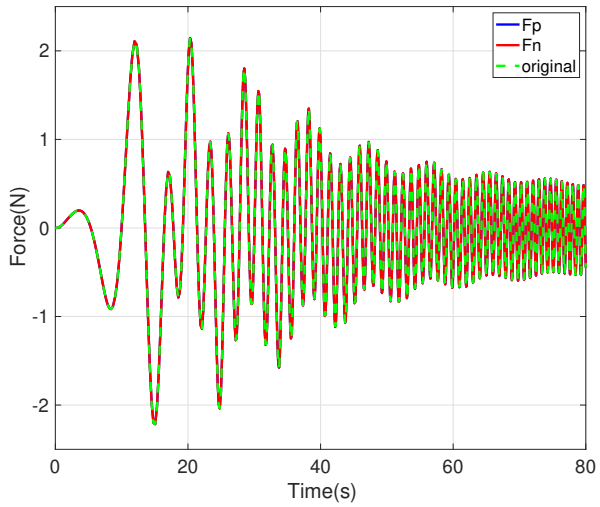

Figure 4.9: Results obtained for complex structure with force control in the Type 1 decomposition.

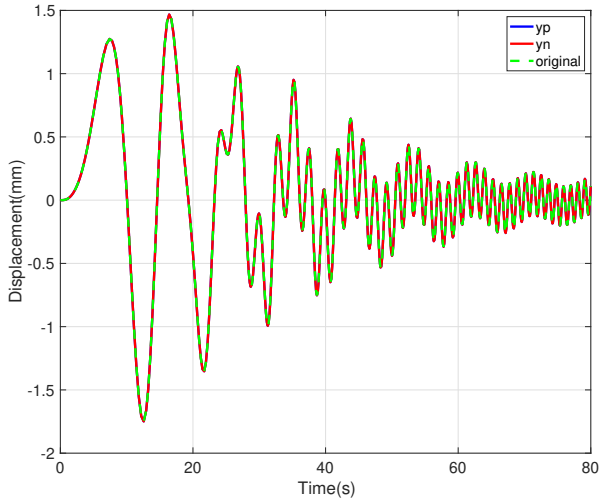

Figure 4.10: Results obtained for complex structure with position control in the Type 1 decomposition.

Chapter 5

Novel Control Architecture for Mass Split Decomposition

Literature covering the topic of DSS or hybrid testing with marginally stable substructures is scarce, as this is a challenging task. Moreover, even the limited available research requires accurate tuning and complex algorithms to achieve DSS synchronisation, with ad-hoc approaches suitable only for specific models. In order to provide a more generic and easier solution, a mass split decomposition is considered in this chapter as a benchmark system for a marginally stable substructure. The benefit of mass split decomposition is that part of the component can be physically tested while the remainder can be numerically simulated, which is helpful in structural dynamics and other aspects such as the design of vehicle. This chapter discusses the issues arising when designing a control strategy for DSS with marginally stable substructure, the shortfalls of current techniques are highlighted and a novel architecture is proposed to overcome such shortfalls.

5.1 Structural Decomposition

The original structure considered in this chapter is same as the one shown in Figure 3.1. After the decomposition, l-th mass is split into two substructures, resulting in the structure shown in Figure 5.1 . Then the following conditions hold

$$\begin{cases} m_{l1} + m_{l2} = m_l \\ m_{l1} m_{l2} \neq 0 \end{cases} \tag{5.1}$$

The difference is that, in this case, at odds with previous examples, the synchronised signal can only be the internal force, which means both S_1 and S_2 are forces (which are equal in traditional DSS), and the error can only between displacements and their derivatives.

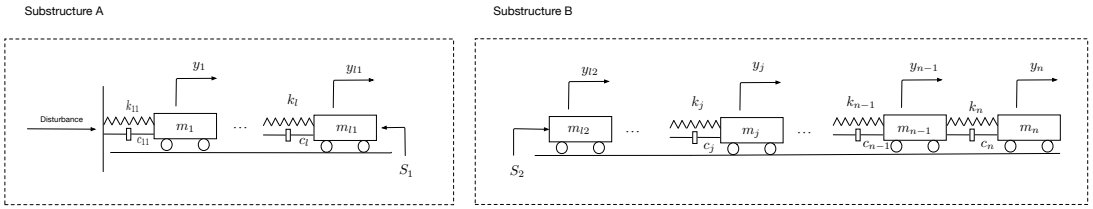

Figure 5.1: Schematics for DSS decomposition for a generic lumped parameter vibration problem, where the interface is placed across mass l.

5.2 Control Design Challenges and Proposed Methodology

In this section the control challenges introduced by the marginal stability of substructure B are discussed and then a control architecture to address these challenges is proposed.

5.2.1 Time Domain Analysis

As proved by the analysis in Chapter 4, the original system and substructure A are stable, while substructure B is only marginally stable. Therefore, the transfer functions in

substructure A and substructure B can be rearranged as

$$\begin{aligned} y_{l1}(s) &= \left(\frac{A_{1(1)}}{s + a_{1(1)}} + \frac{A_{1(2)}}{s + a_{1(2)}} + \cdots + \frac{A_{1(2l)}}{s + a_{1(2l)}} \right) d - \\ &\quad - \left(\frac{A_{2(1)}}{s + a_{1(1)}} + \frac{A_{2(2)}}{s + a_{1(2)}} + \cdots + \frac{A_{2(2l)}}{s + a_{1(2l)}} \right) F \\ y_{l2}(s) &= \left(\frac{B_1}{s} + \frac{B_2}{s^2} + \frac{B_3}{s + a_{2(3)}} + \cdots + \frac{B_{2(n-l+1)}}{s + a_{2[2(n-1+1)]}} \right) F \end{aligned} \tag{5.2}$$

where $a_{1(i)}$ and $a_{2(i)}$ have negative real parts.

According to (5.2) $y_{l1}(s)$ always shows a bounded response for bounded inputs, whereas the first two terms in (5.2) imply that unbounded responses can be exhibited by substructure B even in presence of bounded inputs given that B_1 and B_2 are not zero. In the time domain, this implies that the response of substructure B can include an offset and a drift, i.e.

$$\begin{aligned} y_{l1} &= y_1^*(t) \\ y_{l2} &= y_2^*(t) + C_1 t + C_2 \end{aligned} \tag{5.3}$$

where $y_1^*(t)$ and $y_2^*(t)$ are the components of the time domain response due to the external excitation, and C_1 and C_2 depend on the terms B_1 and B_2 in equation (5.2)

It can be observed that y_{l2} exhibits a linear drift and become unbounded $\big($when F is bounded and stable or marginally stable (poles at the imaginary axis but not at the origin)$\big)$, while $y_2^*(t)$ is always bounded. Moreover, when F has poles at the origin or unstable, y_{l2} may also exhibit nonlinear drifts. It should also be noted that if F is unbounded, then y_{l1} will be unbounded and nonlinear drifts may also be included. It is also worth noting that velocities in substructure B may drift, except when F is stable or has poles on the imaginary axis but not at the origin. Accelerations in both substructures are always bounded if F is bounded, as well as displacements and velocities in substructure A.

5.2.2 Challenges using Traditional Control Framework with Displacements as Synchronised Signal

As demonstrated in section 5.2.1, all displacements in substructure B can drift and become unbounded even for bounded inputs, hence it is dangerous to physically test substructure B in practice, although this is possible in theory. Therefore, it is beneficial to have substructure B tested numerically, to avoid potential damage to the physical substructure. When substructure B only has single degree of freedom and a carefully tuned controller is designed [54, 56, 108], substructure B can be physically tested, but this does not generalise to systems with multiple DoF. According to this approach, y_{l2} and its derivatives are the numerical signals, whereas, y_{l1} and its derivatives are the physical signals. In a successful DSS decomposition, y_{l2} and its derivatives should be equal to y_{l1} and its derivatives. The error based feedback controller shown in Figure 5.2 is a natural choice to attept achieving synchronisation, where $K(s)$ is the feedback controller which adjusts the magnitude of the internal force F in order to minimise the error $e(t)$.

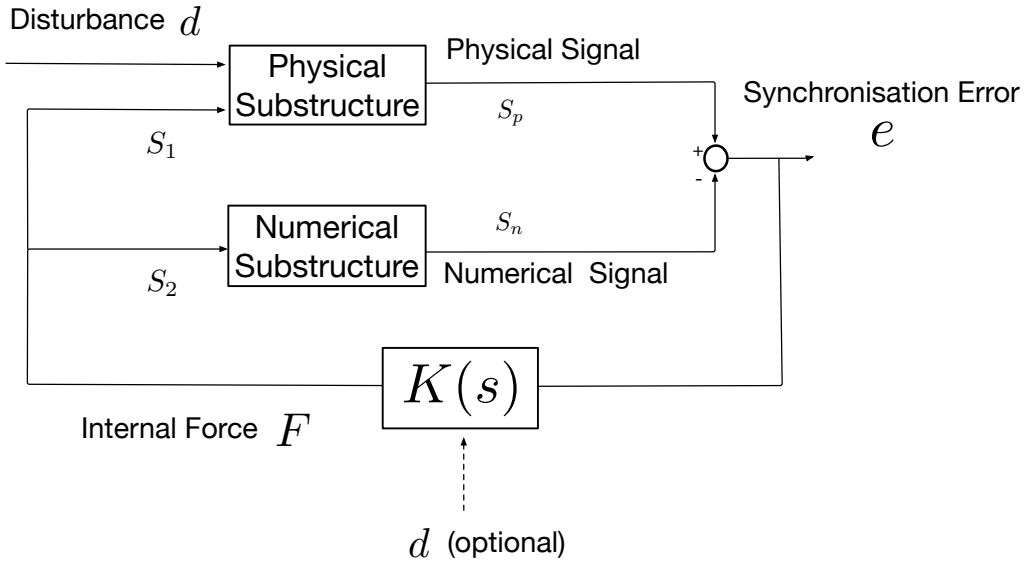

Figure 5.2: Traditional feedback control plant for mass split models

In traditional DSS position control design [56] the synchronisation error refers to positions at the interface, i.e. $e(t) = y_{l1}(t) - y_{l2}(t)$. However, the presence of a marginally stable system (substructure B in this case) implies that the error e can be unbounded due to the terms C_1 and C_2 in (5.2), and two cases need to be considered. In the first case, the controller $K(s)$ is unable to eliminate the divergence of error e - i.e. it does not contain a term s^2 at the numerator - and therefore the internal force F will become unbounded as well, inducing drifts or divergence in both y_{l1} and y_{l2}. Clearly, in this case the DSS closed-loop performance is very different from the original original structure, which always shows bounded response to bounded disturbances d. Moreover, an unbounded y_{l1} and F will lead to damage in the experimental apparatus used in substructure A. Another option is to design the controller $K(s)$ so that it is able to eliminate the divergence of e - i.e. it contains a term s^2 at the numerator - and therefore the internal force F is bounded. However, due to the term C_1 in (5.3), y_{l2} can still be drifting unbounded. The same procedure can be used to show that the same issues arise whenever position-related signals are used as controller inputs. Therefore, the strategy of synchronising positions that is at the root of the most of DSS position control strategies is not suitable in presence of a marginally stable substructure, such as in the mass-split case considered here. In this situation, no control strategy can make the DSS closed-loop response equal to the original system response for every combination of initial conditions and disturbances.

5.2.3 Proposed Control Architecture

In order to overcome this drawback, the following solution is proposed in this thesis: replace displacements with velocities in $e(t)$ and add a local stabilising controller to substructure B. In fact, according to Equation (5.3), velocities at the interface can be written as

$$\begin{aligned} \dot{y}_{l1} &= \dot{y}_1^*(t) \\ \dot{y}_{l2} &= \dot{y}_2^*(t) + C_1 \end{aligned} \tag{5.4}$$

Note that, at odd with (5.3), all the quantities in (5.4) are bounded when F is stable or marginally stable (poles on the imaginary axis but not at the origin), therefore the controller only needs to eliminate the offset C_1 and ensure that the forced responses $\dot{y}_1^*$ and $\dot{y}_2^*$ converge towards each other. This can be easily achieved by having a common factor s in the numerator of the feedback controller transfer function, for example. This is a much simpler control design task, as the controller does not have to deal with potentially unbounded drifts in neither $F(t)$ nor $e(t)$. Note also that a similar principle can be applied to synchronise the error between accelerations, as $\ddot{y}_{l2}$ is stable, therefore, the acceleration based synchronisation is similar to the standard DSS or hybrid testing. However, using acceleration as synchronised signal means that all signals including accelerations, velocities and displacements should be monitored compared with the proposed velocity synchronisation, which only requires to monitor velocities and displacements. Therefore, the first proposed modification to the control strategy depicted in Figure 5.2 is the replacement of position with velocity when calculating the synchronisation error $e(t)$, i.e. setting $e(t) = \dot{y}_1(t) - \dot{y}_2(t)$.

After having replaced positions with velocities and having designed a controller based on this synchronisation error, the DSS behaviour can still differ from the original system response if C_1 is still present due to non-zero initial conditions in substructure B. In fact, in this case the controller response reads

$$F(s) = K(s)e(s) = K(s)\left(\dot{y}_{l1}(s) - \dot{y}_{l2}(s)\right) \tag{5.5}$$

with $\dot{y}_{l1}$ and $\dot{y}_{l2}$ as in (5.4). Standard DSS controller design strategies will then derive $K(s)$ so that the forced responses $\dot{y}_1^*$ and $\dot{y}_2^*$ converge to each other. Indeed, techniques

such as Linear Substructuring Control (LSC, see [101]) are based on basically inverting the dynamics of the system to be controlled, therefore the controller will have a factor s at the numerator, indicating that the constant C_1 would be neglected. This implies that, if C_1 is not zero then a drift in y_{l2} would still occur. In fact, controller $K(s)$ is aimed at eliminating the error between velocities, and any minor offset in the cancellation of this error may translate to position drifts on a long timescale.

One way to solve this issue is to use other signals such as the combination of displacements and their derivatives, as well as the disturbance, instead of the error e as the input for the feedback controller. However, this would require a radical change in the control design approach used for these systems. Therefore, the methodology proposed here is based on relaxing the constraint $|S_1| = |S_2|$, i.e. on allowing the numerical force to be different from the physical force generated by the actuator in the physical substructure. Relaxing this constraint makes substructure A and substructure B partially decoupled, enabling accurate control in absence of potential drifts, as will be shown for the benchmark example considered in the next section. The resulting control architecture is shown in Figure 5.3, where an additional local controller $K_2(s)$ is added in the numerical substructure to make it asymptotically stable. The action of such controller is then simply added to the output of the original velocity-based DSS controller. The numerator of $K_2(s)$ should be set as small as possible to ensure minimal effect on substructure B when e is equal to zero. Note that this architecture leaves complete freedom to the designer in terms of choosing the preferred control design for both the local stabilising controller and the overall DSS synchronisation controller, and does not require any accurate tuning to achieve synchronisation.

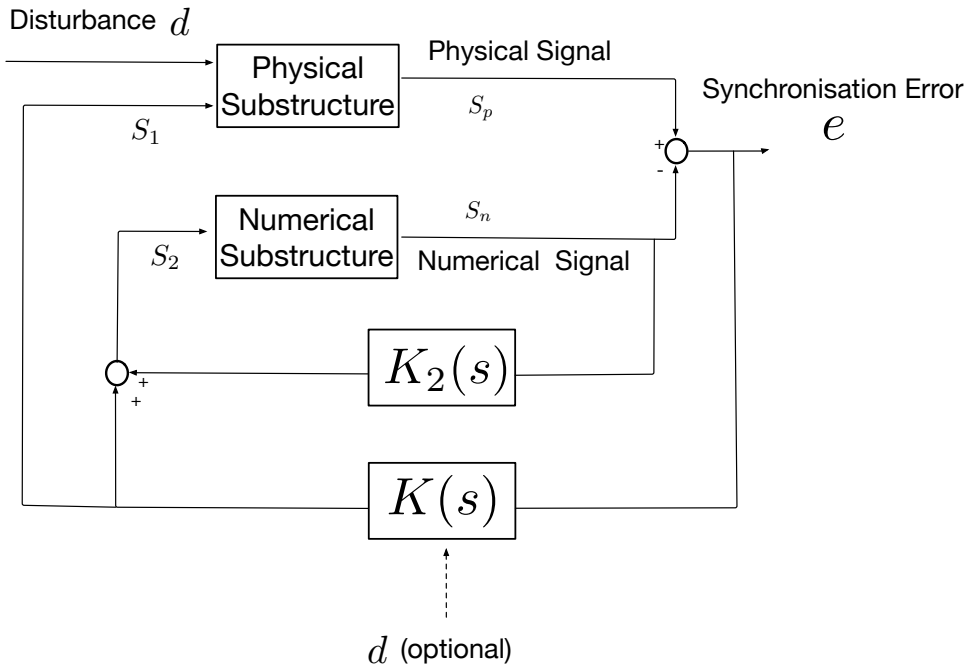

Figure 5.3: Proposed feedback control scheme with extra stabiliser for marginally stable DSS

Another, even simpler, alternative for solving the problem of potential drifts is based on the observation that the occurrence of the problematic case $(C_1, C_2) \neq (0, 0)$ is due to the initial conditions of the numerical system not being zero. However, very often, setting values for such initial conditions is under complete control of the user performing hybrid testing. Therefore, whenever possible, the initial conditions of substructure B should be set to zero so that the additional local stabilising controller may become superfluous (although its presence still makes the control architecture more robust).

5.3 Numerical Example

In this section a five mass-spring-damper system is used to both highlight the challenges related to DSS control of marginally stable structures and to demonstrate the effectiveness of

the control architecture proposed in section 5.2. Parameters used for simulation are listed in Table 5.1, corresponding to natural frequencies $f_n = (0.0730, 0.1965, 0.3073, 0.3941, 0.4514)$ Hz. The disturbance $d(t)$ is a chirp signal in which the frequency increases from $0Hz$ to $0.5Hz$ over $45s$ and then is maintained constant for further $35s$, which is similar to the signal shown in Figure 4.3. The amplitude of the disturbance is fixed to $1mm$.

Table 5.1: Numerical values of parameters used for simulation examples

Index	Mass m_i	Stiffness k_i	Damping c_i
1	$500kg$	$1200N/m$	$300Ns/m$
2	$470kg$	$1100N/m$	$290Ns/m$
3	$440kg$	$1000N/m$	$280Ns/m$
4	$410kg$	$900N/m$	$270Ns/m$
5	$380kg$	$800N/m$	$260Ns/m$

The third mass will be split into two masses and parameters are listed as follows

$$\begin{cases} m_{31} = 0.6m_3 = 264kg \\ m_{32} = 0.4m_3 = 176kg \end{cases} \tag{5.6}$$

At the start, the initial conditions in both substructures are different. In substructure B the initial conditions of the leftmost mass are not equal to zero, while in substructure A the initial conditions for m_{31} are not equal to zero as well, i.e.

$$\begin{cases} y_{31} = 1mm \\ \dot{y}_{31} = 0.7mm/s \\ y_{32} = 0.5mm \\ \dot{y}_{31} = 0.2mm/s \end{cases} \tag{5.7}$$

At first the linear substructring controller (LSC) [52] is used to control the whole system with $e = \dot{y}_{31} - \dot{y}_{32}$. LSC is a feedforward plus feedback control scheme introduced in Chapter 2, where the control input reads $u(s) = K_d(s)d(s) + K_e(s)e(s)$. To design the feedforward gain $K_d(s)$ and the feedback gain $K_e(s)$, the error and the actuator dynamics are written as

$$e(s) = G_d(s)d(s) - G_2F'(s) = G_d(s)d(s) - G_u u(s) \tag{5.8}$$

$$F(s) = S_1(s) = \frac{b}{s+a}u(s) \tag{5.9}$$

For the purpose of the numerical example considered here, the actuator dynamics parameters were set to $a = b = 10$. The feedforward gain then reads [52]

$$\begin{aligned} K_d(s) &= \frac{G_d(s)}{G_u(s)} \\ &= \frac{4.1464s^2(s+10)(s+4)(s+3.793)}{(s^2+0.05669s+0.2106)(s^2+0.4385s+1.525)(s^2+1.081s+3.74)} \\ &\times \frac{(s+3.571)(s^2+0.9769s+3.052)(s^2+2.534s+8.311)}{(s^2+1.781s+6.162)(s^2+2.262s+7.969)} \end{aligned} \tag{5.10}$$

whereas the feedback gain $K_e = 10$ was determined using root loci methods. Note that, as shown in Figure 5.4 the displacement in substructure B grows unbounded, as the traditional controller is not able to eliminate the divergence of displacements and the offset of velocities in marginally stable substructures, in accordance with the analysis of section 5.2.

LSC is then used to control S_1 while a proportional integral (PI) controller is added to stabilise the substructure B and control S_2, as well as eliminating the offset between displacements. In this case, the proportional gain was set to $k_p = 50$, whereas the integral gain was set to $k_I = 25$. Note that this choice of parameters ensure that the amplitude response of the controller K_2 is much smaller than the amplitude of the frequency response

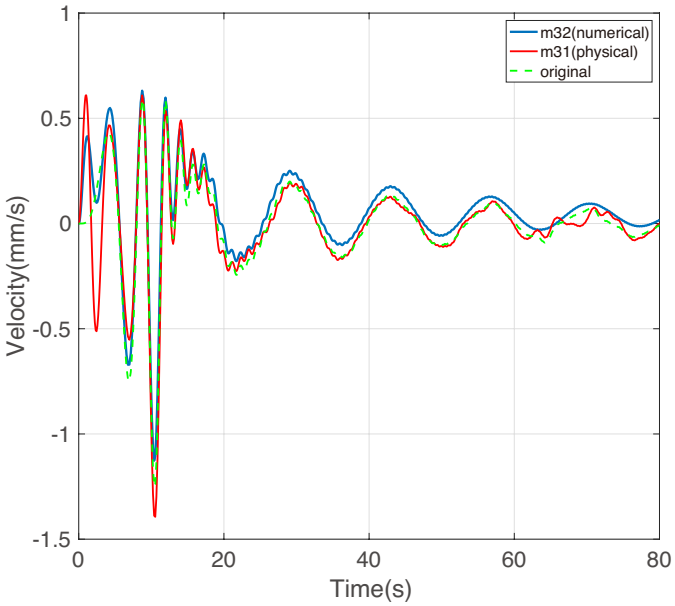

(a)

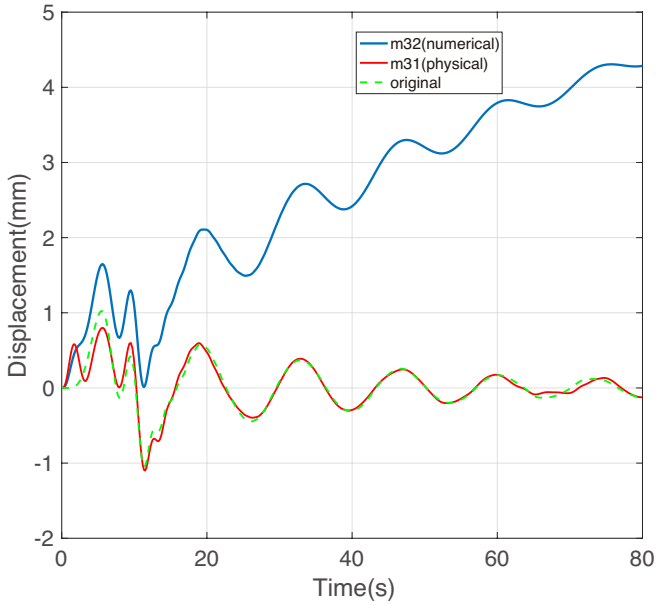

(b)

Figure 5.4: Velocities (a) and displacements (b) at the interface obtained with the traditional control architecture of Figure 5.2 with $e = \dot{y}_{31} - \dot{y}_{32}$ and non-zero initial conditions.

of substructure B, therefore the dynamic response of this latter is minimally influenced by the controller. Figure 5.5 shows that the proposed control architecture is capable of synchronising the DSS decomposition. In addition, exact tuning of the PI gains is not required and any stabilising PI controller provides very similar results. It is also advised to use small gains to minimise the effect of the PI controller on the response of substructure B in closed-loop, as demonstrated in the simulation.

Finally in substructure B all initial conditions are set to zero while in substructure A remains the same. Only LSC is used to eliminate the error. Figure 5.6 shows that the response is convergent in this case.

These results highlight that, when substructure B has non-zero initial conditions, a traditional DSS control design approach is not capable of eliminating the drift in substructure B. The proposed control architecture addresses such issue by adding an extra stabilising local controller in substructure B only, which makes the overall closed-loop response close to the original system response, with a minimal extra effort due to the tuning of the additional controller. Note that, in all cases, non-zero initial conditions for substructure A do not affect synchronisation performance, as substructure A is asymptotically stable. On the other hand, initial conditions for substructure B play a key role. In fact, if the users have the power of setting all such conditions to zero before starting the hybrid testing, then the additional local controller $K_2(s)$ of Figure 5.3 may not not needed, as the response of substructure B can track the response of the original system by using the DSS controller $K(s)$ only.

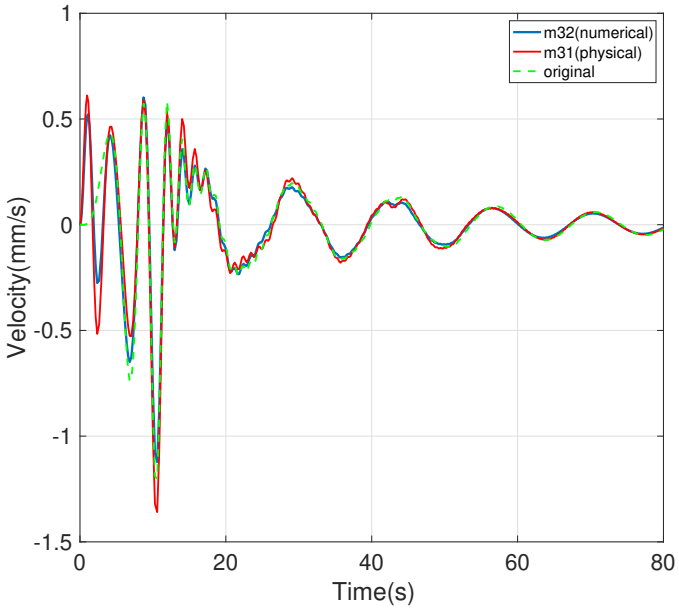

(a)

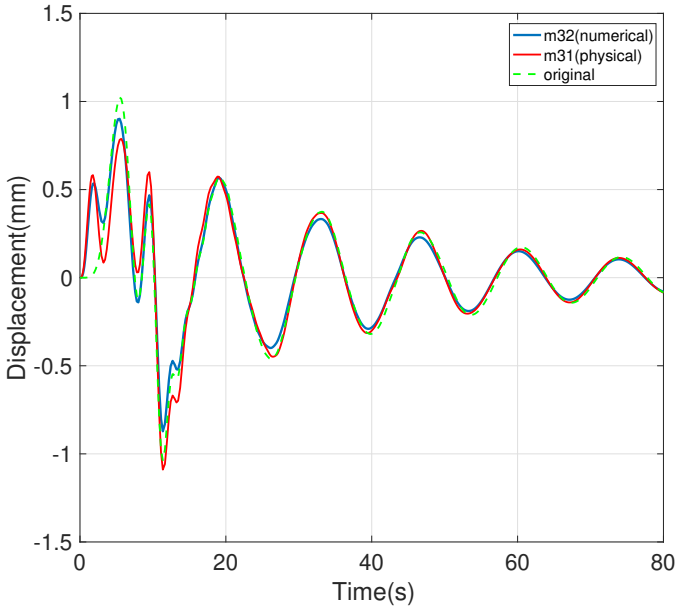

(b)

Figure 5.5: Velocities (a) and displacements (b) at the interface obtained with the proposed control architecture of Figure 5.3 with $e = \dot{y}_{31} - \dot{y}_{32}$, non-zero initial conditions and a stabilising PI local controller for substructure B.

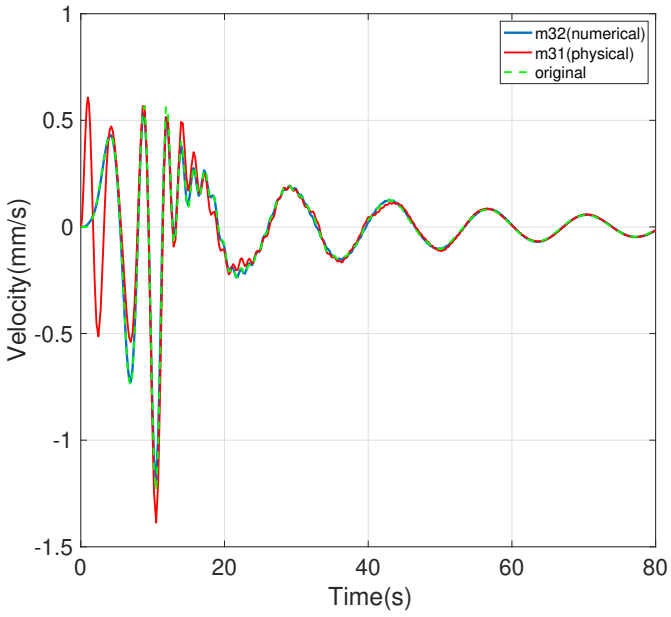

(a)

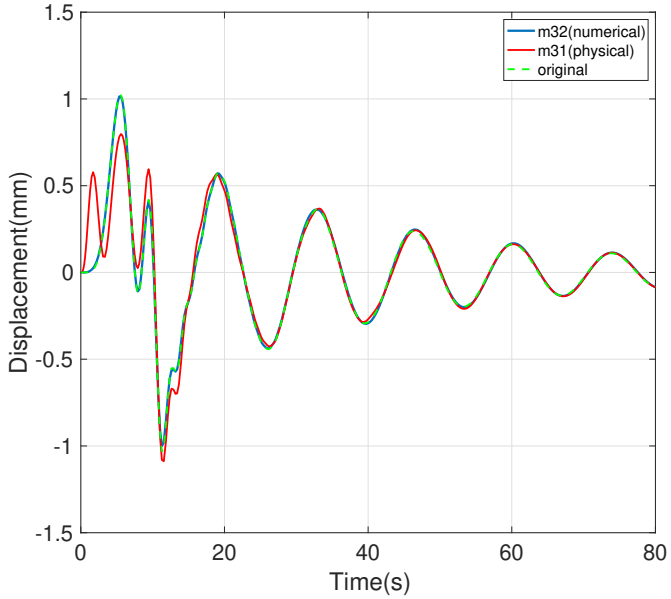

(b)

Figure 5.6: Velocities (a) and displacements (b) at the interface obtained with the traditional control architecture of Figure 5.2 with $e = \dot{y}_{31} - \dot{y}_{32}$, when the user can set the initial conditions of substructure B to zero.

Chapter 6

DSS Testing of Supported Beam with Beam Split

As introduced in Chapter 5, the proposed novel control architecture can significantly reduce the difficulty of DSS synchronisation when a marginally stable substructure is included. In order to expand the applications of the proposed control architecture to more complex structures, a rigid beam is selected for the demonstration in this chapter. A novel decomposition aimed at reducing the required degrees of freedom in the physical substructure is introduced, to show how potential applications can be tackled with the proposed control architecture.

6.1 Beam Structure and Its Decomposition

The structure considered in this chapter is a rigid beam supported at its ends by two elastic supports represented by mass-spring-damper systems. Such structure is shown in Figure 6.1. It is considered as a concept demonstration, aimed at showing that DSS can be applied to a broader family of structures and decomposition strategies, thanks to the novel control

architecture proposed in Chapter 5. The beam will be decomposed at its centre of gravity, with the left part tested physically and the right part tested numerically. Moreover, in the physical substructure the rotational degree will be removed to simplify experimental setup, although the goal of DSS will be to make the interface move as if the rotational degree of freedom is present. Note that the right substructure is a marginally stable system like the one considered in Chapter 5. Although a similar decomposition was proposed in [109], the main focus there was on the finite element model (FEM).

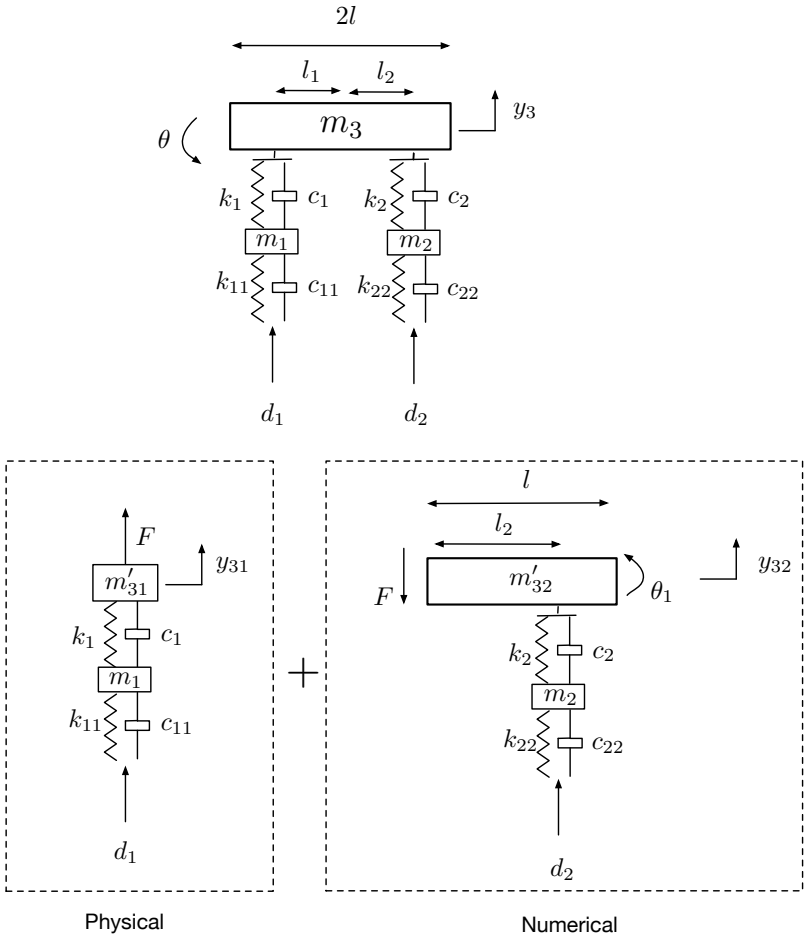

Figure 6.1: Beam structure(top) and its decomposition with beam split(bottom)

The equation of motion of the original system can be written as

$$\begin{cases} m_3\ddot{y}_3 = -k_1(y_3 - \theta l_1 - y_1) - c_1(\dot{y}_3 - \dot{\theta} l_1 - \dot{y}_1) - k_2(y_3 + \theta l_2 - y_2) - c_2(\dot{y}_3 + \dot{\theta} l_2 - \dot{y}_2) \\ I\ddot{\theta} = k_1(y_3 - \theta l_1 - y_1)l_1 + c_1(\dot{y}_3 - \dot{\theta} l_1 - \dot{y}_1)l_1 - k_2(y_3 + \theta l_2 - y_2)l_2 - c_2(\dot{y}_3 + \dot{\theta} l_2 - \dot{y}_2)l_2 \\ m_1\ddot{y}_1 = k_1(y_3 - \theta l_1 - y_1) + c_1(\dot{y}_3 - \dot{\theta} l_1 - \dot{y}_1) - k_{11}(y_1 - d_1) - c_{11}(\dot{y}_1 - \dot{d}_1) \\ m_2\ddot{y}_2 = k_2(y_3 + \theta l_2 - y_2) + c_2(\dot{y}_3 + \dot{\theta} l_2 - \dot{y}_2) - k_{22}(y_2 - d_2) - c_{22}(\dot{y}_2 - \dot{d}_2) \end{cases} \tag{6.1}$$

where d_1 and d_2 are disturbances acting at the supports, y_1, y_2 and y_3 are the vertical displacement of m_1, m_2 and m_3, respectively and θ is the rotational angle of the beam. The equation of motion for the decomposed structure can be written as

$$\begin{cases} m'_{32}\ddot{y}_{32} = -k_2[y_{32} + \theta_1(l_2 - l/2) - y_2] - c_2[\dot{y}_{32} + \dot{\theta}_1(l_2 - l/2) - \dot{y}_2] - F \\ I_1\ddot{\theta} = -k_2[y_{32} + \theta_1(l_2 - l/2) - y_2](l_2 - l/2) \\ \qquad - c_2[\dot{y}_{32} + \dot{\theta}_1(l_2 - l/2) - \dot{y}_2](l2 - l/2) + Fl/2 \\ m'_{31}\ddot{y}_1 = -k_1(y_{31} - y_1) - c_1(\dot{y}_{31} - \dot{y}_1) + F \\ m_1\ddot{y}_1 = k_1(y_{31} - y_1) + c_1(\dot{y}_{31} - \dot{y}_1) - k_{11}(y_1 - d_1) - c_{11}(\dot{y}_1 - \dot{d}_1) \\ m_2\ddot{y}_2 = k_2[y_{32} + \theta_1(l_2 - l/2) - y_2] + c_2[\dot{y}_{32} + \dot{\theta}_1(l_2 - l/2) - \dot{y}_2] \\ \qquad - k_{22}(y_2 - d_2) - c_{22}(\dot{y}_2 - \dot{d}_2) \end{cases} \tag{6.2}$$

where I_1 is the moment of inertia of m'_{32}, y_{31} and y_{32} are the vertical displacement of m'_{31} and m'_{32} respectively.

Table 6.1: Numerical values of parameters used for simulation

Description	Symbols	Value
Mass of original beam	m_3	$400kg$
Moment of inertia of original beam	I	$66.67kgm^2$
Mass of left split mass	m'_{31}	$200kg$
Mass of right split mass	m'_{32}	$200kg$
Moment of inertia of right split beam	I_1	$16.67kgm^2$
Mass of left sprung mass	m_1	$30kg$
Mass of left sprung mass	m_2	$30kg$
Stiffness of left upper spring	k_1	$1600N/m$
Stiffness of right upper spring	k_2	$1500N/m$
Stiffness of left lower spring	k_{11}	$700N/m$
Stiffness of right lower spring	k_{22}	$800N/m$
Damping of left upper damper	c_1	$80Ns/m$
Damping of right upper damper	c_2	$80Ns/m$
Damping of left lower damper	c_{11}	$50Ns/m$
Damping of right lower damper	c_{22}	$50Ns/m$
Half of the original beam length	l	$1m$
Distance from left support to centroid of beam	l_1	$0.6m$
Distance from left support to centroid of beam	l_2	$0.7m$

6.2 Controller Design and Numerical Results

The values of parameters used for simulation are listed in Table 6.1, corresponding to the natural frequencies of the original systems f_n=$(0.2382, 0.2794, 1.4417, 1.4547)Hz$ and the motion of centre of gravity (situated at the DSS interface) is targeted signal for the synchronisation, thus

$$\begin{cases} \dot{y}'_{32} = \dot{y}_{32} - \dfrac{\dot{\theta}_1 l}{2} \\ e = \dot{y}_{31} - \dot{y}'_{32} \end{cases} \tag{6.3}$$

where the synchronisation error $e(t)$ has been defined in terms of velocity, in accordance with the analysis of Chapter 5.

For the purpose of the numerical simulations discussed below, d_1 is a swept sinusoidal wave whose frequency increases from $0Hz$ to $2Hz$ during he first 50 seconds, with a constant amplitude of $8mm$ which is shown in Figure 6.2a. As for d_2, the frequency increases from 0 Hz to 1.8 Hz during the first 45 seconds, with a constant amplitude of $10mm$ which is shown in Figure 6.2b. Note that in this case the goal is to make the vertical displacement of the physical substructure behave as if the rotational freedom was still present.

In the setup considered here, the traditional LSC control procedure would provide a non-causal controller. Therefore, an $\boldsymbol{H}_\infty$ controller was designed to minimise the synchronisation error $e(t)$, to ensure the output is bounded, meaning the state space form is required as described in Chapter 2, with the objective function defined $\frac{||e||^2}{||d_1||^2+||d_2||^2}$. Then the controller can be obtained by using MATLAB and the calculation can refer to Chapter 2, as factors such as sensitivity, weighting factors and uncertainty are not considered at this stage. Note that the details of the controller are listed in appendix B.

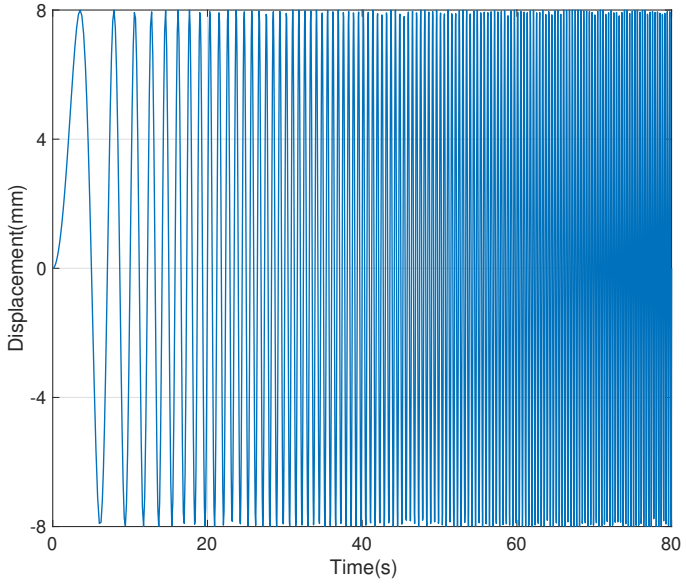

(a)

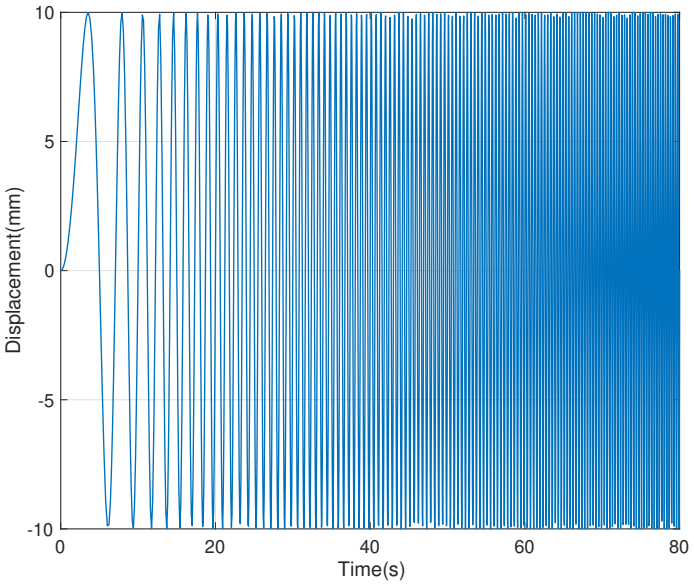

(b)

Figure 6.2: Disturbance d_1 (a) and disturbance d_2 (b) .

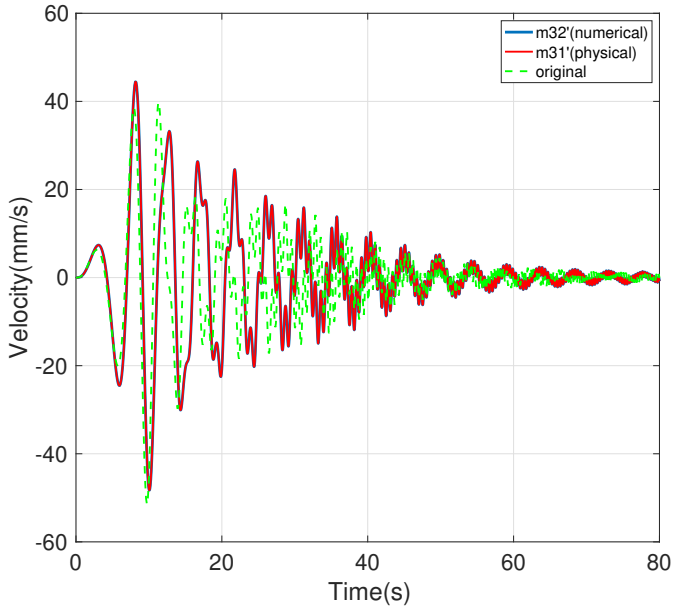

(a)

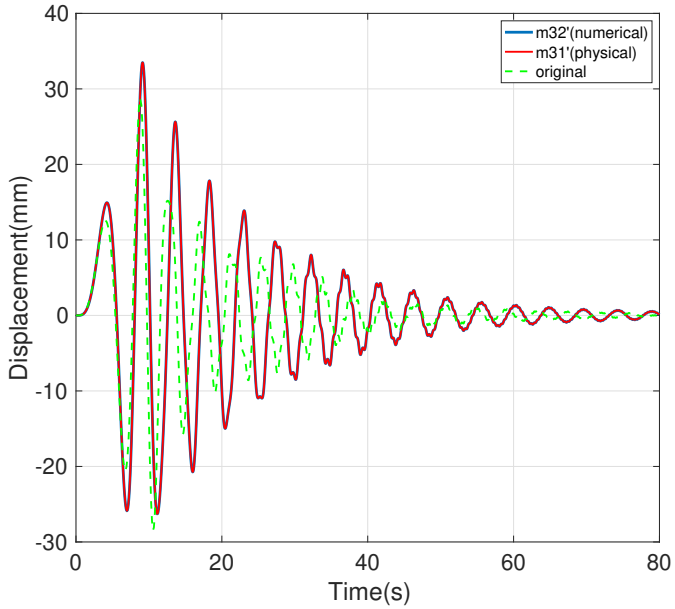

(b)

Figure 6.3: Velocities (a) and displacements (b) of beam system based on single $\boldsymbol{H}_\infty$ control objective for error elimination.

Figure 6.3 shows the behaviour of the decomposed structure. Both displacements and velocities can be synchronised and there is no drift of displacement in the numerical substructure. However, the overall response of the decomposed structure is significantly different from the response of the original structure, in particular there is a phase difference in the response of both velocities and displacements, and amplitudes are different compared with the original response. This is due to the controlled force F overreacting in the effort of minimising $e(t)$.

In order to overcome this issue and reduce the amplitudes, the internal force F is also targeted for the minimisation by defining the control objective $\frac{||e||^2+||F||^2}{||d_1||^2+||d_2||^2}$. The results shown in Figure 6.4 demonstrate that the physical substructure response is close to the original system, while the numerical substructure response is not synchronised with the physical substructure. Once again, the details of the controller are listed in appendix B.

In order to solve the synchronisation issue an extra stabiliser can be added according to the novel control architecture proposed in section 5.2. A proportional integral derivative (PID) controller is therefore added in the numerical substructure, with the velocity error as the input, and the proportional gain $k_p = 200$, the integral gain $k_I = 20$ and the derivative gain $k_d = 10$, resulting in a control architecture similar to Figure 5.3. Figure 6.5 shows that synchronisation of displacements can be achieved by adding an extra local controller and both substructures respond as in the original beam, proving that the concept is implementable in reality. However, the velocity tracking in the numerical substructure at the high frequency range is not as good as it is at the lower frequency range. Solving this issue is beyond the scope of this thesis, with suggestions on how to achieve this discussed in Chapter 2.

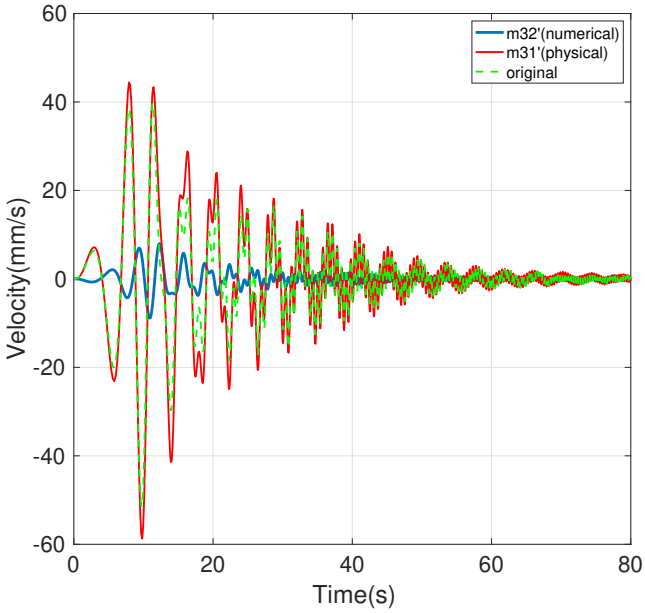

(a)

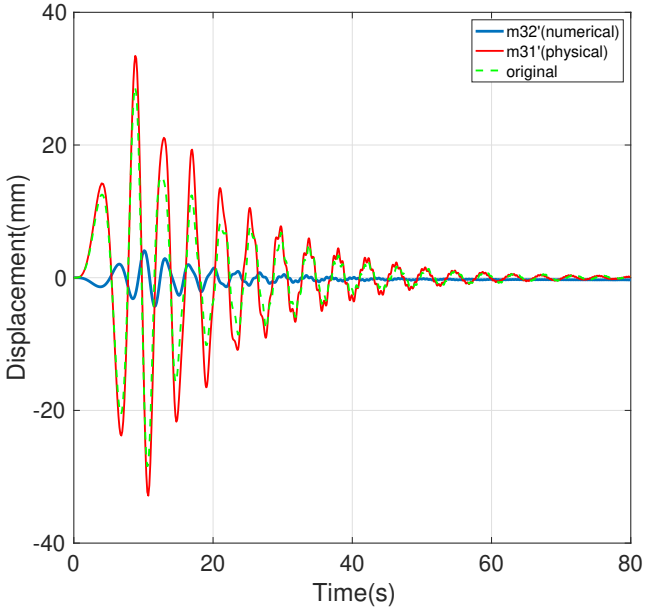

(b)

Figure 6.4: Velocities (a) and displacements (b) of beam system based on double $\boldsymbol{H}_\infty$ control objective for error elimination and minimal control effort.

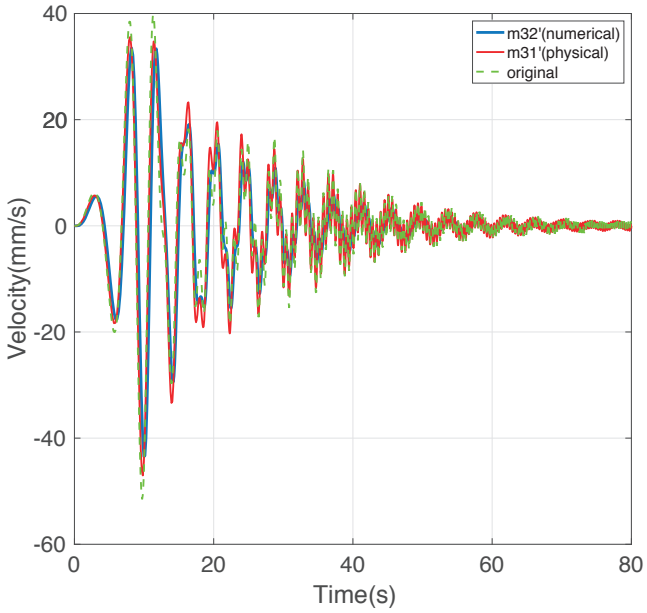

(a)

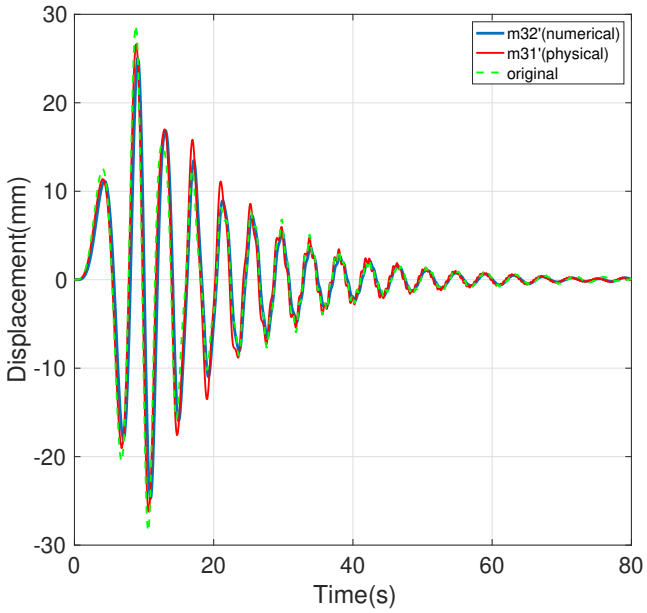

(b)

Figure 6.5: Velocities (a) and displacements (b) of beam system based on double $\boldsymbol{H}_\infty$ control objective for error elimination and minimal control effort with extra PID controller.

Chapter 7

Conclusions and Future Work

The main aim of this thesis was to derive generic conditions for feasibility of control design in DSS hybrid testing, including decomposition strategies that have received little attention in the literature so far. In particular, a generic procedure for DSS control design has been proposed by analysing the generic vibrating structure and relative properties of DSS decomposition strategies, which helps to analyse the different structures based on standard steps. The key is the recursive form of generalised transfer functions of the generic vibrating structure. In fact, it is usually difficult to obtain the fully explicit symbolic expression of the transfer functions needed for DSS control design, but the proposed recursive form allows for a simplified analysis. For example, the relative degree of numerators and denominators can be easily obtained thanks to this formulation, thus the causality analysis can be performed for different DSS decompositions without using any system parameters. Controllability and observability analysis can be made by proving that in each transfer function there are no common roots between the numerators and the denominators. The proof was completed with the help of the implicit expressions for the coefficients in the transfer functions. For underdamped original structures it is shown that they are always

controllable and observable, whereas some extra conditions need to be satisfied for other types of structures. For DSS, extra explicit conditions have been proposed, in addition to those derived for the original structure.

Another major contribution of this thesis is the proposal of a control architecture for DSS testing of structures where the interface splits a mass, a problem that has been largely neglected by the literature. In fact, DSS or hybrid testing with split mass substructures often does not provide satisfactory performance. Researchers developed different controllers to try to solve this problem, but these controllers are only suitable for the specific models they were considering, with significant limitations on real world application. In addition, the vast majority of researches available in the literature focused on the synchronisation of displacements. In this thesis the inherent shortcoming of the traditional positional-error based controller is revealed by showing that, when choosing displacement as signal to be synchronised, the error can be unbounded. This fact, in turn, makes it difficult to achieve satisfactory synchronisation and this issue cannot be solved within the traditional control framework. Furthermore, the analysis presented in this thesis also reveals that the velocities in both substructures are bounded, meaning that, compared with the synchronisation of displacements, it is much easier to achieve the synchronisation of velocities. Using velocities to calculate the synchronisation error ensures the elimination of displacement drifts in the marginally stable substructure, although an extra controller might be required to achieve asymptotic stability. The comprehensive guidance to control the mass split structures observed here provides an efficient solution to this type of problems, without requiring researchers to focus on the specific models anymore.

For the future work the focus can be on the physical tests to more complex structures, as the concept of beam split proposed in Chapter 6 can be experimentally validated at first. The proposed results in this thesis also open the possibility for further work in this

area. For example, extension to nonlinear systems such as beam split with large angular displacement, can be investigated to study how nonlinearity can affect the performance of DSS controllers. In addition, the proposed extension to traditional DSS control design can also enable more complex components to be tested, for example, MR dampers, would be interesting given the wide use of such components in the construction and automotive industry. Furthermore, the use of the H_∞ control framework as in Chapter 6 enables control designers to obtain a priori bounds on the transmission of disturbances across the feedback loop. Therefore, the combination of using H_∞ controllers in nonlinear systems can be implemented. Many scenarios can be included, for example, the design of a building equipped with MR damper to resist the unknown input with the help of DSS, which is helpful to reduce the structural damage during earthquakes. Moreover, a vehicle equipped with MR damper can be designed with the help of DSS, in order to improve the handling and comfort on different terrains. Other potential scenarios include the application of the proposed control architecture to other types of structures, apart from the beam shown in Chapter 6. More complex models with marginally stable substructures and the reduction of degrees of freedom can be tested at a significantly reduced level of difficulty. Finite element models can also be selected as another potential application, to accurately analyse the structure with complex boundary conditions, especially when the marginally stable substructure is included. In addition, delay is also another interesting direction for future research, as there is no generic approach to analyse the effect of delay on DSS behaviour. Ideally, potential applications and analysis approaches should start from the simple systems to develop and test the methodology and then gradually scale it to a generic approach to simplify the analysis of complex systems. Moreover, as shown in Equation (3.34), analytical solutions for individual natural frequencies are relatively straightforward to obtain and the recursive formulation show how characteristic polynomials are multiplied. Therefore it

would be interesting to explore if this allows for an analytical derivation of the natural frequencies of the whole system. This would in turn enable the analysis of how the system parameters and degrees of freedom affect the DSS natural frequencies, which would be helpful to better design test rigs.

References

[1] D. P. Stoten, J.-Y. Tu, and G. Li, "Adaptive control of generalised dynamically substructured systems," *IFAC Proceedings Volumes*, vol. 41, no. 2, pp. 14090–14095, 2008.

[2] J.-Y. Tu, D. P. Stoten, G. Li, and R. A. Hyde, "A state-space approach for the control of dynamically substructured systems," in *2009 IEEE Control Applications,(CCA) & Intelligent Control,(ISIC)*, pp. 1093–1098, IEEE, 2009.

[3] N. Terkovics, S. Neild, M. Lowenberg, R. Szalai, and B. Krauskopf, "Substructurability: the effect of interface location on a real-time dynamic substructuring test," *Proceedings of the Royal Society A*, vol. 472, no. 2192, p. 20160433, 2016.

[4] G. Li, "Dynamically substructured system frameworks with strict separation of numerical and physical components," *Structural Control and Health Monitoring*, vol. 21, no. 10, pp. 1316–1333, 2014.

[5] C. E. Silva, D. Gomez, A. Maghareh, S. J. Dyke, and B. F. Spencer Jr, "Benchmark control problem for real-time hybrid simulation," *Mechanical Systems and Signal Processing*, vol. 135, p. 106381, 2020.

[6] M. Nakashima, "Development, potential, and limitations of real–time online (pseudo–dynamic) testing," *Philosophical Transactions of the Royal Society of London. Series A: Mathematical, Physical and Engineering Sciences*, vol. 359, no. 1786, pp. 1851–1867, 2001.

[7] D. P. Stoten, "A comparative study and unification of two methods for controlling dynamically substructured systems," *Earthquake Engineering & Structural Dynamics*, vol. 46, no. 2, pp. 317–339, 2017.

[8] X. Ning, Z. Wang, H. Zhou, B. Wu, Y. Ding, and B. Xu, "Robust actuator dynamics compensation method for real-time hybrid simulation," *Mechanical Systems and Signal Processing*, vol. 131, pp. 49–70, 2019.

[9] G. Ou, A. I. Ozdagli, S. J. Dyke, and B. Wu, "Robust integrated actuator control: experimental verification and real-time hybrid-simulation implementation," *Earthquake Engineering & Structural Dynamics*, vol. 44, no. 3, pp. 441–460, 2015.

[10] C. Chen and J. M. Ricles, "Tracking error-based servohydraulic actuator adaptive compensation for real-time hybrid simulation," *Journal of Structural Engineering*, vol. 136, no. 4, pp. 432–440, 2010.

[11] Y. Chae, K. Kazemibidokhti, and J. M. Ricles, "Adaptive time series compensator for delay compensation of servo-hydraulic actuator systems for real-time hybrid simulation," *Earthquake Engineering & Structural Dynamics*, vol. 42, no. 11, pp. 1697–1715, 2013.

[12] B. Wu, Z. Wang, and O. S. Bursi, "Actuator dynamics compensation based on upper bound delay for real-time hybrid simulation," *Earthquake Engineering & Structural Dynamics*, vol. 42, no. 12, pp. 1749–1765, 2013.

[13] A. Najafi and B. F. Spencer Jr, "Adaptive model reference control method for real-time hybrid simulation," *Mechanical Systems and Signal Processing*, vol. 132, pp. 183–193, 2019.

[14] G. A. Fermandois, "Application of model-based compensation methods to real-time hybrid simulation benchmark," *Mechanical Systems and Signal Processing*, vol. 131, pp. 394–416, 2019.

[15] B. M. Phillips and B. F. Spencer Jr, "Model-based feedforward-feedback actuator control for real-time hybrid simulation," *Journal of Structural Engineering*, vol. 139, no. 7, pp. 1205–1214, 2012.

[16] C. Chen and J. M. Ricles, "Improving the inverse compensation method for real-time hybrid simulation through a dual compensation scheme," *Earthquake Engineering & Structural Dynamics*, vol. 38, no. 10, pp. 1237–1255, 2009.

[17] C. Chen, J. M. Ricles, T. M. Marullo, and O. Mercan, "Real-time hybrid testing using the unconditionally stable explicit cr integration algorithm," *Earthquake Engineering & Structural Dynamics*, vol. 38, no. 1, pp. 23–44, 2009.

[18] X. S. Gao and S. You, "Dynamical stability analysis of mdof real-time hybrid system," *Mechanical Systems and Signal Processing*, vol. 133, p. 106261, 2019.

[19] A. Maghareh, S. Dyke, S. Rabieniaharatbar, and A. Prakash, "Predictive stability indicator: a novel approach to configuring a real-time hybrid simulation," *Earthquake Engineering & Structural Dynamics*, vol. 46, no. 1, pp. 95–116, 2017.

[20] J. E. Carrion and B. F. Spencer Jr, "Model-based strategies for real-time hybrid testing," tech. rep., Newmark Structural Engineering Laboratory. University of Illinois at Urbana-Champaign, 2007.

[21] R. Christenson, Y. Z. Lin, A. Emmons, and B. Bass, "Large-scale experimental verification of semiactive control through real-time hybrid simulation," *Journal of Structural Engineering*, vol. 134, no. 4, pp. 522–534, 2008.

[22] R. Zhang and B. M. Phillips, "Cyber-physical approach to the optimization of semiactive structural control under multiple earthquake ground motions," *Computer-Aided Civil and Infrastructure Engineering*, vol. 34, no. 5, pp. 402–414, 2019.

[23] J. Shan, Y. Ouyang, and W. Shi, "Adaptive control of earthquake-excited nonlinear structures with real-time tracking on prescribed performance criteria," *Structural Control and Health Monitoring*, vol. 25, no. 10, p. e2247, 2018.

[24] T. Asai, C.-M. Chang, and B. Spencer Jr, "Real-time hybrid simulation of a smart base-isolated building," *Journal of Engineering Mechanics*, vol. 141, no. 3, p. 04014128, 2015.

[25] X. Shao, A. M. Reinhorn, and M. V. Sivaselvan, "Real-time hybrid simulation using shake tables and dynamic actuators," *Journal of Structural Engineering*, vol. 137, no. 7, pp. 748–760, 2010.

[26] S. Günay and K. M. Mosalam, "Enhancement of real-time hybrid simulation on a shaking table configuration with implementation of an advanced control method," *Earthquake Engineering & Structural Dynamics*, vol. 44, no. 5, pp. 657–675, 2015.

[27] Y. Qian, G. Ou, A. Maghareh, and S. J. Dyke, "Parametric identification of a servohydraulic actuator for real-time hybrid simulation," *Mechanical Systems and Signal Processing*, vol. 48, no. 1-2, pp. 260–273, 2014.

[28] G. Ou, S. J. Dyke, and A. Prakash, "Real time hybrid simulation with online model updating: An analysis of accuracy," *Mechanical Systems and Signal Processing*, vol. 84, pp. 223–240, 2017.

[29] M. Zapateiro, H. R. Karimi, N. Luo, and B. F. Spencer Jr, "Real-time hybrid testing of semiactive control strategies for vibration reduction in a structure with mr damper," *Structural Control and Health Monitoring*, vol. 17, no. 4, pp. 427–451, 2010.

[30] S. Kim, R. Christenson, B. Phillips, and B. Spencer, "Geographically distributed real-time hybrid simulation of mr dampers for seismic hazard mitigation," in *20th Analysis and Computation Specialty Conference - Proceedings of the Conference*, 20th Analysis and Computation Specialty Conference - Proceedings of the Conference, pp. 382–393, 9 2012.

[31] H. N. Mahmoud, A. S. Elnashai, B. F. Spencer Jr, O.-S. Kwon, and D. J. Bennier, "Hybrid simulation for earthquake response of semirigid partial-strength steel frames," *Journal of structural engineering*, vol. 139, no. 7, pp. 1134–1148, 2013.

[32] C. Chen, J. M. Ricles, T. L. Karavasilis, Y. Chae, and R. Sause, "Evaluation of a real-time hybrid simulation system for performance evaluation of structures with rate dependent devices subjected to seismic loading," *Engineering Structures*, vol. 35, pp. 71–82, 2012.

[33] S. Günay and K. M. Mosalam, "Seismic performance evaluation of high-voltage disconnect switches using real-time hybrid simulation: Ii. parametric study," *Earthquake engineering & structural dynamics*, vol. 43, no. 8, pp. 1223–1237, 2014.

[34] R. K. Fruhwirth, G. Thonhauser, W. Mathis, *et al.*, "Hybrid simulation using neural networks to predict drilling hydraulics in real time," in *SPE Annual Technical Conference and Exhibition*, Society of Petroleum Engineers, 2006.

[35] P. Bonnet, C. Lim, M. Williams, A. Blakeborough, S. Neild, D. Stoten, and C. Taylor, "Real-time hybrid experiments with newmark integration, mcsmd outer-loop control and multi-tasking strategies," *Earthquake Engineering & Structural Dynamics*, vol. 36, no. 1, pp. 119–141, 2007.

[36] R. M. Botelho and R. E. Christenson, "Robust stability and performance analysis for multi-actuator real-time hybrid substructuring," in *Dynamics of Coupled Structures, Volume 4*, pp. 1–7, Springer, 2015.

[37] X. Gao, N. Castaneda, and S. J. Dyke, "Experimental validation of a generalized procedure for mdof real-time hybrid simulation," *Journal of Engineering Mechanics*, vol. 140, no. 4, p. 04013006, 2014.

[38] H. Xu, C. Zhang, H. Li, and J. Ou, "Real-time hybrid simulation approach for performance validation of structural active control systems: a linear motor actuator based active mass driver case study," *Structural Control and Health Monitoring*, vol. 21, no. 4, pp. 574–589, 2014.

[39] D. McCrum and M. Williams, "An overview of seismic hybrid testing of engineering structures," *Engineering Structures*, vol. 118, pp. 240–261, 2016.

[40] M. Hakuno, M. Shidawara, and T. Hara, "Dynamic destructive test of a cantilever beam, controlled by an analog-computer," in *Proceedings of the Japan society of civil engineers*, vol. 1969, pp. 1–9, Japan Society of Civil Engineers, 1969.

[41] Y.-T. Leung, "An accurate method of dynamic substructuring with simplified computation," *International Journal for Numerical Methods in Engineering*, vol. 14, no. 8, pp. 1241–1256, 1979.

[42] A. Hale and L. Meirovitch, "A general substructure synthesis method for the dynamic simulation of complex structures," *Journal of Sound and Vibration*, vol. 69, no. 2, pp. 309–326, 1980.

[43] M. Nakashima, H. Kato, and E. Takaoka, "Development of real-time pseudo dynamic testing," *Earthquake Engineering & Structural Dynamics*, vol. 21, no. 1, pp. 79–92, 1992.

[44] J. Y. Tu, "Development of numerical-substructure-based and output-based substructuring controllers," *Structural Control and Health Monitoring*, vol. 20, no. 6, pp. 918–936, 2013.

[45] D. D. Klerk, D. J. Rixen, and S. N. Voormeeren, "General framework for dynamic substructuring: History, review and classification of techniques," *AIAA Journal*, vol. 46, pp. 1169–1181, May 2008.

[46] A. Plummer, "Model-in-the-loop testing," *Proceedings of the Institution of Mechanical Engineers, Part I: Journal of Systems and Control Engineering*, vol. 220, no. 3, pp. 183–199, 2006.

[47] A. Bouscayrol, "Different types of hardware-in-the-loop simulation for electric drives," in *2008 IEEE International Symposium on Industrial Electronics*, pp. 2146–2151, IEEE, 2008.

[48] S. Klein, R. Savelsberg, F. Xia, D. Guse, J. Andert, T. Blochwitz, C. Bellanger, S. Walter, S. Beringer, J. Jochheim, *et al.*, "Engine in the loop: Closed loop test

bench control with real-time simulation," *SAE International journal of commercial vehicles*, vol. 10, no. 2017-01-0219, pp. 95–105, 2017.

[49] A. Vidanapathirana, S. Dewasurendra, and S. Abeyaratne, "Model in the loop testing of complex reactive systems," in *2013 IEEE 8th International Conference on Industrial and Information Systems*, pp. 30–35, IEEE, 2013.

[50] D. P. Stoten, T. Yamaguchi, and Y. Yamashita, "Dynamically substructured system testing for railway vehicle pantographs," *Journal of Physics: Conference Series*, vol. 744, no. 1, p. 012204, 2016.

[51] A. Facchinetti and S. Bruni, "Hardware-in-the-loop hybrid simulation of pantograph–catenary interaction," *Journal of Sound and Vibration*, vol. 331, no. 12, pp. 2783–2797, 2012.

[52] D. P. Stoten and R. A. Hyde, "Adaptive control of dynamically substructured systems: The single-input single-output case," *Proceedings of the Institution of Mechanical Engineers, Part I: Journal of Systems and Control Engineering*, vol. 220, no. 2, pp. 63–79, 2006.

[53] M. Wallace, J. Sieber, S. Neild, D. Wagg, and B. Krauskopf, "Stability analysis of real-time dynamic substructuring using delay differential equation models," *Earthquake engineering & structural dynamics*, vol. 34, no. 15, pp. 1817–1832, 2005.

[54] S. Neild, D. Stoten, D. Drury, and D. Wagg, "Control issues relating to real-time substructuring experiments using a shaking table," *Earthquake engineering & structural dynamics*, vol. 34, no. 9, pp. 1171–1192, 2005.

[55] O. Bursi, A. Gonzalez-Buelga, L. Vulcan, S. Neild, and D. Wagg, "Novel coupling rosenbrock-based algorithms for real-time dynamic substructure testing," *Earthquake engineering & structural dynamics*, vol. 37, no. 3, pp. 339–360, 2008.

[56] J.-Y. Tu, W.-D. Hsiao, and C.-Y. Chen, "Modelling and control issues of dynamically substructured systems: adaptive forward prediction taken as an example," *Proceedings of the Royal Society A*, vol. 470, no. 2168, p. 20130773, 2014.

[57] J. Kullaa, "Virtual sensing of structural vibrations using dynamic substructuring," *Mechanical Systems and Signal Processing*, vol. 79, pp. 203–224, 2016.

[58] B. Wu and H. Zhou, "Sliding mode for equivalent force control in real-time substructure testing," *Structural Control and Health Monitoring*, vol. 21, pp. 1284–1303, 2014.

[59] G. Li, J. Na, D. P. Stoten, and X. Ren, "Adaptive neural network feedforward control for dynamically substructured systems," *IEEE Transactions on Control Systems Technology*, vol. 22, pp. 944–954, May 2014.

[60] M. Wallace, D. Wagg, S. Neild, P. Bunniss, N. Lieven, and A. Crewe, "Testing coupled rotor blade–lag damper vibration using real-time dynamic substructuring," *Journal of Sound and Vibration*, vol. 307, no. 3-5, pp. 737–754, 2007.

[61] J. Guo, Z. Tang, S. Chen, and Z. Li, "Control strategy for the substructuring testing systems to simulate soil-structure interaction," *Smart Structures and Systems*, vol. 18, no. 6, pp. 1169–1188, 2016.

[62] C.-P. Lamarche, R. Tremblay, P. Léger, M. Leclerc, and O. Bursi, "Comparison between real-time dynamic substructuring and shake table testing techniques for nonlinear seismic applications," *Earthquake engineering & structural dynamics*, vol. 39, no. 12, pp. 1299–1320, 2010.

[63] C. Dion, N. Bouaanani, R. Tremblay, C.-P. Lamarche, and M. Leclerc, "Real-time dynamic substructuring testing of viscous seismic protective devices for bridge structures," *Engineering structures*, vol. 33, no. 12, pp. 3351–3363, 2011.

[64] S.-C. Wu and E. J. Haug, "Geometric non-linear substructuring for dynamics of flexible mechanical systems," *International journal for numerical methods in engineering*, vol. 26, no. 10, pp. 2211–2226, 1988.

[65] V. K. Goel, J. N. Grauer, T. C. Patel, A. Biyani, K. Sairyo, S. Vishnubhotla, A. Matyas, I. Cowgill, M. Shaw, R. Long, *et al.*, "Effects of charite artificial disc on the implanted and adjacent spinal segments mechanics using a hybrid testing protocol," *Spine*, vol. 30, no. 24, pp. 2755–2764, 2005.

[66] X. Wang and J. K. Mills, "Dynamic modeling of a flexible-link planar parallel platform using a substructuring approach," *Mechanism and machine theory*, vol. 41, no. 6, pp. 671–687, 2006.

[67] M. Wallace, D. Wagg, and S. Neild, "An adaptive polynomial based forward prediction algorithm for multi-actuator real-time dynamic substructuring," *Proceedings of the Royal Society A: Mathematical, Physical and Engineering Sciences*, vol. 461, no. 2064, pp. 3807–3826, 2005.

[68] P. Gawthrop, M. Wallace, S. Neild, and D. Wagg, "Robust real-time substructuring techniques for under-damped systems," *Structural Control and Health Monitoring*, vol. 14, no. 4, pp. 591–608, 2007.

[69] J. M. Londoño, G. Serino, D. J. Wagg, S. A. Neild, and A. J. Crewe, "On the assessment of passive devices for structural control via real-time dynamic substructuring," *Structural Control and Health Monitoring*, vol. 19, no. 8, pp. 701–722, 2012.

[70] Y. Kyrychko, K. Blyuss, A. Gonzalez-Buelga, S. Hogan, and D. Wagg, "Real-time dynamic substructuring in a coupled oscillator–pendulum system," *Proceedings of the Royal Society A: Mathematical, Physical and Engineering Sciences*, vol. 462, no. 2068, pp. 1271–1294, 2006.

[71] D. Stoten, C. Lim, and S. Neild, "Assessment of controller strategies for real-time dynamic substructuring of a lightly damped system," *Proceedings of the Institution of Mechanical Engineers, Part I: Journal of Systems and Control Engineering*, vol. 221, no. 2, pp. 235–250, 2007.

[72] S. S. You and D. Fricke, "Advances of virtual testing and hybrid simulation in automotive performance and durability evaluation," *SAE International Journal of Materials and Manufacturing*, vol. 4, no. 1, pp. 98–110, 2011.

[73] P. Terwiesch, T. Keller, and E. Scheiben, "Rail vehicle control system integration testing using digital hardware-in-the-loop simulation," *IEEE Transactions on Control Systems Technology*, vol. 7, no. 3, pp. 352–362, 1999.

[74] M. Spiryagin, Y. Q. Sun, C. Cole, T. McSweeney, S. Simson, and I. Persson, "Development of a real-time bogie test rig model based on railway specialised multibody software," *Vehicle System Dynamics*, vol. 51, no. 2, pp. 236–250, 2013.

[75] A. Gonzalez-Buelga, D. Wagg, and S. Neild, "Parametric variation of a coupled pendulum-oscillator system using real-time dynamic substructuring," *Structural Control and Health Monitoring: The Official Journal of the International Association for Structural Control and Monitoring and of the European Association for the Control of Structures*, vol. 14, no. 7, pp. 991–1012, 2007.

[76] W. Hong, S. Kang, J. Lee, Y. Byun, and C. Choi, "Characterization of railroad track substructures using dynamic and static cone penetrometer," in *5th International Conference on Geotechnical and Geophysical Site Characterisation, ISC 2016*, Australian Geomechanics Society, 2016.

[77] M. S. Allen and R. L. Mayes, "Recent advances to estimation of fixed-interface modal models using dynamic substructuring," in *Dynamics of Coupled Structures, Volume 4*, pp. 157–170, Springer, 2018.

[78] R. L. Mayes and M. Arviso, "Design studies for the transmission simulator method of experimental dynamic substructuring.," tech. rep., Sandia National Laboratories, 2010.

[79] S. N. Voormeeren, "Dynamic substructuring methodologies for integrated dynamic analysis of wind turbines," 2012.

[80] S. Voormeeren, P. Van Der Valk, and D. Rixen, "Generalized methodology for assembly and reduction of component models for dynamic substructuring," *AIAA journal*, vol. 49, no. 5, pp. 1010–1020, 2011.

[81] S. Besset and L. Jezequel, "Dynamic substructuring based on a double modal analysis," *Journal of Vibration and acoustics*, vol. 130, no. 1, 2008.

[82] C. Soize and H. Chebli, "Random uncertainties model in dynamic substructuring using a nonparametric probabilistic model," *Journal of Engineering Mechanics*, vol. 129, no. 4, pp. 449–457, 2003.

[83] S. Voormeeren and D. Rixen, "A family of substructure decoupling techniques based on a dual assembly approach," *Mechanical Systems and Signal Processing*, vol. 27, pp. 379–396, 2012.

[84] W. D'Ambrogio and A. Fregolent, "Inverse dynamic substructuring using the direct hybrid assembly in the frequency domain," *Mechanical Systems and Signal Processing*, vol. 45, no. 2, pp. 360–377, 2014.

[85] M. Law, H. Rentzsch, and S. Ihlenfeldt, "Predicting mobile machine tool dynamics by experimental dynamic substructuring," *International Journal of Machine Tools and Manufacture*, vol. 108, pp. 127–134, 2016.

[86] P. Reuss, B. Zeumer, J. Herrmann, and L. Gaul, "Consideration of interface damping in dynamic substructuring," in *Topics in Experimental Dynamics Substructuring and Wind Turbine Dynamics, Volume 2*, pp. 81–88, Springer, 2012.

[87] M. van der Seijs and D. Rixen, *Experimental dynamic substructuring: analysis and design strategies for vehicle development.* PhD thesis, Delft University of Technology, 2016.

[88] D. De Klerk, "Dynamic response characterization of complex systems through operational identification and dynamic substructuring-an application to gear noise propagation in the automotive industry," 2009.

[89] Z. Mourelatos, "An efficient crankshaft dynamic analysis using substructuring with ritz vectors," *Journal of Sound and vibration*, vol. 238, no. 3, pp. 495–527, 2000.

[90] D. De Klerk and S. Voormeeren, "Uncertainty propagation in experimental dynamic substructuring," in *Proceedings of the Twenty Sixth International Modal Analysis Conference, Orlando, FL*, Society for Experimental Mechanics Bethel, CT, 2008.

[91] S. Voormeeren, D. De Klerk, and D. Rixen, "Uncertainty quantification in experimental frequency based substructuring," *Mechanical Systems and Signal Processing*, vol. 24, no. 1, pp. 106–118, 2010.

[92] T. Kranjc, J. Slavič, and M. Boltežar, "An interface force measurements-based substructure identification and an analysis of the uncertainty propagation," *Mechanical Systems and Signal Processing*, vol. 56, pp. 2–14, 2015.

[93] A. Oppenheim, A. Willsky, H. Nawab, and S. Hamid, *Signals and Systems*. Pearson Education, 1998.

[94] R. Curtain and K. Morris, "Transfer functions of distributed parameter systems: A tutorial," *Automatica*, vol. 45, no. 5, pp. 1101–1116, 2009.

[95] Q. Gao and H. R. Karimi, *Stability, Control and Application of Time-delay Systems*. Butterworth-Heinemann, 2019.

[96] M. E. S. Graham C. Goodwin, Stefan F. Graebe, *Control System Design*. Prentice Hall, 2000.

[97] P. Gawthrop, S. Neild, A. Gonzalez-Buelga, and D. Wagg, "Causality in real-time dynamic substructure testing," *Mechatronics*, vol. 19, no. 7, pp. 1105–1115, 2009.

[98] R. Kalman, "On the general theory of control systems," *IRE Transactions on Automatic Control*, vol. 4, pp. 110–110, December 1959.

[99] P. Antsaklis and A. Michel, *A Linear Systems Primer*. No. p.284-p.295, Birkhäuser, 2007.

[100] K. Warwick, *Control systems: an introduction*. Prentice Hall International Series in Systems and Control Engineering, Prentice Hall, 2nd ed ed., 1996.

[101] D. P. Stoten, J. Y. Tu, and G. Li, "Synthesis and control of generalized dynamically substructured systems," *Proceedings of the Institution of Mechanical Engineers, Part I: Journal of Systems and Control Engineering*, vol. 223, no. 3, pp. 371–392, 2009.

[102] C. N. Lim, S. A. Neild, D. P. Stoten, D. Drury, and C. A. Taylor, "Adaptive control strategy for dynamic substructuring tests," *Journal of Engineering Mechanics*, vol. 133, no. 8, pp. 864–873, 2007.

[103] R. Enokida and K. Kajiwara, "Nonlinear signal-based control with an error feedback action for nonlinear substructuring control," *Journal of Sound and Vibration*, vol. 386, pp. 21 – 37, 2017.

[104] Y.-J. Cha, A. K. Agrawal, A. Friedman, B. Phillips, R. Ahn, B. Dong, S. J. Dyke, B. F. Spencer, J. Ricles, and R. Christenson, "Performance validations of semiactive controllers on large-scale moment-resisting frame equipped with 200-kn mr damper using real-time hybrid simulations," *Journal of Structural Engineering*, vol. 140, no. 10, p. 04014066, 2014.

[105] T. Yamaguchi and D. P. Stoten, "Synthesised H_∞ / μ control design for dynamically substructured systems," *Journal of Physics: Conference Series*, vol. 744, no. 1, p. 012205, 2016.

[106] F. Lin, *Robust control design: an optimal control approach*, vol. 18. John Wiley & Sons, 2007.

[107] A. Stoorvogel, *The H_∞ control problem: a state space approach*. Prentice Hall International Series in Systems and Control Engineering, Prentice Hall, 2000.

[108] D. A. Barton, "Control-based continuation: Bifurcation and stability analysis for physical experiments," *Mechanical Systems and Signal Processing*, vol. 84, pp. 54–64, 2017.

[109] A. Fregolent *et al.*, "Substructure decoupling without using rotational dofs: Fact or fiction?," *Mechanical Systems and Signal Processing*, vol. 72, pp. 499–512, 2016.

Appendix A

Distribution of Roots for Polynomials with Even Maximum Degree and Positive Coefficients

The aim of this appendix is to prove that polynomials with even degrees and unconditionally positive coefficients only admit roots with negative real parts and purely imaginary roots. This proof is used in Chapter 3 to show that the original whole system and substructure A are asymptotically stable and that substructure B is marginally stable.

Let us then consider a polynomial $P(s)$ with a maximum even degree $2n$ and positive coefficients

$$P(s) = a_{2n}s^{2n} + a_{2n-1}s^{2n-1} + \cdots + a_i s^i + \cdots + a_0 \tag{A.1}$$

$$a_i > 0, \quad 0 \leq i \leq 2n \tag{A.2}$$

No positive or zero real roots for $P(s)$ exist, as can be easily shown by direct substitution. Therefore, the roots of $P(s)$ can only include negative real roots, imaginary roots and complex roots. Moreover, a polynomial with a even maximum degree should have an even number of real roots, an even number of conjugated imaginary roots, an even number of conjugated complex roots, or a combination of these three possibilities.

The following proof is composed of two parts. In the first part it is demonstrated that: i) if $P(s)$ admits complex roots with positive real parts then its coefficients are not unconditionally positive, and ii) if $P(s)$ does not admit complex roots with positive real parts then its coefficients are unconditionally positive. These implications are then used in the second part of the proof to prove, exploiting the contraposition principle, that polynomials $P(s)$ with even degree and unconditionally positive coefficients only admit roots with negative real part and, potentially, purely imaginary roots.

Let us then start the proof by considering the case where $P(s)$ only admits conjugated imaginary roots only, i.e.

$$P(s) = \prod_{q=1}^{n} (a_{2(q)} s^2 + a_{0(q)}), \quad a_{2(q)} > 0, a_{0(q)} > 0 \tag{A.3}$$

Therefore, it is obvious that after the expansion the coefficients of odd degree terms s^{2j-1} are equal to zero and all the others are positive. This contradicts the positivity of coefficients of $P(s)$, therefore $P(s)$ can not admit only purely imaginary roots.

admit is when $P(s)$ only admits negative real roots and conjugated complex roots with negative real parts, i.e.

$$P(s) = \prod_{q=1}^{n} (a_{2(q)} s^2 + a_{1(q)} s + a_{0(q)}) \tag{A.4}$$

where

$$\begin{cases} a_{2(q)} > 0 \\ a_{1(q)} > 0 \\ a_{0(q)} > 0 \end{cases} \tag{A.5}$$

Induction can be used to show that all coefficients in $P(s)$ are unconditionally positive. This condition is already satisfied when $n = 1$. Let us then assume that this condition is also satisfied when $n = j$ thus

$$P(s) = a_{2j}s^{2j} + a_{2j-1}s^{2j-1} + \cdots + a_i s^i + \cdots + a_0 \tag{A.6}$$

where

$$a_i > 0, \quad 0 \leq i \leq 2j \tag{A.7}$$

Then when $n = j + 1$ the following condition holds

$$\begin{aligned} P(s) &= (a_{2(j+1)}s^2 + a_{1(j+1)}s + a_{0(j+1)})(a_{2j}s^{2j} + a_{2j-1}s^{2j-1} + \cdots + a_i s^i + \cdots + a_0) \\ &= a_{2j+2}s^{2j+2} + a_{2j+1}s^{2j+1} + a'_{2j}s^{2j} + \cdots + a'_i s^i + \cdots + a'_0 \end{aligned} \tag{A.8}$$

where

$$\begin{cases} a_{2j+2} = a_{2(j+1)}a_{2j} > 0 \\ a_{2j+1} = a_{2(j+1)}a_{2j-1} + a_{1(j+1)}a_{2j} > 0 \\ a'_i = a_{2(j+1)}a_{i-2} + a_{1(j+1)}a_{i-1} + a_{0(j+1)}a_i > 0 \quad 2 \leq i \leq 2j \\ a'_1 = a_{1(j+1)}a_0 + a_{0(j+1)}a_1 > 0 \\ a'_0 = a_{0(j+1)}a_0 > 0 \end{cases} \tag{A.9}$$

Therefore, if $P(s)$ only admits negative real roots and conjugated complex roots with negative real parts, then all of its coefficients are unconditionally positive.

If $P(s)$ only admits imaginary roots, conjugated complex roots with negative real parts and negative real roots, the following equation holds

$$\begin{aligned} P(s) &= \prod_{q=1}^{j}(a_{2(q)}s^2 + a_{0(q)}) \prod_{q=1}^{j_1}(a'_{2(q)}s^2 + a'_{1(q)}s + a'_{0(q)}) \\ &= a_{2j+2j_1}s^{2j+2j_1} + a_{2j+2j_1-1}s^{2j+2j_1-1} + \cdots + a_i s^i + \cdots + a_0 \end{aligned} \tag{A.10}$$

$$\begin{cases} a_{2(q)} > 0 \\ a_{0(q)} > 0 \\ a'_{2(q)} > 0 \\ a'_{1(q)} > 0 \\ a'_{0(q)} > 0 \end{cases} \tag{A.11}$$

Then a similar induction procedure can be used to show that all the coefficients a_i are unconditionally positive.

Another case is that when $P(s)$ only admits conjugated complex roots with positive real parts. In this situation the following equation holds

$$P(s) = \prod_{q=1}^{n}(a_{2(q)}s^2 - a_{1(q)}s + a_{0(q)}) \tag{A.12}$$

where

$$\begin{cases} a_{2(q)} > 0 \\ a_{1(q)} > 0 \\ a_{0(q)} > 0 \\ a_{1(q)}^2 - 4a_{2(q)}a_{0(q)} < 0 \end{cases} \tag{A.13}$$

then the induction can be used to show that in the expanded form of $P(s)$, the coefficients for s^i are always negative when i is odd, and the coefficients for s^i are always positive when i is even, thus

$$P(s) = a_{2n}s^{2n} - a_{2n-1}s^{2n-1} + \cdots + (-1)^i a_i s^i + \cdots + a_0 \tag{A.14}$$

where

$$a_i > 0, \quad 0 \leq i \leq 2n \tag{A.15}$$

In fact, this condition is already satisfied for $n = 1$ and $n = 2$. let us then assume that this condition is also satisfied when $n = j$, thus

$$P(s) = a_{2j}s^{2j} - a_{2j-1}s^{2j-1} + \cdots + (-1)^i a_i s^i + \cdots + a_0 \tag{A.16}$$

where

$$a_i > 0, \quad 0 \leq i \leq 2j \tag{A.17}$$

Then for $n = j + 1$ the following condition holds

$$\begin{aligned} P(s) &= (a_{2(j+1)}s^2 - a_{1(j+1)}s + a_{0(j+1)})(a_{2j}s^{2j} - a_{2j-1}s^{2j-1} + (-1)^i a_i s^i + \cdots + a_0) \\ &= a_{2j+2}s^{2j+2} - a_{2j+1}s^{2j+1} + a'_{2j} + \cdots + a'_i s^i + \cdots + a'_0 \end{aligned} \tag{A.18}$$

where

$$\begin{cases} a_{2j+2} = a_{2(j+1)}a_{2j} \\ a_{2j+1} = a_{2(j+1)}a_{2j-1} + a_{1(j+1)}a_{2j} \\ a'_i = (-1)^{i-2}a_{2(j+1)}a_{i-2} + (-1)^i a_{1(j+1)}a_{i-1} + (-1)^i a_{0(j+1)}a_i \quad 2 \le i \le 2j \\ a'_1 = -(a_{1(j+1)}a_0 + a_{0(j+1)}a_1) \\ a'_0 = a_{0(j+1)}a_0 \end{cases} \tag{A.19}$$

Therefore, a'_i are always negative for odd values of i and a'_i are always positive for even values of i. This contradicts the positivity of coefficients of $P(s)$, therefore $P(s)$ can not admit roots with only positive real parts.

Finally if $P(s)$ admits negative real roots, conjugated complex roots with negative real parts and conjugated complex roots with positive real parts, then

$$\begin{aligned} P(s) &= \prod_{q=1}^{j}(a_{2(q)}s^2 + a_{1(q)}s + a_{0(q)}) \prod_{q=1}^{j_1}(a'_{2(q)}s^2 - a'_{1(q)}s + a'_{0(q)}) \\ &= (a_{2j}s^{2j} + a_{2j-1}s^{2j-1} + \cdots + a_i s^i + \cdots + a_0) \\ &\times (a'_{2j_1}s^{2j_1} - a'_{2j_1-1}s^{2j_1-1} + \cdots + (-1)^i a'_i s^i + \cdots + a'_0) \\ &= a''_{2j+2_j-1}s^{2(j+j_1)} + a''_{2j+2j_1-1}s^{2(j+j_1)-1} + \cdots + a''_i s^i + \cdots + a''_0 \end{aligned} \tag{A.20}$$

where

$$\begin{cases} a_i > 0, & 0 \le i \le j \\ a'_i > 0, & 0 \le i \le j_1 \\ (a'_{1(q)})^2 - 4a'_{2(q)}a'_{0(q)} < 0 & \\ a''_{2j+2j_1} = a_{2j}a'_{2j_1} & \\ a''_0 = a_0 a'_0 & \end{cases} \tag{A.21}$$

and if $j \le j_1$

$$\begin{cases} a''_i = \sum_{q=0}^{i-2j} (-1)^q a_{i-q}a'_q, & 2j \le i \le 2j + 2j_1 - 1 \\ a''_i = \sum_{q=0}^{i} (-1)^{i-q} a_q a'_{i-q}, & 0 \le i \le 2j \end{cases} \tag{A.22}$$

if $j > j_1$

$$\begin{cases} a''_i = \sum_{q=0}^{i-2j_1} (-1)^{i-q} a_q a'_{i-q}, & 2j_1 \le i \le 2j + 2j_1 - 1 \\ a''_i = \sum_{q=0}^{i} (-1)^q a_{i-q}a'_q, & 0 \le i \le 2j_1 \end{cases} \tag{A.23}$$

Therefore, apart from a''_{2j+2j_1} and a''_0, other coefficients are not always positive. The same conclusion applies when $P(s)$ includes purely imaginary roots, negative real roots and complex roots with positive real parts and when $P(s)$ only includes purely imaginary roots and complex roots with positive real parts.

In summary, two main conclusions can be drawn from the conditions above. The first

one is that if $P(s)$ does not include complex roots with positive real parts then its coefficients are unconditionally positive. The second conclusion is that if $P(s)$ does include complex roots with positive real parts then its coefficients are not unconditionally positive. Then the law of contraposition - stating that a conditional statement implies that its contrapositive holds as well - can be used to show that two additional conditions hold. The first one is that if the coefficients of $P(s)$ are not unconditionally positive then $P(s)$ admits complex roots with positive real parts. The second condition is that if the coefficients of $P(s)$ are unconditionally positive then $P(s)$ does not include any complex root with positive real part. All together, these conditions imply that a polynomial $P(s)$ with even degree and unconditionally positive coefficients only admits negative real roots, complex roots with negative real parts and purely imaginary roots. The proof is therefore complete.

Appendix B

Controllers for Beam Split Model

The details of the controllers used in Chapter 6 are provided. The transfer function form of the controller K with the objective function $min\frac{||e||^2}{||d_1||^2+||d_2||^2}$ is listed as follows

$$K^T(s) = \begin{bmatrix} \frac{84514(s+50)(s-0.1125)(s+0.002163)(s^2+2.636s+11.31)(s^2+5.258s+21.49)}{(s+156)(s+1)(s^2+2.175s+9.42)(s^2+4.746s+22)(s^2+194.1s+2.974\times10^4)} \\ \frac{64778(s+50)(s+0.00199)(s+0.001721)(s^2+2.636s+11.31)(s^2+8.433s+32.48)}{(s+156)(s+1)(s^2+2.175s+9.42)(s^2+4.746s+22)(s^2+194.1s+2.974\times10^4)} \\ \frac{2.3357\times10^5(s+50)(s+0.04051)(s+0.001235)(s^2+2.636s+11.31)(s^2+5.206s+21.54)}{(s+156)(s+1)(s^2+2.175s+9.42)(s^2+4.746s+22)(s^2+194.1s+2.974\times10^4)} \\ \frac{1.5553\times10^5(s+50)(s+0.002199)(s+0.001782)(s^2+2.636s+11.31)(s^2+8.432s+32.48)}{(s+156)(s+1)(s^2+2.175s+9.42)(s^2+4.746s+22)(s^2+194.1s+2.974\times10^4)} \\ \frac{1.1435\times10^5(s+50)(s-0.05434)(s+0.002371)(s^2+2.636s+11.31)(s^2+5.929s+26.52)}{(s+156)(s+1)(s^2+2.175s+9.42)(s^2+4.746s+22)(s^2+194.1s+2.974\times10^4)} \\ \frac{2.5453\times10^9(s+155.9)(s+50)(s+0.00214)}{(s+1.094\times10^8)(s+156)(s+1)}\times \\ \times\frac{(s+0.001647)(s^2+2.636s+11.31)(s^2+31.78s+754.1)}{(s^2+2.175s+9.42)(s^2+4.746s+22)(s^2+194.1s+2.974\times10^4)} \\ \frac{2.2155\times10^6(s+50)(s^2+0.00388s+3.774\times10^{-}6)(s^2+3.101s+10.02)(s^2+4.91s+22.44)}{(s+156)(s+1)(s^2+2.175s+9.42)(s^2+4.746s+22)(s^2+194.1s+2.974\times10^4)} \\ \frac{1.1852\times10^6(s+50)(s^2+0.00388s+3.789\times10^{-}6)(s^2+7.351s+21.15)(s^2+4.91s+22.44)}{(s+156)(s+1)(s^2+2.175s+9.42)(s^2+4.746s+22)(s^2+194.1s+2.974\times10^4)} \\ \frac{1.7234\times10^6(s+50)(s+0.002007)(s+0.001874)(s^2+3.623s+14.01)(s^2+4.91s+22.44)}{(s+156)(s+1)(s^2+2.175s+9.42)(s^2+4.746s+22)(s^2+194.1s+2.974\times10^4)} \\ \frac{1.1187\times10^{10}(s+195.2)(s+50)(s^2+0.00388s+3.767\times10^{-}6)(s^2+4.91s+22.44)(s^2-9.057s+855.6)}{(s+9.582\times10^7)(s+156)(s+1)(s^2+2.175s+9.42)(s^2+4.746s+22)(s^2+194.1s+2.974\times10^4)} \end{bmatrix} \quad \text{(B.1)}$$

And then the transfer function form of the controller K with the objective function $min\frac{||e||^2+||F||^2}{||d_1||^2+||d_2||^2}$ is listed as follows

$$K^T(s) = \begin{bmatrix} \frac{7.3123\times10^{-4}(s+0.01744)(s+0.002171)(s^2+5.394s+22.33)}{(s+1)(s+0.01555)(s+0.008409)(s^2+4.91s+22.44)} \\ \frac{3.5418\times10^{-4}(s+2.761\times10^4)(s^2+0.003954s+4.156\times10^{-6})(s^2+9.86s+44.13)}{(s+2.672\times10^4)(s+1)(s+0.01555)(s+0.008409)(s^2+4.91s+22.44)} \\ \frac{1.7191\times10^{-3}(s-0.001712)(s+0.0007492)(s^2+5.404s+22.34)}{(s+1)(s+0.01555)(s+0.008409)(s^2+4.91s+22.44)} \\ \frac{8.4994\times10^{-4}(s+2.761\times10^4)(s^2+0.003912s+4.071\times10^{-6})(s^2+9.861s+44.13)}{(s+2.672\times10^4)(s+1)(s+0.01555)(s+0.008409(s^2+4.91s+22.44)} \\ \frac{8.7835\times10^{-4}(s+2.762\times10^4)(s+0.01018)(s+0.002381)(s^2+5.835s+27.87)}{(s+2.672\times10^4)(s+1)(s+0.01555)(s+0.008409)(s^2+4.91s+22.44)} \\ \frac{0.79066(s-6.162)(s^2+0.003944s+4.137\times10^{-6})(s^2+10.04s+106.9)}{(s+2.672\times10^4)(s+1)(s+0.01555)(s+0.008409)(s^2+4.91s+22.44)} \\ \frac{3.4855\times10^{-3}(s+16.37)(s+2.559)(s^2+0.003926s+4.091\times10^{-6})}{(s+1)(s+0.01555)(s+0.008409)(s^2+2.636s+11.31)} \\ \frac{0.054529(s+2.287\times10^4)(s+2.169)(s-0.3411)(s^2+0.003926s+4.091\times10^{-6})}{(s+2.339\times10^4)(s+1)(s+0.01555)(s+0.008409)(s^2+2.636s+11.31)} \\ \frac{0.013629(s+1.816\times10^4)(s+4.183)(s-1.776)(s^2+0.003926s+4.091\times10^{-6})}{(s+2.339\times10^4)(s+1)(s+0.01555)(s+0.008409)(s^2+2.636s+11.31)} \\ \frac{71.357(s+0.604)(s^2+0.003926s+4.091\times10^{-6})(s^2+7.297s+83.69)}{(s+1)(s+0.01555)(s+0.008409)(s^2+2.636s+11.31)} \end{bmatrix} \quad \text{(B.2)}$$